Westside Turbidite Field Trip
San Joaquin Valley – California
April 27, 2014

2014 AAPG Pacific Section Convention

Trip Leaders Mike Clark and Glenn Sharman

Field trip sponsored by

San Joaquin Geological Society

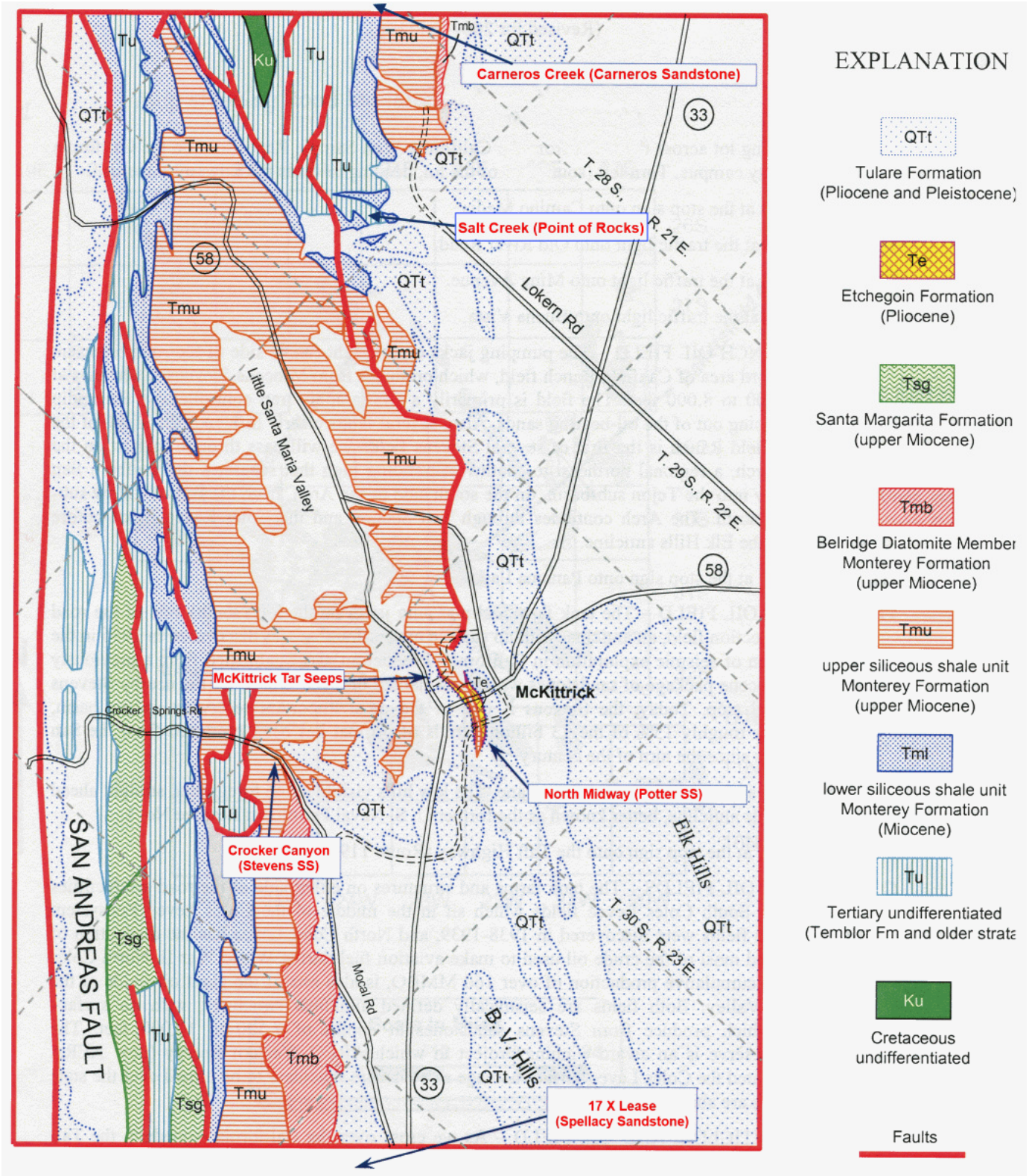

Geologic map of the west side of the southern San Joaquin Basin, showing locations of the field trip stops (modified from Dibblee, 1973).

Field Trip Itinerary

We have a long day ahead of us. If we can leave the outcrops on schedule, it will help us to see everything we have planned. Thank you for your cooperation.

7:00 Meet at Convention Center

Handouts, introductions, logistics, and safety considerations

7:30 Leave for Midway-Sunset Field (allow 60 minutes driving time)

8:30 Arrive at Midway 17X Lease (allow **60 minutes**) to examine a **Stevens submarine canyon**. We will also look at granitic bedrock, a Pleistocene fan delta, and Miocene turbidites that are interbedded with diatomites. A total of three short stops (one overview and two road cuts).

9:30 Leave for North Midway Field (allow 15 minutes driving time)

9:45 Arrive at North Midway (allow **60 minutes**) to examine a **Potter mass transport complex**, and the Belridge Diatomite. There is also a short hike to an 1890s asphalt mine driven into fluvial deposits of the Pleistocene Tulare Formation.

10:45 Start return hike to cars

11:00 Leave for McKittrick (allow 15 minutes driving time)

11:15 Bathroom stop at Chevron field office

11:30 Leave for Highway 58 oil seep (allow 15 minutes driving time)

11:45 Arrive at Highway 58 oil seep - LUNCH STOP (allow **60 minutes**). Here we will be able to see an **active tar seep** and the vertical shaft of an **1890s tar mine**.

12:45 Leave for Carneros Creek (allow 30 minutes driving time)

1:15 Arrive at Carneros Creek (allow **60 minutes**) to examine **Carneros turbidites**.

2:15 Start return hike to cars

2:30 **Leave for Salt Creek (allow 30 minutes driving time)**

3:00 Arrive at Salt Creek (allow **60 minutes**) to examine **Point of Rocks turbidites**.

4:00 Start return hike to cars

4:15 **Leave for Convention Center (allow 60 minutes driving time)**

5:15 Arrive back at Convention Center

Table of Contents

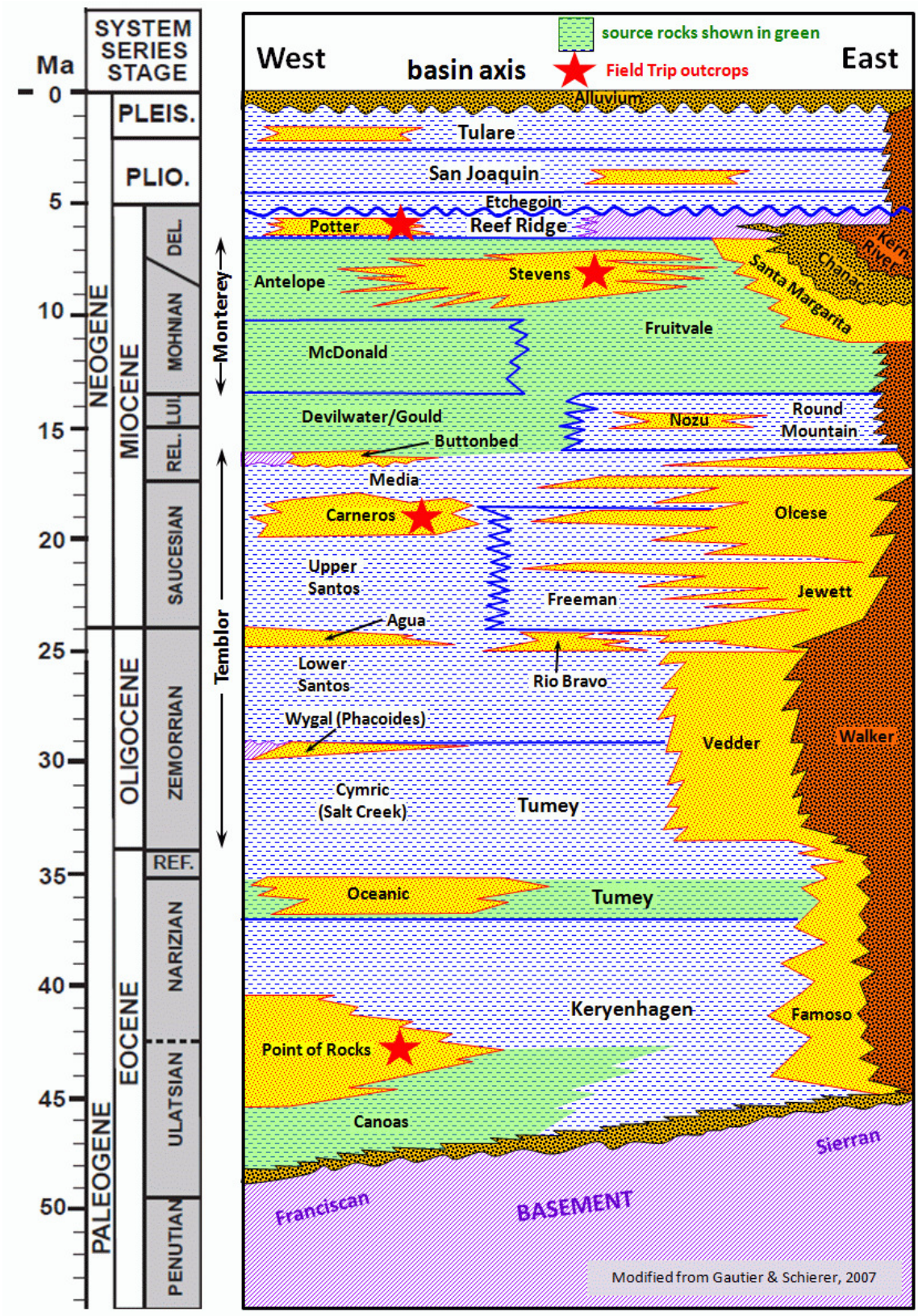

Stratigraphic section showing stratigraphy of the southern San Joaquin basin.

INTRODUCTION

Miocene Depositional Systems of the Southern San Joaquin Basin

S. A. Reid

(Article excerpted by Permission of Pacific Section — SEPM)

Introduction

The Miocene and Pliocene stratigraphic section at Elk Hills contains a continuous record of deposition at the center of the southern San Joaquin basin. Although the section consists of mostly claystone and mudstone, five distinct sandy intervals are present which form the petroleum reservoirs of the Elk Hills field (Figure 1).

Major factors which influenced sand sedimentation in the basin center are local and regional uplift, San Andreas fault offset chronology, location of fluvial sediment discharge points, degree of tidal range, and eustatic sea level changes. Significant Miocene tectonic events included termination of subduction and establishment of the San Andreas strike-slip system and clockwise rotation of the Tehachapi and San Emigdio Ranges. Pliocene Basin and Range uplift in addition to compression on the San Andreas fault caused uplift of all ranges surrounding the southern basin.

Tectonic events in and around the basin had the most impact on development of depositional systems. Tectonics controlled the shape of the basin, the location of seaways and basin circulation patterns. The degree of restriction influenced the generation and preservation of diatoms and their associated organic material. Tectonics controlled the timing of uplift, and the location of provenance areas such as the Gabilan highland and highlands adjacent to the La Honda basin. The shape of western Stevens sand units (late Miocene) was controlled by San Andreas fault compression which created intraslope basins.

Effects of eustatic sea-level changes on the southern San Joaquin basin are more difficult to assess. One significant event most likely related to an eustatic sea-level change was the 10.5 Ma lowstand, which resulted in deposition of the Kern River-fed eastern Stevens submarine fan on the Bakersfield arch. Middle Miocene Olcese sequences, early Pliocene episodes of Etchegoin delta front progradation, and late Pliocene *Mya* sand depositional cycles are other examples of probable sea-level-controlled deposition.

Carneros Sandstone Paleogeography (19 Ma)

Uplift and erosion of northern portions of the Temblor Range and highlands bordering the adjacent La Honda basin continued through the early Miocene (Graham and others, 1989)and initiated deposition of the Carneros submarine fan (Figure 2). A thin Carneros section deposited on an unconformity indicates localized uplift in the northern Temblor Range (Pence, 1985). This uplift event caused a local, relative drop in sea level which forced sediment to bypass the shelf and to be deposited basinward. A major submarine fan sourced from the northern Temblor Range and north of the La Honda basin prograded east and southeast onto the central San Joaquin basin floor. Although a significant global sea level change is interpreted at 21 Ma (Haq and others, 1987), and initial Carneros sedimentation may have coincided with this lowstand, Carneros sedimentation continued through 19 Ma, well into an inferred global sea level highstand. Shelf sedimentation continued in westside areas less affected by the uplift (Pence, 1985). Coarse grained, shallow marine sedimentation also continued on the east side of the basin on a broad shelf adjacent to the low, eroding western slope of the Sierra Nevada. Although sea-level lowstands (including the 21 Ma lowstand) may have resulted in sequence boundaries (Bloch and Olson, 1990), sediments continued to stay on the shelf.

Gould Shale and Button Bed Paleogeography (16.5 Ma)

The paleogeography at 16.5 Ma is representative of much of the medial and early late Miocene, a time when the basin experienced the mildest tectonic activity of the Miocene-Pliocene interval (Figure 3). Movement of the San Andreas fault progressed with little associated uplift, resulting in few highlands to restrict marine circulation between the basin and the Pacific (Bartow, 1991). In the southern basin, rotation of the Tehachapi and San Emigdio Ranges was nearly complete (Goodman and Malin, 1992).

On the stable Sierra Nevada shelf, the effects of eustatic sea level changes should be the most apparent. Bloch and Olson (1990) correlate unconformities within the Olcese to sea level lowstands, and correlate the transgression of each Olcese sequence to relative rises in sea level. Bartow (1991) also documents the effects of sea level changes, and interprets widespread eastside shoaling at 16.5 Ma coincident with a major lowstand. No deep sea fan system development is associated with the 16.5 Ma lowstand, indicating all sandy sediments were contained on the broad shelf. In addition, the development of a very thick interval of shale throughout much of the basin center indicates coarse sediments seldom passed beyond the shelf edge, even at times of low relative sea level. In the Tejon area, localized deposition in nonmarine, shallow marine and turbidite facies indicates the continuing effects of an uplifted, nearby source area.

Monterey Formation and Stevens sandstone Paleogeography (10 Ma)

Discussion: Three contemporaneous events in the late Miocene at 10 Ma radically altered the paleogeography of the basin: (1) partial blockage of the basin along the west side by granitic blocks moved by the San Andreas fault, (2) formation of a drainage system and Sierran discharge point similar to the modern Kern River, and (3) a major sea level lowstand (Figure 4). These events resulted in formation of major petroleum reservoir rocks and the principle petroleum source rocks of the San Joaquin basin.

After removing about 250 km (155 mi) of post-medial Miocene San Andreas fault offset, granitic highlands of the Gabilan Range in the late Miocene lay west of the southern San Joaquin basin (Graham and others, 1989). Numerous streams drained east across the fault escarpment, forming an apron of fan deltas and a narrow northwest-trending band of shelf sediments (Santa Margarita Formation) in the area of the southern Temblor Range (Ryder and Thomson, 1989). Sand spilled across this narrow shelf onto the slope, creating small depositional lobes and channel-fill turbidite systems of the Williams, Republic, and Webster sand units of the western Stevens (Link and Hall, 1990). The Gabilan highland restricted ocean access of the basin on the western side, although seaways to the Pacific existed to the north and south (Bartow, 1991). Throughout the central and western areas, the basin geometry favored diatom blooms and preservation of their organic-rich tests in Antelope Shale (Graham and Williams, 1985).

Redirection of the Kern River through stream capture, as outlined by MacPherson (1978), resulted in a major shift in the terminus of southern Sierra Nevada drainage in the late Miocene. Sierra-derived detritus transported along the new drainage exited the Sierra Nevada highlands northeast of Bakersfield. As a result of this drainage shift, much higher volumes of sand entered the basin, resulting in extensive shelf deposits (Santa Margarita) and a large river floodplain (Chanac).

Eastern Stevens submarine fan deposition and the creation of the Rosedale and Fruitvale canyons are interpreted to have been the result of sea-level changes (MacPherson, 1978; Hewett and Jordan, 1993). Three upper Mohnian sea-level lowstands are interpreted as marking the beginning of the Coulter, Gosford, and Bellevue fan sequences (Hewett and Jordan, 1993). A precise tie of sea-level lowstands to eustatic sea-level changes, uplift of shelf areas, or other factors is difficult because of the poor age control in the subsurface. However, the most significant eustatic sea-level lowstand of the Miocene occurred at 10.5 to 10.0 Ma (Haq and others, 1987) and was contemporaneous with Stevens deposition in the eastern part of the basin.

Monterey Formation and western Stevens sandstone Paleogeography (8.5 Ma)

Discussion: Continued northward progression of the Gabilan granitic source area by the San Andreas fault moved the site of Santa Margarita sand deposition on the western side of the basin to the central Temblor Range (Ryder and Thomson, 1989)(Figure 5). Seaways continued to connect the San Joaquin basin to the Pacific Ocean north and south of the Gabilan highland (Bartow, 1991). Changes in plate motion (summarized by Bartow, 1991) or activation of eastern-directed thrust wedges of Franciscan rocks (Imperato, 1993) may have triggered a brief but important west side tectonic event, which resulted in a broad slope as far east as Elk Hills punctuated by several small anticlines and synclines. Western Stevens turbidites, originating from the Gabilan highland west of the North Midway-McKittrick area, prograded across the synclinal basins and around anticlinal ridges and onto the Buttonwillow basin floor southeast of Lost Hills.

By 8.5 Ma, sea level was once again at a global highstand (Haq and others, 1987; Bartow, 1991). Although the Kern River continued to supply abundant sediments, indicated by widespread Chanac and Santa Margarita subsurface deposits, no Sierra Nevada-derived sediments spilled across the shelf break to form submarine fans. However, San Emigdio highlands to the south continued to contribute clastics across a narrow shelf to feed smaller submarine fan systems in the Maricopa subbasin (Quinn, 1990). North of the Bakersfield arch, conditions continued to favor diatom generation and preservation (Graham and Williams, 1985).

Reef Ridge Shale Paleogeography (7 Ma)

Discussion: The end of the Miocene along the western San Joaquin basin was relatively stable (Figure 6). Reef Ridge deposits tend to fill the intraslope basins and cover the anticlinal structures of the west side. Although the Gabilan block continued moving northwest opposite the southern basin, the block no longer contributed a sufficient volume of sediments into the basin to reach the base of the western slope. Seaways north and south of the Gabilan block continued to connect the San Joaquin basin to the open ocean (Bartow, 1991). The end of the Miocene also brought further reductions in diatom sedimentation. A shallowing of the basin, shifting ocean circulation patterns, and/or temperature changes may be responsible for reduced diatom production. Sediments derived from the Sierra Nevada continued to be restricted to the eastern shelf areas. Increases in clay sedimentation across the central and southern basin may indicate (1) more clay available from the Kern and other drainage systems, (2) clay sedimentation no longer diluted by diatom contribution, and/or (3) development of tidal currents with reworking of nearshore deposits and shifting clay deposition to deeper areas of the basin. Whatever the cause, a thick clay layer covered nearly all western and eastern Stevens turbidites in the San Joaquin basin.

References Cited

Bartow, J. A., 1991, The Cenozoic evolution of the San Joaquin Valley, California: U. S. Geological Survey Professional Paper 1501, 40 p.

Bloch, R. B., and Olson, H. C., 1990, Stratigraphy and structural history of the lower and middle Miocene section, eastside San Joaquin Valley, in Kuespert, J. G., and Reid, S. A., eds, Structure, stratigraphy and hydrocarbon occurrences of the San Joaquin basin, California: Pacific Section SEPM, v. 64, p. 287-291

Carter, J. B., 1985, Depositional environments of the type Temblor Formation, Chico Martinez Creek, Kern County, California, in Graham, S. A., ed., Geology of the Temblor Formation, western San Joaquin basin, California: Pacific Section SEPM, v. 44, p. 5-18.

COSUNA, 1984, Correlation of Stratigraphic Units of North America (COSUNA) Project; southern, central and northern California province correlation charts: AAPG, Tulsa, Ok.

Dibblee, T. W., Jr., and Warne, A. H., 1988, Inferred relation of the Oligocene to Miocene Bealville Fanglomerate to the Edison fault, Caliente Canyon area, Kern County, California, in Graham, S. A., and Olson, H. C., eds, Studies of the Geology of the San Joaquin basin: Pacific Section SEPM, v. 60, p. 223-231.

Dunwoody, J. A., Chairman, 1986, South San Joaquin Valley correlation section from San Andreas fault to Sierra Nevada foothills: Pacific Section AAPG, Correlation Section no. 8.

Goodman, E. D., and Malin, P. E., 1992, Evolution of the southern San Joaquin basin and mid-Tertiary "transitional" tectonics, central California: Tectonics, v. 11, no. 3, p. 378-498.

Graham, S. A., 1978, Role of Salinian block in evolution of San Andreas fault system, California: AAPG Bulletin, v. 62, p. 2214-2231.

Graham, S. A., Stanley, R. G., Bent, J. V., and Carter, J. R., 1989, Oligocene and Miocene paleogeography of central California and displacement along the San Andreas fault: GSA Bulletin, v. 101, p. 711-730.

Graham, S. A., and Williams, L. A., 1985, Tectonic, depositional and diagenetic history of Monterey Formation (Miocene), central San Joaquin basin, California: AAPG Bulletin, v. 69, p. 385-411.

Haq, B. U., Hardenbol, J., and Vail, P. R., 1987, Chronology of fluctuating sea levels since the Triassic: Science, V. 235, p. 1156-1166.

Hewlett, J. S., and Jordan, D. W., 1993, Stratigraphic and combination traps within a seismic sequence framework, Miocene Stevens turbidites, Bakersfield arch, California, in Weimer, P., and Posamentier, H., Siliciclastic sequence stratigraphy, recent developments and applications: AAPG Memoir 58, 492 p.

Hirst, B., 1988, Early Miocene tectonism and associated turbidite deposystems of the Tejon area, Kern County, California, in Graham, S. A., and Olson, H. C., eds, Studies of the Geology of the San Joaquin basin: Pacific Section SEPM, v. 60, p. 207-221.

Imperato, D. P., 1993, Overview of middle-late Cenozoic structure, tectonics and sedimentation of Elk Hills and Vicinity (abstract): AAPG Bulletin, v. 77, p. 701.

Link, M. H., and Hall, B. R., 1990, Architecture and sedimentology of the Miocene Moco T and Webster turbidite reservoirs, Midway Sunset Field, California, in Kuespert, J. G., and Reid, S. A., eds, Structure, stratigraphy and hydrocarbon occurrences of the San Joaquin basin, California: Pacific Section SEPM, v. 64, p. 115-129.

MacPherson, B. A., 1978, Sedimentation and trapping mechanism in upper Miocene Stevens and older turbidite fans of southeastern San Joaquin Valley, California: AAPG Bulletin, v. 62, p. 2243-2278.

Pence, J. J., 1985, Sedimentology of the Temblor Formation in the northern Temblor Range, California, in Graham, S. A., ed., Geology of the Temblor Formation, western San Joaquin basin, California: Pacific Section SEPM, v. 44, p. 19-34.

Quinn, M. J., 1990, Upper Miocene Stevens sands in the Maricopa depocenter, southern San Joaquin Valley, California, in Kuespert, J. G., and Reid, S. A., eds, Structure, stratigraphy and hydrocarbon occurrences of the San Joaquin basin, California: Pacific Section SEPM, v. 64, p. 97-113.

Reid, S. A., 1990, Trapping characteristics of upper Miocene turbidite deposits, Elk Hills field, Kern County, California, in Kuespert, J. G., and Reid, S. A., eds, Structure, stratigraphy and hydrocarbon occurrences of the San Joaquin basin, California: Pacific Section SEPM, v. 64, p.

Ryder, R. T., and Thomson, A., 1989, Tectonically controlled fan delta and submarine fan sedimentation of late Miocene age, southern Temblor Range, California: U. S. Geological Survey Professional Paper 1442, 59 p.

Schwartz, D. E., 1988, Characterizing the lithology, petrophysical properties, and depositional setting of the Belridge Diatomite, South Belridge field, Kern County, California, in Graham, S. A., and Olson, H. C., eds, Studies of the Geology of the San Joaquin basin: Pacific Section SEPM, v. 60, p. 281-301.

Webb, G. W., 1981, Stevens and earlier Miocene turbidite sandstones, southern San Joaquin Valley, California: AAPG Bulletin, v. 65, p. 438-465.

This article by Tony Reid is excerpted from pages 131-150 of the following publication by the Pacific Section—SEPM (Society for Sedimentary Geology)

Fritsche, A. E., 1995, Cenozoic Paleogeography of the Western United States - II: Pacific Section—SEPM, Book 75, 309 p.

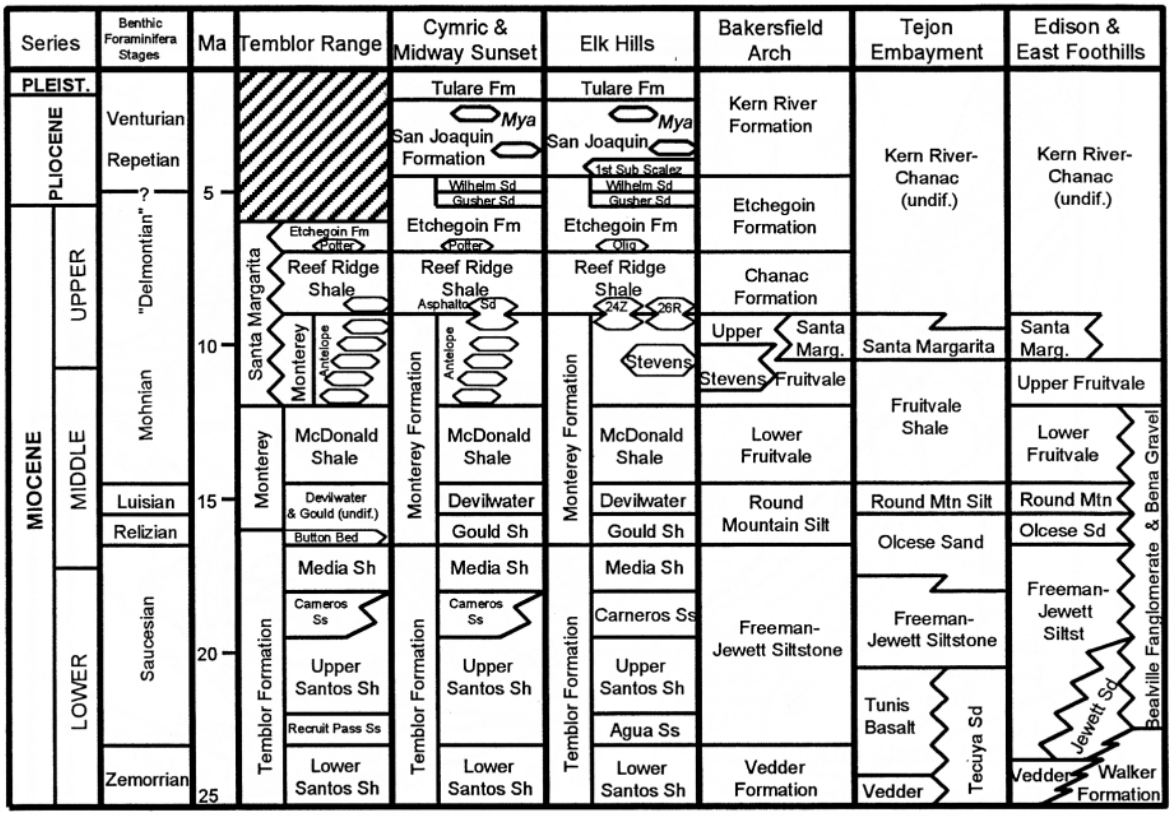

Figure 1. Correlation chart of Miocene and Pliocene stratigraphic units of the southern San Joaquin basin. Correlations are generally based on COSUNA (1984), with the following modifications: in the Temblor Range, Santa Margarita-Monterey relationship is from Ryder and Thomson (1989); at Elk Hills, ages of Miocene turbidites are from Reid (1990); Miocene Tejon correlations are from Hirst (1988); Edison area age distribution of the Bealville Fanglomerate and Bena Gravel is from Dibblee and Warne (1988).

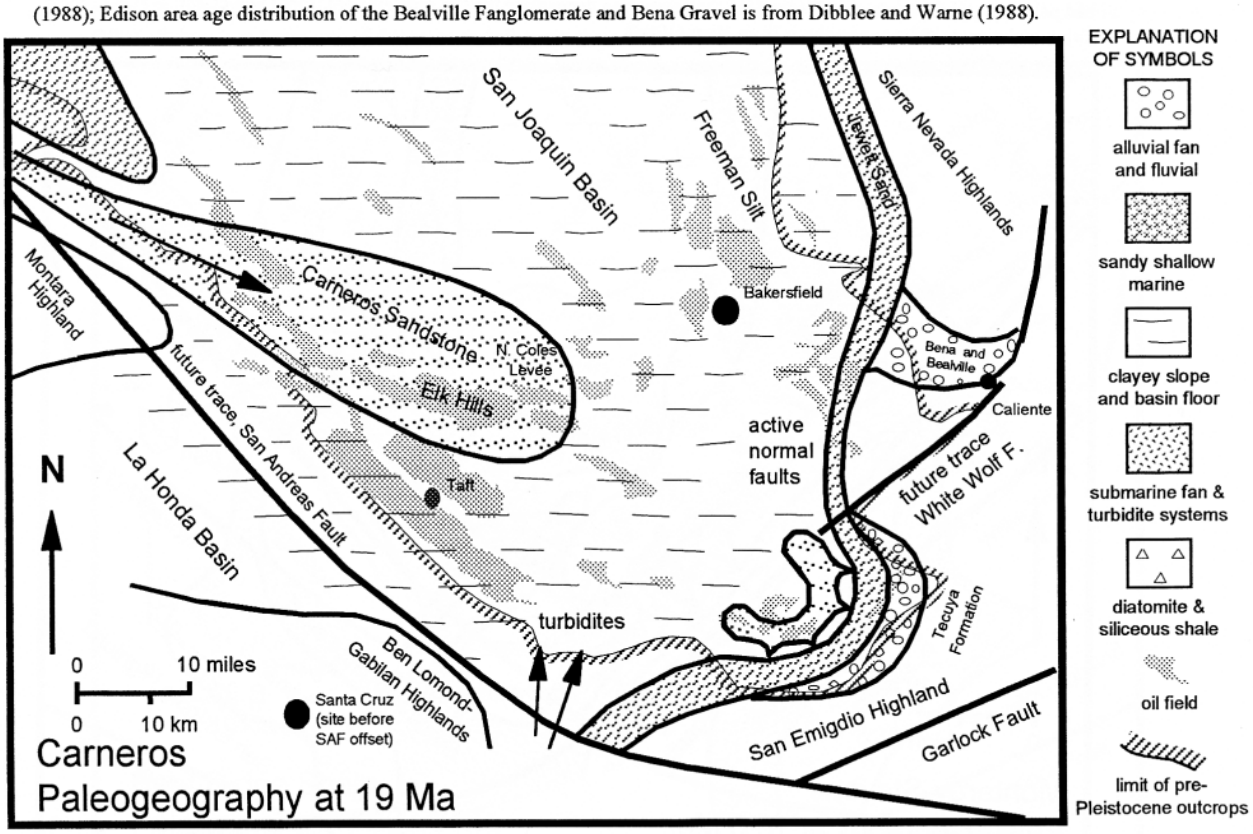

Figure 2. Paleogeography of the San Joaquin basin at 19 Ma, early Miocene, showing the depositional environments represented by the Carneros Sandstone and correlative units. Restoration of 315 to 320 km of San Andreas fault offset, La Honda basin paleogeography and western Carneros fan location are from Graham and others (1989). Northern Temblor shelf is based on Pence (1985). Nonmarine deposits of the Caliente area are from Dibblee and Warne (1988). Tejon embayment paleogeography is from Hirst (1988). The eastern limit of the Carneros is based on subsurface data from Elk Hills and North Coles Levee fields (Dunwoody, 1986).

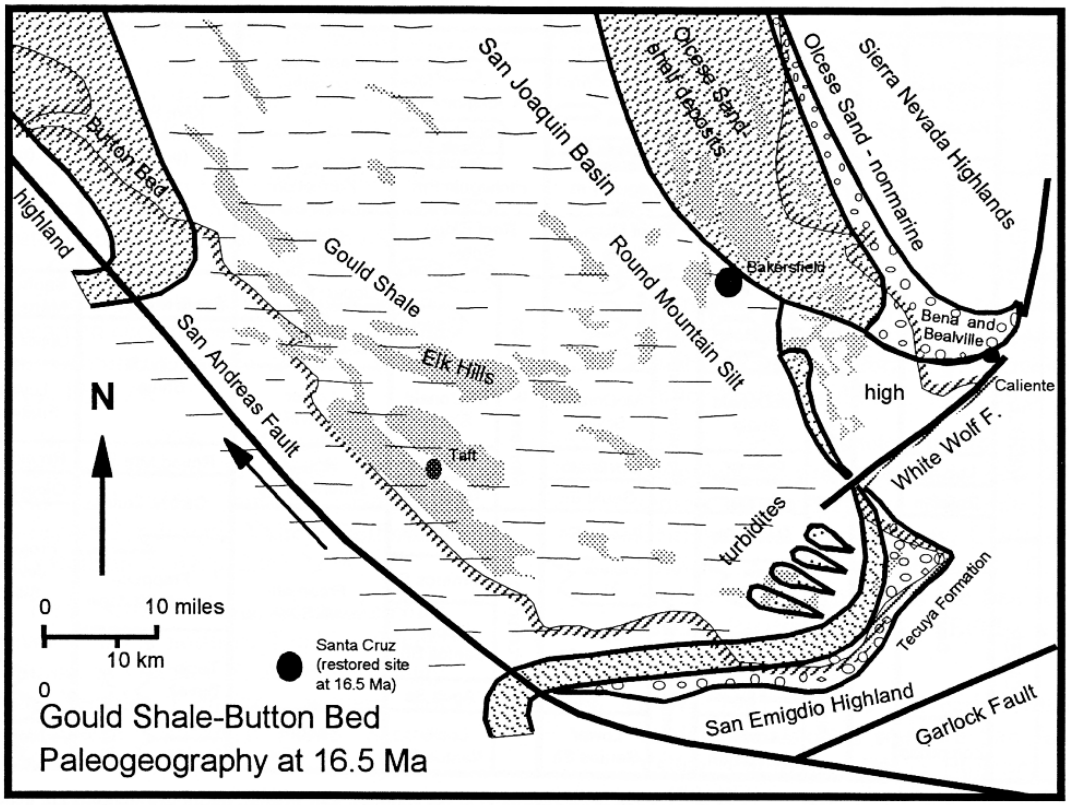

Figure 3. Paleogeography of the San Joaquin basin at 16.5 Ma, medial Miocene, showing the depositional environments represented by the Gould Shale and correlative units. See Figure 2 for explanation of symbols. Northern Temblor Button bed paleogeography is based on Carter (1985). Nonmarine deposits of the Caliente area are from Dibblee and Warne (1988). Tejon embayment paleogeography is from Hirst (1988).

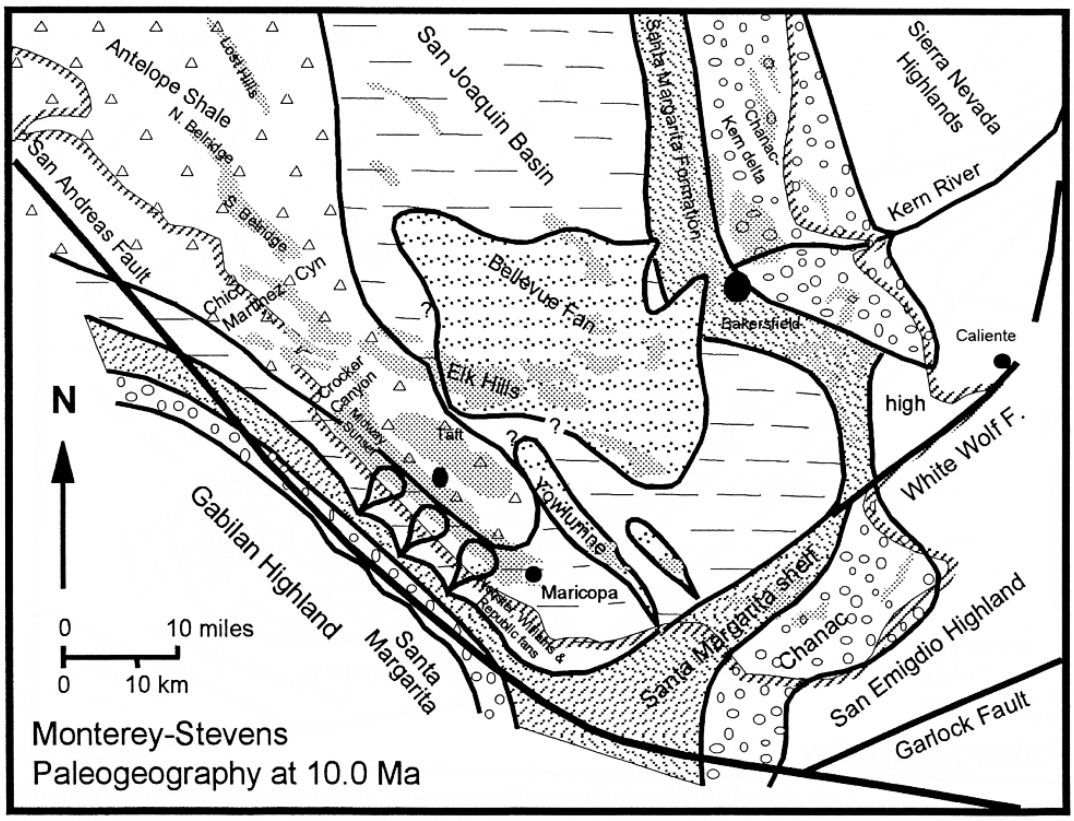

Figure 4. Paleogeography of the San Joaquin basin at 10 Ma, late Miocene, showing the location of Stevens sand turbidite complexes and correlative units. See Figure 2 for explanation of symbols. Location of the Gabilan highland is from Graham (1978). Distribution of western Santa margarita depositional environments is from Ryder and Thomson (1989). Subsurface distribution of eastern and western Stevens sand units are from MacPherson (1978), Webb (1981), and Quinn (1990). Subsurface occurrence of Antelope Shale is from Graham and Williams (1985).

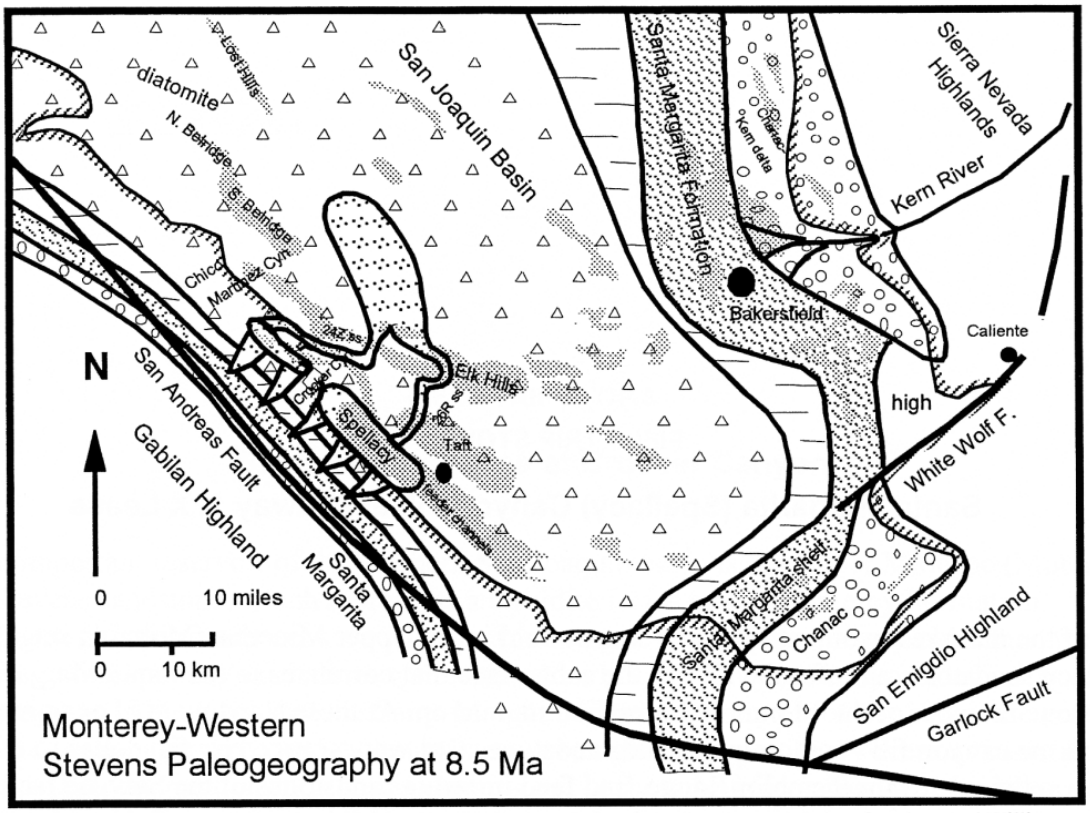

Figure 5. Paleogeography of the San Joaquin basin at 8.5 Ma, late Miocene (approximate N Point of Graham and Williams, 1985), showing location of western Stevens turbidite complexes and correlative units. See Figure 2 for explanation of symbols Location of the Gabilan highland is from Graham (1978). Distribution of western Santa Margarita depositional environments is from Ryder and Thomson (1989). Subsurface distribution of western Stevens sand units is from Webb (1981) and Reid (1990). Subsurface occurrence of diatomite and siliceous shale is from Graham and Williams (1985).

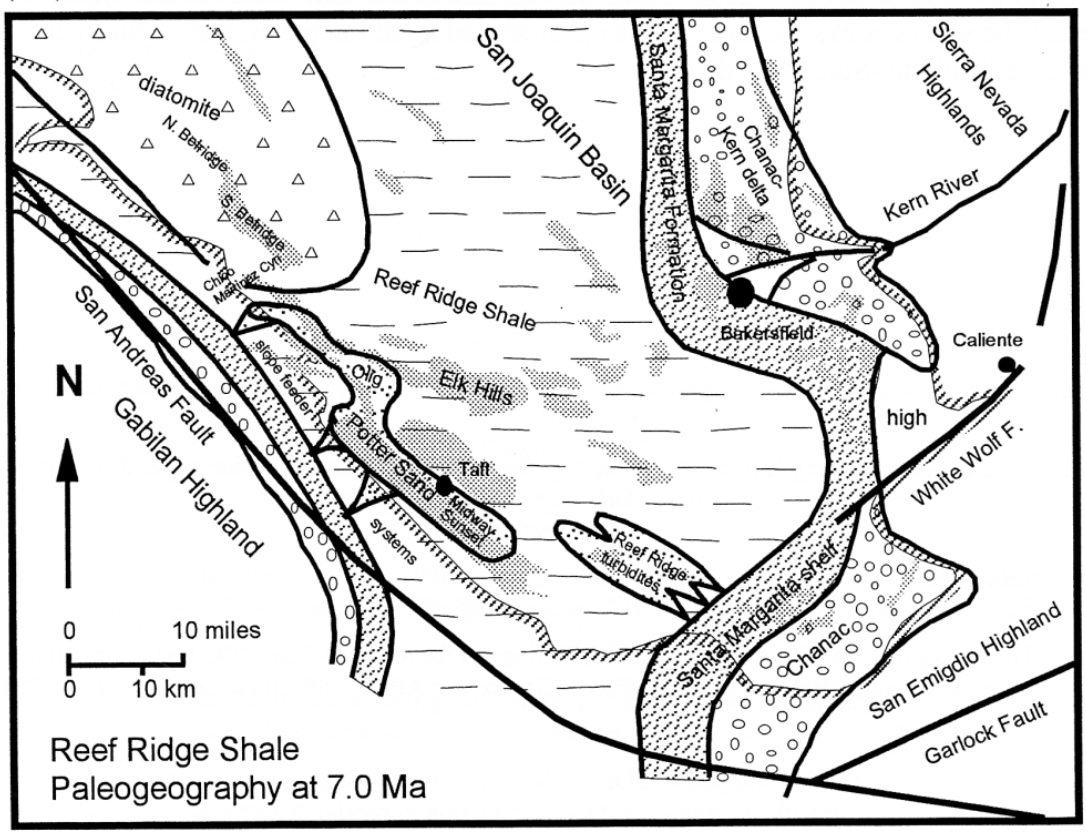

Figure 6. Paleogeography of the San Joaquin basin at 7 Ma, late Miocene, showing the depositional environments represented by the Reef Ridge Shale and correlative units. See Figure 2 for explanation of symbols. Location of the Gabilan highland is from Graham (1978). Distribution of western Santa Margarita depositional environments is from Ryder and Thomson (1989). Subsurface distribution of westerly-sourced turbidites is based on Schwartz (1988).

FIELD TRIP STOP 1

Stevens Sandstone at Midway 17X Lease

One of the main reservoirs at Midway-Sunset field is the Upper Miocene (Mohnian stage) Spellacy sandstone, and informal unit in the subsurface that correlates to the Santa Margarita sandstone member of the Monterey Formation in outcrop. We will examine at these stops submarine canyon fill conglomerates and sandstones that were sourced by fan deltas to the west of us, on the far side of the Temblor Range. These canyons then fed sediment, in turn, to turbidite sandstones of the Stevens facies of the Monterey that produce to the east of us in the subsurface of Midway-Sunset field.

Also evident at these stops are a diatomaceous facies of the Monterey, which in some localities is referred to as the Antelope Shale. Organic-rich siliceous shales and diatomites of the Monterey Formation represent the source rocks for most of the oil produced from the basin, and virtually all of the oil produced at midway-Sunset field.

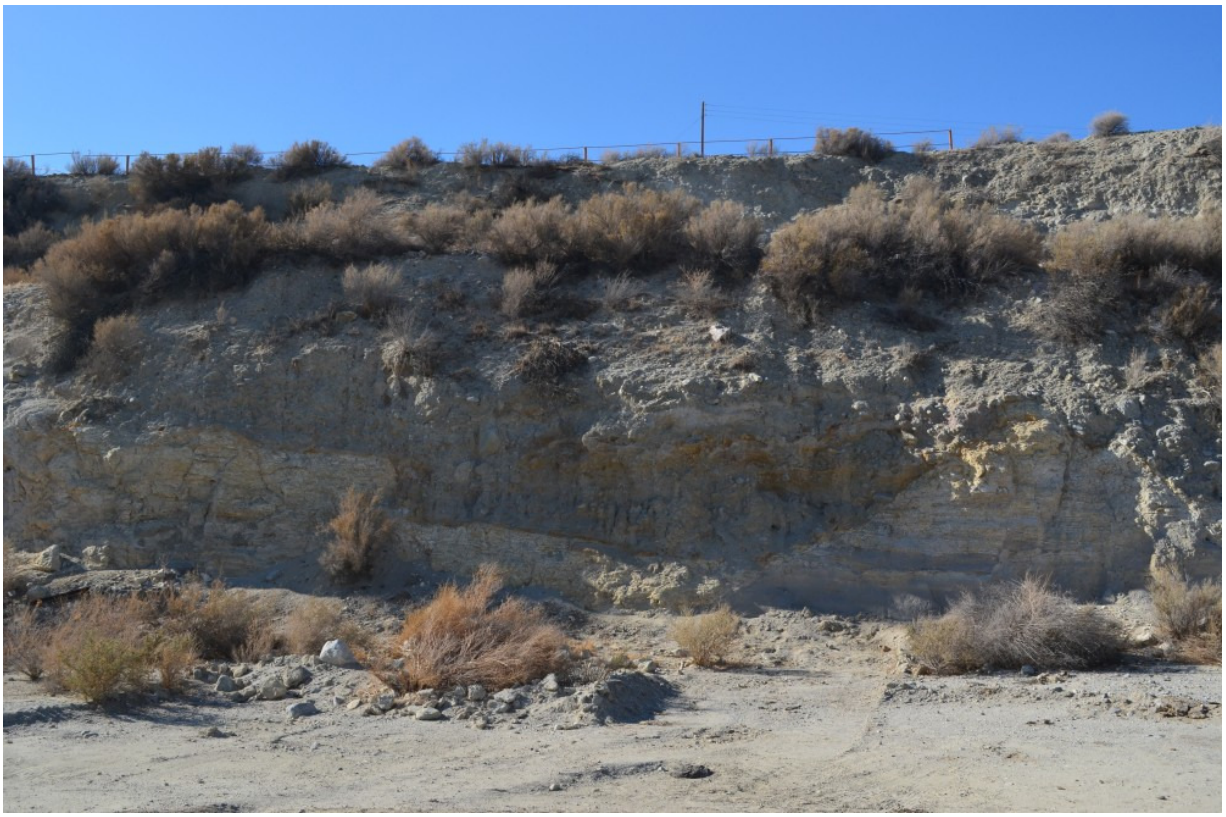

The accompanying article by the late Tor Nilsen has been modified from the original through the inclusion of Figures 1, 5 & 6 by the guidebook authors. The original did not include these figures. The unaltered article appears on pages 331-334 in the following publication by the Pacific Section—AAPG.

Nilsen, T. H., Wylie, A.S. and Gregory, G. J., 1996, Geology of the Midway-Sunset Oil Field and Adjacent Temblor Range, San Joaquin Basin, California: Pacific Section—AAPG, Fieldtrip Guidebook GB75, 428 p.

Santa Margarita Sandstone Member and Belridge Diatomite Member of the Monterey Formation at Midway 17X Lease

Tor Nilsen

Overview

A series of stops will be made here in the area of the Chevron Section 17X development (Figure 1), chiefly to observe (1) the infilling of a late Miocene submarine canyon in the lower part of the Santa Margarita Member of the Monterey Formation, (2) the unconformity between the Tulare Formation and the upper Miocene strata, and (3) the lower part of the Tulare Formation (Figures 2, 3 and 4). the abundant excavations of well pads in the 17X lease in the Midway area of Midway-Sunset field provide excellent exposures of numerous stratigraphic relationships and sedimentologic features. The stops will be made in ascending stratigraphic order, starting with the base of the submarine canyon complex. The wells in the development produce from some of the same units that are exposed in the area, providing a close correlation of outcrop to subsurface stratigraphic data.

An overview of the area can be obtained from a high top located about ½ km southwest of the development. From here, the overall configuration and deep incision of the basal part of the submarine canyon complex of the Santa Margarita Member can be observed. These conglomerates in the subsurface are known as the Spellacy sandstone, which produces low-gravity oil from the 17X wells (Figures 5 & 6). This is an outstanding example of being able to stand next to producing wells and being able to see in adjacent outcrops the same units that produce from the subsurface.

From the overview, note the generally low topography and continuous exposures of canton-margin, white-weathering diatomite in the drainages to the northwest and southeast of the ridge we are standing on. In the drainage to the northeast in the SE ¼ of Section 18-T32S-R23E, a large paleo-landslide block of rotated and deformed Belridge Diatomite Member is present along the northwestern flank of the canyon; this unit recognized in Figure 4 by the belt of northeast-trending strikes and variable dip directions in the Belridge Diatomite member, is mapped by Nilsen (1995, Plate I) as unit Tmb3.

Stratigraphy

The basal subunit of the submarine canyon complex here (NE/4 of Sec 19-T32S-R23E) consists of amalgamated resistant bends of medium- to coarse-grained sandstone characterized by massive to crude parallel stratification The overlying subunit consists of boulder conglomerate that has incised into the underlying sandstone subunit; abundant boulders of granitic rock from this subunit lie scattered across the landscape and crop out locally in small road cuts. More canyon-fill conglomerate subunits, separated by laterally discontinuous diatomite beds, are present southeast of the 17X development area.

Within the 17X development, the upper part of the exposed canyon-fill succession can be observed at several road pad cuts. At the 235-17X well, an erosive basal contact of boulder conglomerate truncation the Belridge diatomite is well exposed in the gently northeast-dipping succession (Figure 2). Note that the prominent modern soil, more than a meter thick, truncates both diatomite and conglomerate and underlies the modern topographic surface. This widespread calcareous and caliche-rich soil has been mistaken by some previous workers for the Tulare Formation. The coarser beds of conglomerate are present in the stratigraphically deepest parts of the incision., thus forming a fining-upward parasequence; along the margins of the conglomerate body, thin-beds of sandstone appear to form levee or overbank deposits. However, careful examination of these apparent beds suggests that many are actually intrusive sills probably derived from the canyon-fill. Five paleocurrent measurements taken from the pad cut from scour orientations, clast imbrications, and medium-scale cross bedding indicate sediment transport to the northeast.

At well pads 202-17X, 243-17X, and 254-17X, a remarkable exposure of the base of an incision can be observed (Figure 3). The Belridge Diatomite Member is intensely faulted, scoured, and locally undercut by conglomerate. Highly variable strikes and dips both within the fault blocks and of the faults that bound the blocks appear to record an apparent "plucking" of the diatomite, with a number of large blocks of diatomite included within the boulder and cobble conglomerate. The outcrop indicates the diatomite underwent synsedimentary faulting, disruption, and intrusion during cutting and filling of the canyon. Three paleocurrent measurements from cobble imbrications indicate sediment transport toward the northeast.

At well pad 223-17X, the canyon fill is well exposed in strike section and shows a well-defined organization into a series of fining-upward parasequences, with downcutting of at least 40 ft along the basal contact with the Belridge Diatomite

Member. The conglomerate dips about 20 degrees to the southwest and contains a variety of clasts, including granite, quartzite, sandstones, schistose rocks, apparent metavolcanic rocks, and rip-up clasts of diatomite. A number of half-round clasts of basement rocks indicate multiple cycles of transport and deposition of some clasts. paleocurrent measurements from cobble imbrications yielded sediment transport directions toward the north.

At well pads 231-17X, 242-17X and 267-17X, a more or less continuous section is exposed that extends from the Belridge Diatomite Member upward into canyon-fill conglomerate and sandstone of the Santa Margarita Member that is abruptly truncated by an angular unconformity and overlain by the basal deposits of the Tulare Formation. The Belridge Diatomite here is almost flat-lying, but flexed into a series of small anticlines and synclines that may have formed as a result of small-scale deformation near the crest of a large anticline (Figure 4). The diatomite contains thin lenses and intrusions (?) of coarse-grained sandstone. The overlying Santa Margarita Member consists of a stack of conglomerate and sandstone beds organized into fining-upward couplets with erosive and channelized bases. the channels are small and present throughout the outcrop, suggesting a braidform system of thalweg channels within the canyon. the channels appear to be shallow and to have a northwest-southeast orientation. Most of the conglomerate is composed of basement clasts, but locally siliceous shale-rip-up clast conglomerate is present. The pre-Tulare Formation above the unconformity appears to buttress against or onlap onto the Miocene conglomerate. the Tulare Formation consists mostly of debris flows with some interbeds of stream-transported gravel.

At well pads 344-17X and 200-17X, large pad cuts and road cuts provide excellent opportunities to examine the gently dipping lower part of the Tulare Formation. The unit here consists almost wholly of a stack of thin- to medium-bedded pebble conglomerate beds that are composed almost entirely of sub-angular to angular diatomite clasts and detritus. The beds appear to have been derived from the adjacent Temblor Range to the southwest and deposited by subaerial debris flows on a debris-flow-dominated alluvial fan.

References

Calloway, D.C., (1968), Cross section, Midway-Sunset to Buena Vista Hills in (Karp, S.E., ed.) Geology and iol fields, West Side Southern San Joaquin Valley, Pacific Section of AAPG, SEPM and SEG Field Trip Guidebook, p. 82.

Gregory, G.J. (1996), Geology of the Midway-Sunset Oil Field in (Nilsen, T.H., Wylie, A.S. and Gregory, G.J., eds.) Geology of Midway-Sunset Oil Field: AAPG Field Trip Guidebook, Pacific Section AAPG, Bakersfield, CA, p. 55-88.

Sturm, D.H. (1996), Spellacy Reservoir Sandstones, Midway-Sunset Field in (Nilsen, T.H., Wylie, A.S. and Gregory, G.J., eds.) Geology of the Midway-Sunset Oil Field: AAPG Field Trip Guidebook, Pacific Section AAPG, Bakersfield, CA, p. 155-174.

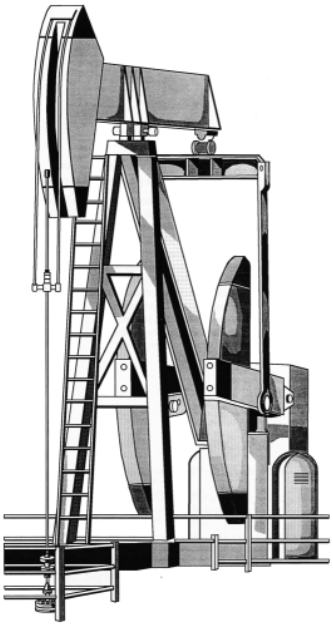

Figure 1: Aerial photograph of the Midway 17X Lease showing outcrop locations described in the text for Santa Margarita Sandstone and Belridge Diatomite outcrop locations.

Figure 2: Erosive contact at the base of a submarine canyon exposed at Field Trip Stop 1b. Gray-colored granitic conglomerate (Santa Margarita Member) that fills the canyon incises into and truncates white-colored Opal A facies diatomite (Belridge Member).

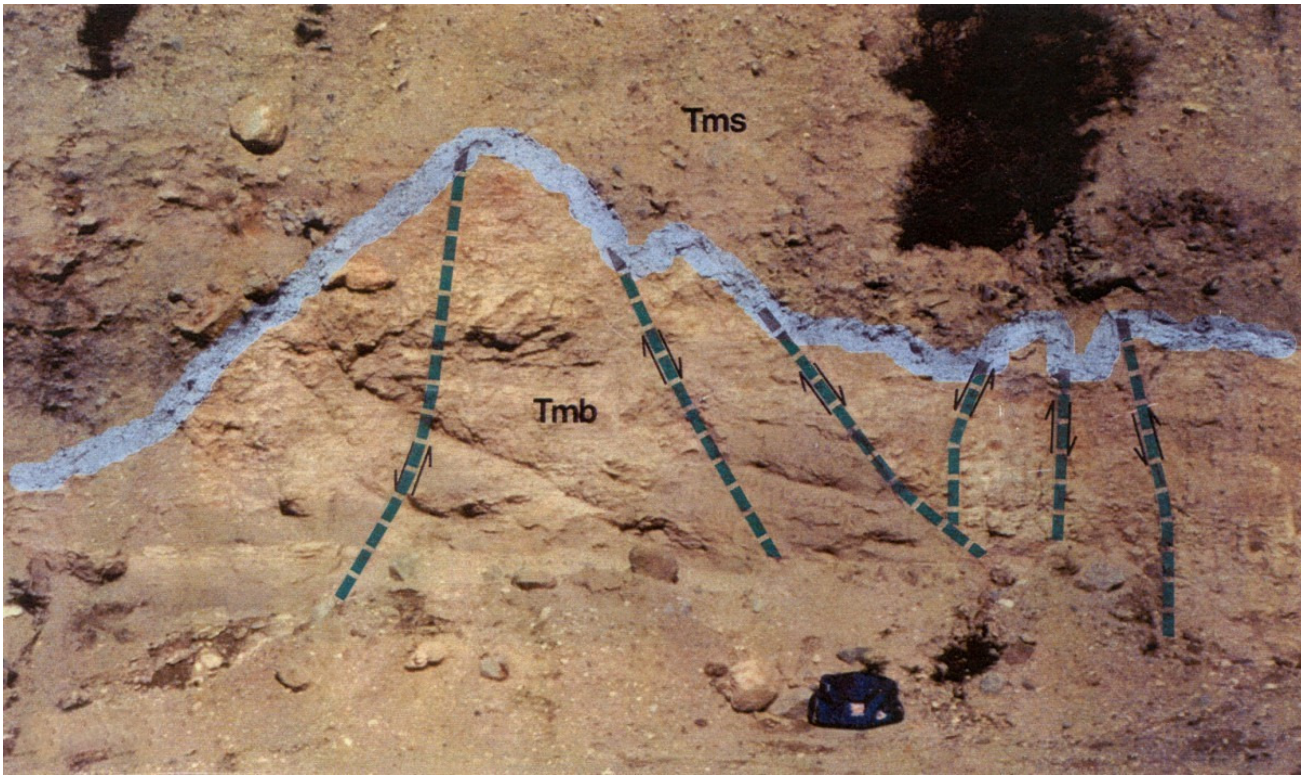

Figure 3: Erosive contact at base of the submarine canyon at Stop 1c overlies faulted diatomite.

Abbreviations: Tmb=Belridge Diatomite; Tms=Santa Margarita (Spellacy) Sandstone

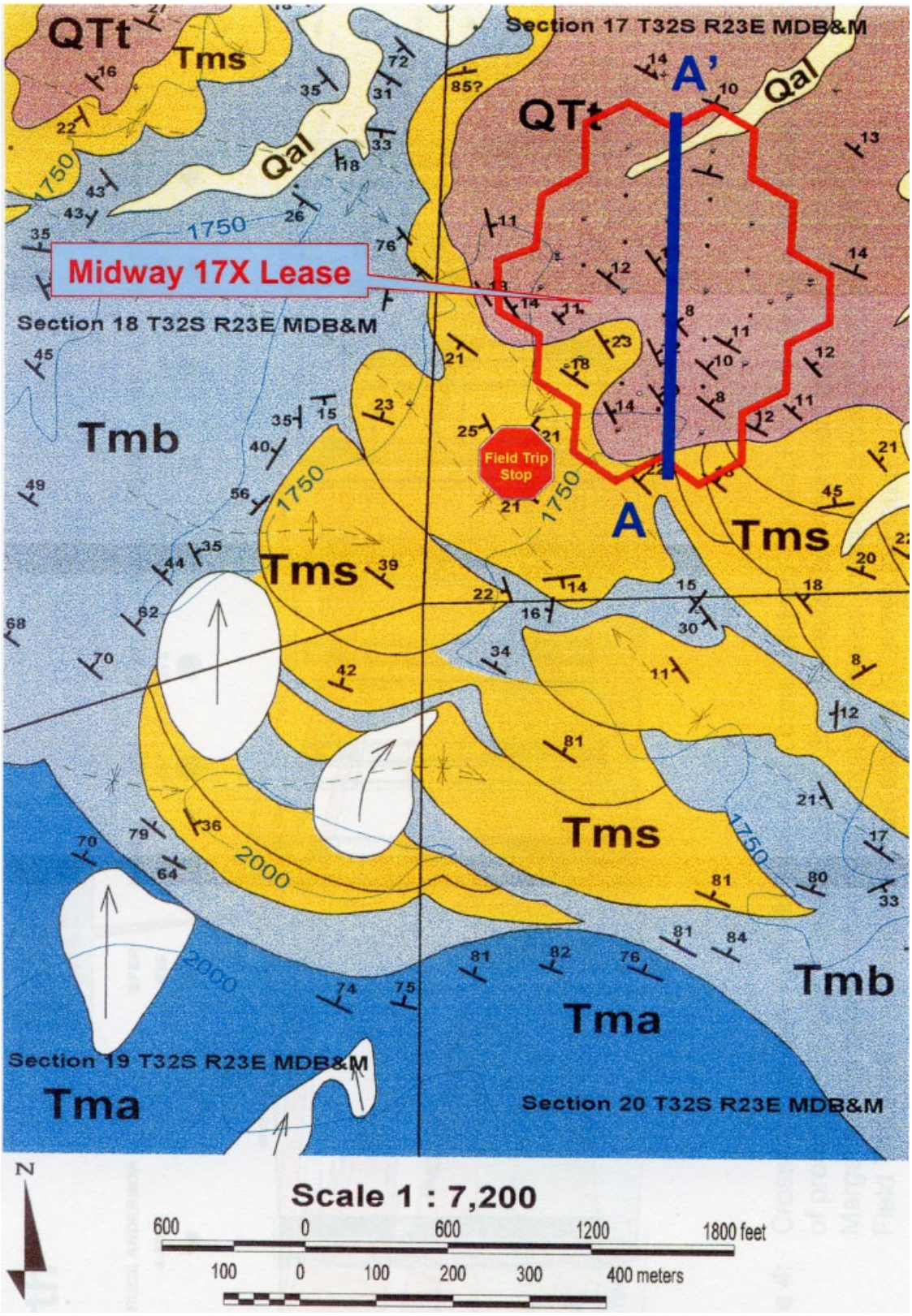

Figure 4: Geologic map showing location of the 17X lease Field Trip stops and location of cross-section A-A'.

Tms = Spellacy Sandstone; Tmb - Belridge Diatomite; Tma = Antelope Shale

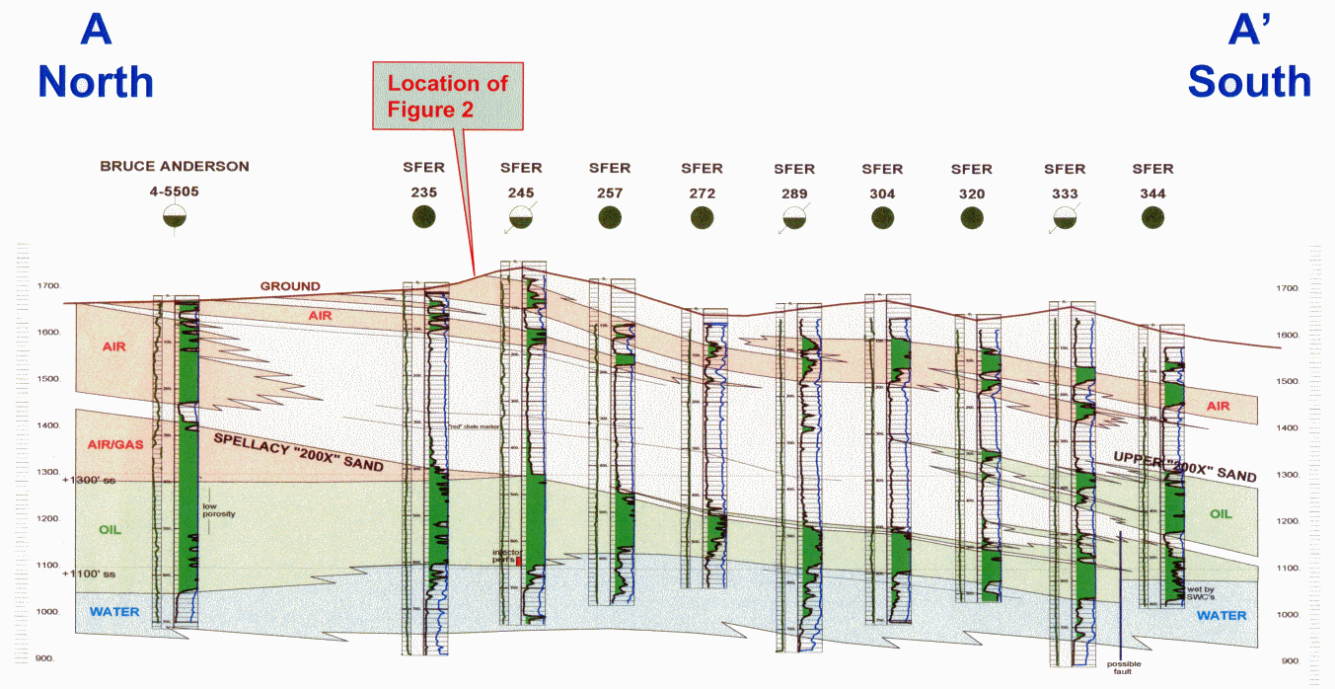

Figure 5: Cross-section A-A', which runs from N-S through the 17X Lease. Canyon-filling conglomerates of the Santa Margarita Sandstone (outcrop nomenclature) grade basinward (south) into productive Spellacy Sandstone conglomerates (subsurface nomenclature). Location of the cross-section is shown in Figure 4.

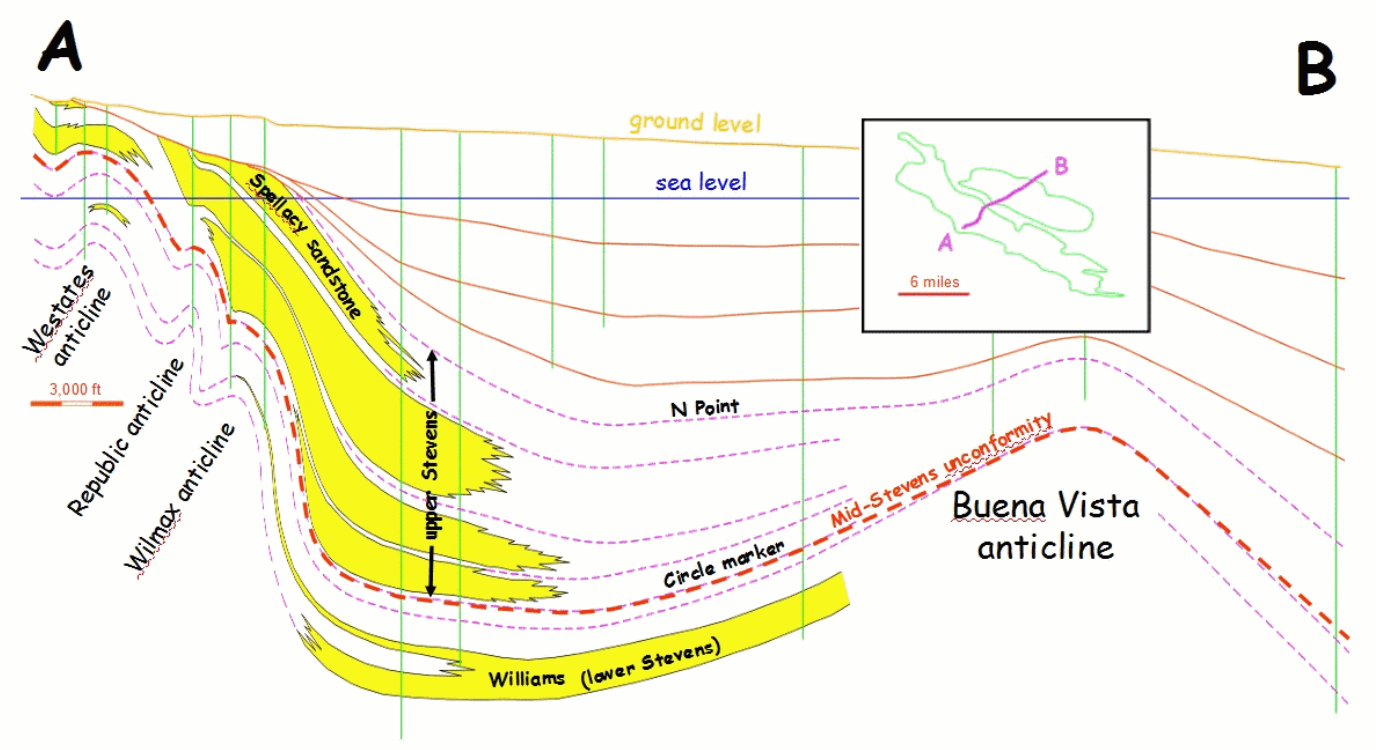

Figure 6: Cross-section showing basinward thickening from SW to NE of Stevens sandstone lobes. The Spellacy represents the uppermost lobe of this package and originates from Santa Margarita submarine canyons in the 17X Lease that are located on the left side of the section (modified from Calloway, 1968 by Sturm, 1996 and Gregory, 1996).

Come Join Us!

Tuesday Night Dinner Meetings
of the
San Joaquin Geological Society (SJGS)

''So Senteur! Planning on roaming the neighborhood
with some of your SJGS buddies tonight?"

(Apologies to Gary Larson of the Far Side)

FIELD TRIP STOP 2

Stevens Sandstone at Crocker Canyon

Another important subsurface reservoir of the southern San Joaquin basin is the Upper Miocene (Mohnian stage) Stevens sandstone, which is a turbidite facies of the Monterey Formation. The Crocker Canyon Sandstone that we will examine at this stop correlates to the Stevens Sandstone of the subsurface. Although the Crocker Canyon Sandstone is clearly older than the Santa Margarita/Spellacy sandstones exposed on the Midway 17X lease, it is analogous to the Spellacy turbidite lobes that the Santa Margarita canyons grade into in the down-basin direction.

Some geologists interpret the Stevens as basin floor submarine fans. However, the relationships at this outcrop and in the subsurface are more consistent with confined turbidite lobes that ponded along the axes of synclines oriented parallel to the faulted margin of the ancient basin. Here and there, Stevens channels during late Miocene time cut through the bounding anticlines, which enabled turbidite sands ponded along the axes synclines to remobilize, spill over into, and pond in the down-basin direction along the axes of adjacent synclines (see Figure 3).

The accompanying article by the late Tor Nilsen is modified from the original through the inclusion of Figures 3 & 4 by the guidebook authors. The original did not include these figures. The original, unaltered article appears on pages 391-395 in the following publication by the Pacific Section—AAPG.:

Nilsen, T. H., Wylie, A.S. and Gregory, G. J., 1996, Geology of the Midway-Sunset Oil Field and Adjacent Temblor Range, San Joaquin Basin, California: Pacific Section—AAPG, Fieldtrip Guidebook GB75, 428 p.

Crocker Canyon Sandstone Member and the Antelope Shale Member of the Monterey Formation

By Tor Nilsen

Excellent exposures of deep-marine sandstone of the Crocker Sandstone Member and siliceous shale of the Antelope Shale Member are present in the canyon, primarily along the south side, but also locally along the north side (Figure 1). These outcrops form the type section of the Crocker Sandstone Member as redefined in this guidebook by Nilsen (1995). The outcrop has been previously described in some detail by Kiser and others (1988) and McCullough and others (1990); the latter measured a section through the sandstone member and prepared a schematic line drawing of the uppermost beds of sandstone, reproduced herein as Figure 2. McCullough and others (1990) measured 313 m of strata, which they divided into six distinct lithofacies:

1. Diatomaceous laminated siltstone and shale, with interbedded chert and sand lenses, inferred to be Facies G of Mutti and Ricci Lucchi (1972), consisting of pelagic and hemipelagic fines.
2. Sandstone that is poorly sorted and contains abundant rip-up clasts of siliceous shale, inferred to be Facies F of Mutti and Ricci Lucchi (1972), consisting of submarine slump deposits.
3. Interbedded coarse-grained sandstone and silty shale. The sandstone beds are described as being laterally continuous, regularly bedded, and having sharp flat bases; they are inferred to be Facies C of Mutti and Ricci Lucchi (1972), deposits typical of nonchannelized sedimentation.
4. Sandstone that is massive, poorly graded and sorted, medium to coarse grained, as thick as 2 m, and with common scour marks and convoluted lamination along bedding surfaces; these beds are inferred to be Mutti and Ricci Lucchi (1972, 1975) Facies B2, typically deposited in channelized deep-sea settings.
5. Sandstone that is very coarse grained and very poorly sorted, contains abundant granitic pebbles, and is generally normally graded and amalgamated; it is inferred to be conglomeratic Facies A4 of Mutti and Ricci Lucchi (1972, 1975), typically deposited in submarine channels.
6. Pebbly sandstone that is very coarse grained, very poorly sorted, ungraded, and contains abundant small and large rip-up clasts of silty shale and slump features; it is inferred to be conglomeratic Facies A4 of Mutti and Ricci Lucchi (1972, 1975), typical of unstable submarine channel deposits.

These lithofacies are stacked in a generally coarsening-upward parasequence in which the coarser grained sandstones of lithofacies 4, 5 and 6 are most abundant at the top of the sandstone body. The entire sequence was interpreted by Kiser and others (1988) and McCullough and others (1990) to be in inner-fan channel complex in a sandy submarine fan system, with the distal fan deposits located in the subsurface to the east, where they form prominent reservoirs. McCullough and others (1990) infer the diatomaceous pelagic and hemipelagic units of lithofacies 1 below the sandstone body to consist of overbank and slope deposits, and the interbedded sandstone and mudstone deposits of lithofacies 3 to have been deposited as channel-margin or crevasse-splay deposits, possibly from adjacent channel systems.

The regional mapping of the Crocker Sandstone Member by Nilsen (1995) provides additional information and a different basis for a paleoenvironmental interpretation of the succession at this outcrop. Interpretation of the succession as an inner-fan channel system by Kiser and others (1988), Ryder and Thomson (1989), and McCullough and others (1990) is also somewhat inconsistent with published examples of modern and ancient inner-fan systems. Firstly, the succession exposed coarsens upward and is abruptly terminated at its top by overlying pelagic and hemipelagic siliceous shales; classic inner-fan channels fine and thin upward, leaving a record of gradual abandonment and overlying finer grained and thinner bedded levee/channel margin deposits. Secondly, the succession contains no easily documented channeling or incision that should mark both the base of the channel and the walls of either the main channel or of the thalweg channel; although there is abundant evidence of scour and amalgamation, as well as incorporation of blocks of silceous shale within the sandstone body, no clear incisions deeper than the thickness of a single bed can be observed, and no coarse-grained channel lag is present at the base of the putative channel system. Thirdly, the measured

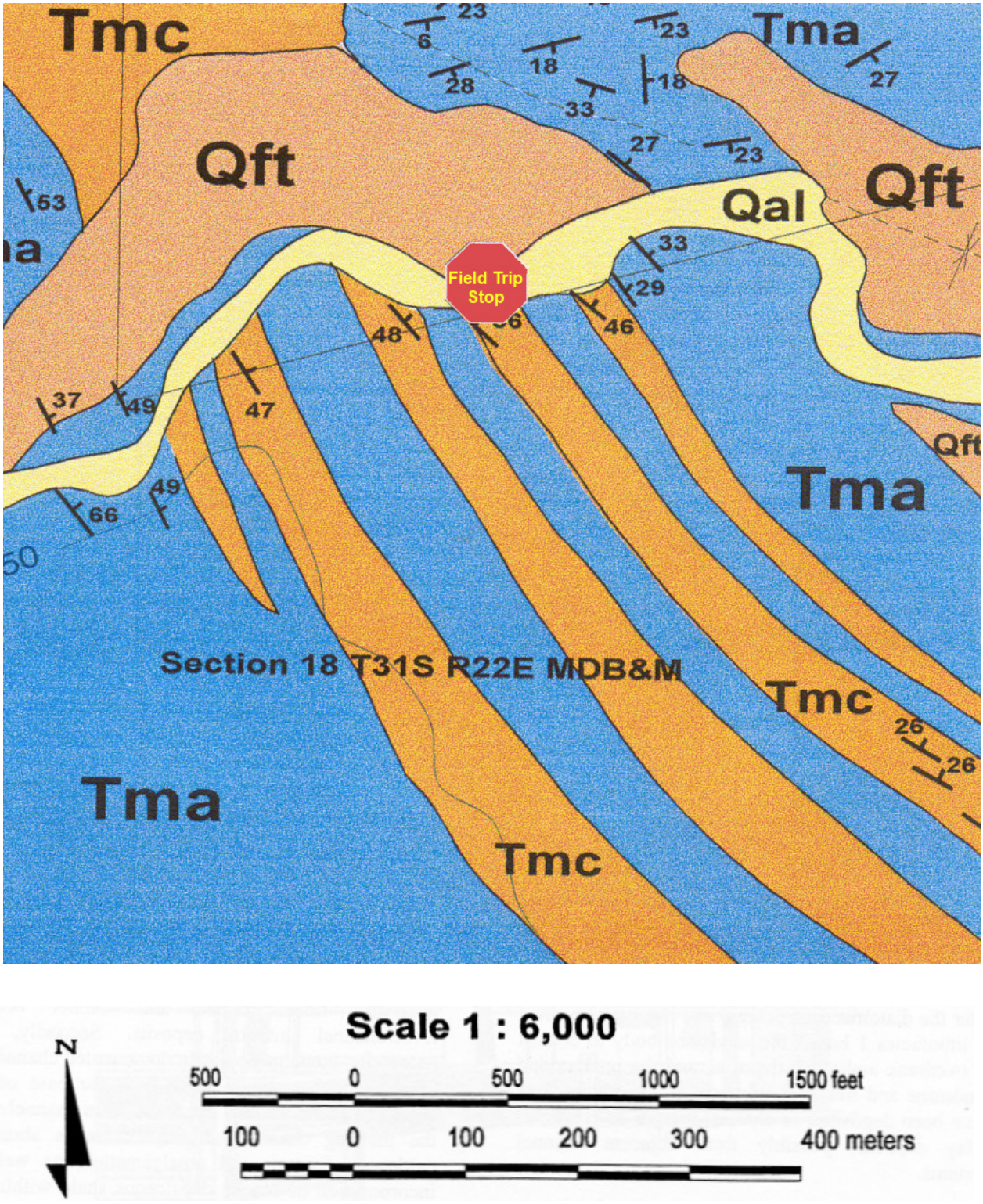

Figure 1: Geologic map showing location of the Crocker Canyon stop (from Nilsen, 1995).

Tmc = Crocker Canyon Sandstone; Tma = Antelope Shale

section of McCullough and others (1990) clearly shows a succession of sandstone beds or bodies separated by thick intervals of siliceous shale of lithofacies 1; rather than a simple channel complex, the succession appears to consist of at least four separate sandstone bodies, the bases of which are at 87 m above the base of the section for the lowest, 127 m for the second 220 m for the third, and 270 m for the fourth and uppermost body (Figure 2).

Nilsen's (1995) regional mapping clearly shows that four distinctive sandstone bodies make up the Crocker Sandstone Member in the area of sections 18 and 19 (Figure 1, Pl. 1 in Nilsen et al., 1996); these bodies have been mapped for a distance of more than a mile northward to the Crocker Canyon exposures. A fifth and lowest sandstone body crops out in the canyon and appears to thicken northward of the canyon, where the mapping indicates the presence of multiple sandstone bodies wrapping around the Crocker Canyon syncline and related folds. The Crocker Sandstone Member pinches out in the central part of sec. 8, T.31S., R.22E. to the northeast of the type section, thus defining a lens-shaped cross-sectional area about 3-4 mi wide when unfolded, a geometry similar to that of the partly correlative Williams and Republic Sandstone Members to the southeast, which also lie within the Antelope Shale Member of the Monterey Formation.

The Crocker Sandstone member in outcrop appears to consist of an entire sand-rich submarine fan system, deposited during at least five distinctive pulses separated by hemipelagic shale intervals. The succession coarsens upward because the entire Crocker submarine fan has prograded into the Midway basin, with each successive pulse or parasequence representing a more proximal and thus coarser-grained and thicker-bedded part of the fan. The pulses are probably controlled by the mixed effect of tectonic uplift/subsidence and regional sea-level fluctuations, with the latter probably having a more profound effect. The lack of channeling at the base of the succession indicates that the deposits do not fill an erosive channel. Instead, the entire fan system appears to infill a tectonically generated synclinal axis within the Antelope Shale Member, with the successive sandstone bodies onlapping against the synclinal basin walls, rather than erosively cutting down into them (see Nilsen et al., 1996, for further discussion of the proposed depositional model). The onlap can be observed at several places within the outcropping section, but requires standing back from the outcrop and viewing it from a distance; different dips for the infilling sandstone bodies and the underlying folded siliceous shales are readily apparent.

References

Kiser, S.C., Bowersox, J. R., and Miller, E. E., 1988, Upper Miocene turbidite deposition, Crocker Canyon area, section 18, T. 31S, R 22E, southwest San Joaquin Valley, California *in* (Randall, J. W., and Countryman, R. L., eds.) Selected Papers: San Joaquin Geological Society, v. 7, p. 22-31.

Lowe D.R. (1982), Sediment gravity flows: II. Depositional models with special reference to the deposits of high-density turbidity currents, Journal of Sedimentology, v. 52, p. 279-297.

McCullough, P.T., Horton, R. A., and Reid, S. A., 1990, Relationships of upper Miocene turbidites and diatomaceous shales, Crocker Canyon area, Kern County, California *in* (Kuespert, J. G. and Reid, S. A. eds.) Structure, Stratigraphy and Hydrocarbon Occurrences of the San Joaquin Basin, California: Pacific Section—SEPM and Pacific Section—AAPG, Fieldtrip Guidebook GB65, p. 313-318.

Mutti, E. and Ricci-Lucchi, F., 1975, Turbidite facies and facies associations *in* Examples of Turbidite Facies and Facies Associations from Selected Formations of the Northern Apennines: 9th International Congress of Sedimentology, Nice, France, fieldtrip Guidebook A11, p. 21-36.

Mutti, E., and Ricci-Lucchi, F., 1972, Le trobiditi dell' Apennino Setentrionale: Introduzione all'analisi di facies: Memorie della Societa Geologica Italiana, v. 11, p. 21-36 (translated by T. H. Nilsen, 1978 in International Geological Review, v 20, p. 125-166).

Nilsen, T. H., 1995, Geologic map of post-lower Miocene strata, central Temblor Range, California: Unpublished map prepared for Santa Fe Energy Resources, scale 1:10,000.

Nilsen, T. H., Wylie, A.S. and Gregory, G. J., 1996, Geology of the Midway-Sunset Oil Field and Adjacent Temblor Range, San Joaquin Basin, California: Pacific Section—AAPG, Fieldtrip Guidebook GB75, 428 p.

Reid, S.A. (1990) Trapping characteristics of Upper Miocene turbidite deposits, ELk Hills Field, Kern County, California in (Kuespert, J.G. and Reid, S.A., eds.) Structure, stratigraphy and hydrocarbon occurrences of the San Joaquin Basin, California, Pacific Section SEPM Guidebook #64 and Pacific Section AAPG Guidebook #G865, p. 141-156.

Ryder, R. T. and Thomson, A., 1989, Tectonically controlled fan delta and submarine fan sedimentation of late Miocene age, southern Temblor Range, California: United States Geological Survey, Professional Paper 1442, 59 p.

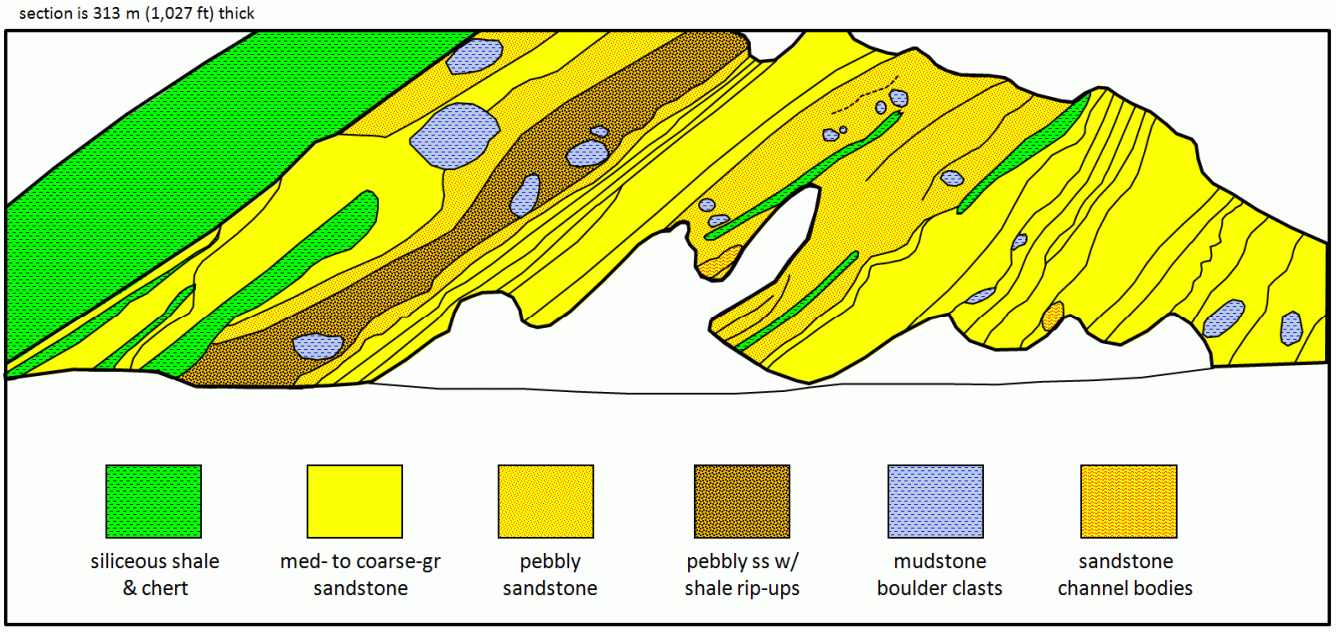

Figure 2: Schematic outcrop drawing of Crocker Sandstone Member of Monterey Formation exposed at Crocker Canyon (modified from McCullough et al., 1990).

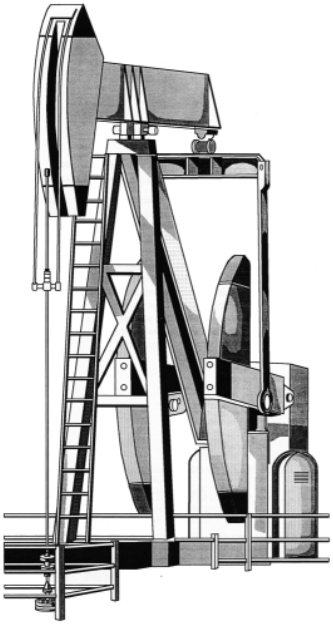

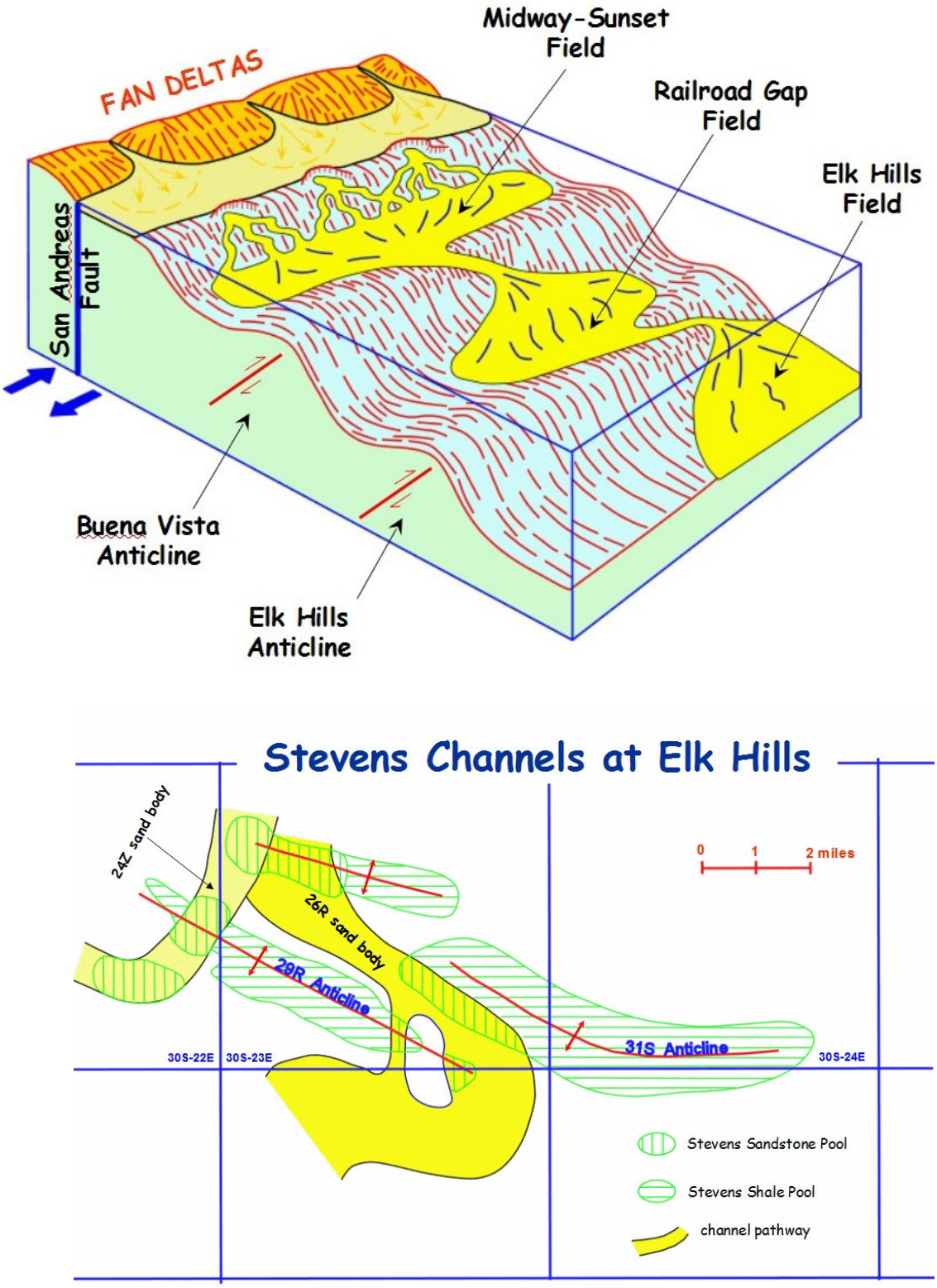

Figure 3: Upper diagram (Ryder & Thomson, 1989) shows deposition of Stevens sandstones as confined fans that pond along synclines (e.g., the Crocker Canyon Sandstone at Midway-Sunset). Channels that cut across the bounding anticlines are able to deliver sand to adjacent synclines (e.g., Railroad Gap and Elk Hills fields). Some of these channel sandstones at Elk Hills field, as shown in the Lower diagram (Reid, 1990), are confined between anticlines (e.g., the 26 R Sand), whereas others cut across them (e.g., the 24Z Sand).

FIELD TRIP STOP 3

Potter Sandstone Mass Transport Complex at North Midway

One of the important reservoirs in the northern part of Midway-Sunset field is the Uppermost Miocene (Delmontian stage) Potter sandstone, an informal unit of the Reef Ridge Formation. We will examine at this stop a Potter mass transport complex that contains massive blocks of diatomite that presumably were scoured from the walls of a submarine canyon complex landward of us, and carried basinward by submarine slumps and slides. These canyons ultimately fed sediment to Potter turbidite sandstones that produce oil in the subsurface of North Midway.

The massive blocks of diatomite evident in at this stop are a diatomaceous facies of the Reef Ridge Formation, and probably correlate, at least in part, to opal A facies diatomites that produce several miles to the north at the giant South Belridge and Lost Hills fields. There is also diatomite production from analogous facies here at North Midway and nearby at McKittrick field. Although organic-rich siliceous shales and diatomites of the Reef Ridge have been suggested as potential source rocks for some of the oil produced here, fingerprinting of the oils and likely source beds indicates that the oil was probably generated from older Mohnian-age shales in the lower part of the Antelope Formation, which is a unit more or less synonymous with the Monterey Formation.

Potter Sandstone at North Midway-Sunset Field

Mike Ponek

Field History

The North Midway field is located southeast of the town of McKittrick, an oil field boomtown that developed with growth of westside oil fields. The north end of the field is approximately 1-1/2 miles southeast of the McKittrick Field and is a northern extension of the giant Midway Sunset Field.

The first test of the prospective area was drilled in May 1901 in the southeast quarter of section 34, T31S/R22E. This test hole was abandoned at 1060' with TD in the Tulare Formation. The next test well #92 was drilled in July, 1920 by the Associated Oil Company to a depth of 1794 feet. Well #92 penetrated the top of the Potter sand and was commercially productive. The locations for these early wells were staked on the basis of surface geology. During the 1920's only the southern portion of the North Midway Field was exploited.

The northern portion of the field, located in section 34, was later developed by Tidewater Oil Company during the mid-1940s. Tidewater's initial well #65 was drilled to a depth of 2880 feet, penetrating the Potter oil sand in what is now the main productive trend at North Midway Field. The Potter sands in this area are steeply dipping to overturned. This same Potter trend is being developed today in sections 27 and 28.

The Potter sands are usually encountered between 800 to 1600 feet deep and produce 20 to 60 barrels of oil per day, per well. Initially, the wells are cyclic steamed. Subsequent steam injection has aided in the recovery of the heavy oil from the Potter sands. The Tulare Formation is also productive in the North Midway Field, usually to a depth of 1000 feet, and produces 10 to 15 barrels of oil per day, per well. The Tulare wells are cyclic steamed.

Geologic History

Structural growth and uplift in the North Midway area resulted in many overlapping depositional relationships. The Potter sand member of the Reef Ridge Formation was deposited in Latest Delmontian time along the margin of a constricting and shallowing marine basin. The mode of deposition for the Potter sands is still under dispute. However, at North Midway, submarine canyons appear to have provided pathways for the lower siliciclastic units, resulting in a series of interfingering conglomeratic sands interbedded with diatomaceous siltstones.

Displacement of the granitic highlands northwest along the San Andreas Fault and the structural development and uplift in the Temblor during Early Pliocene time resulted in a shallowing marine basin. This setting provided the site for deposition of the Etchegoin Formation. Severe structural deformation has uplifted and overturned the Pliocene and Miocene section. The Pleistocene Tulare Formation predominantly onlaps all older deposits. These structural complexities are evident in the outcrops and log data at North Midway Field in sections 27 and 28.

Stratigraphy

The Potter reservoir at North Midway consists of five sand units as shown on the type log (Figure 1). Core from the lower IV and V sands are poorly sorted and usually conglomeratic, containing granitic cobbles, rounded chert and quartzite pebbles. This character is evident in outcrop. The upper I – III sand units of the Potter are moderately to well sorted and medium to coarse grained. Unfortunately the I - III sands do not outcrop at North Midway. At the North Midway field stops we will explore the various Potter and diatomaceous shale outcrops.

References

Calloway, D.C. (1962) - Distribution of Upper Miocene sands and their relation to production in the North Midway Area, Midway-Sunset Field, California, San Joaquin Geological Society Selected Papers, v. 1, p. 47-55.

DOGGR (1998), "Midway-Sunset Oil Field" in California Oil & Gas Fields: Volume 1 - Central California, Calif. Div. of Gas & Geothermal Resources (DOGGR), v. 1, p. 277-278.

Gardiner, R.L., Wylie, A.S. and Gagner, M.J. (1996) The Potter Sandstone, Midway-Sunset Field, Kern County, California in (Nilsen, T.H., Wylie, A.S. and Gregory, G.J., eds.) Geology of the Midway-Sunset Oil Field, Pacific Section AAPG Field Trip Guidebook, p. 175-191.

Woodward, W.T. (1943), North Midway area of the Midway-Sunset Oil Field, Calif. Div. of Mines Bull. 118, p. 519.

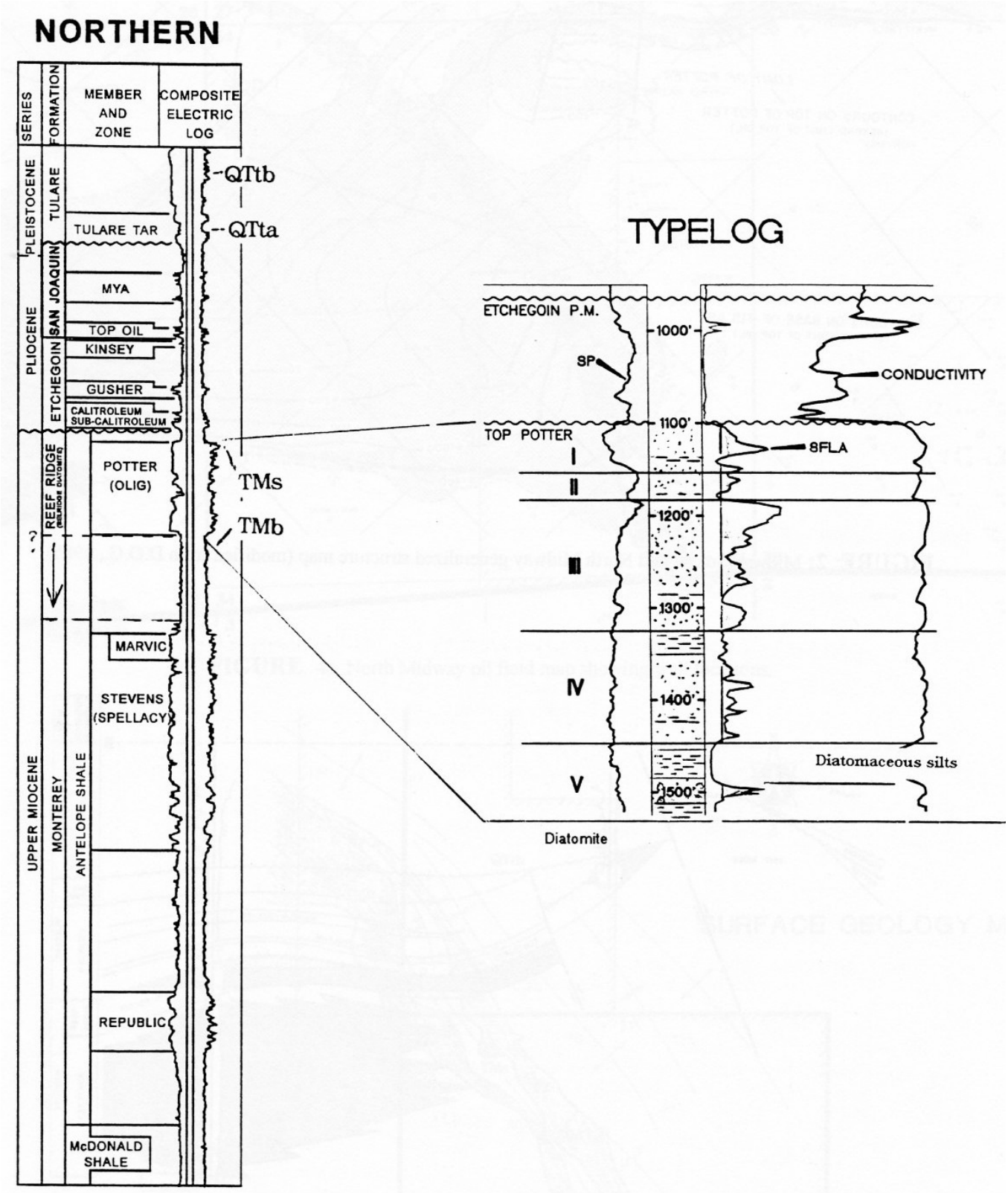

FIGURE 1: North Midway stratigraphic column and type log (from DOGGR, 1992).

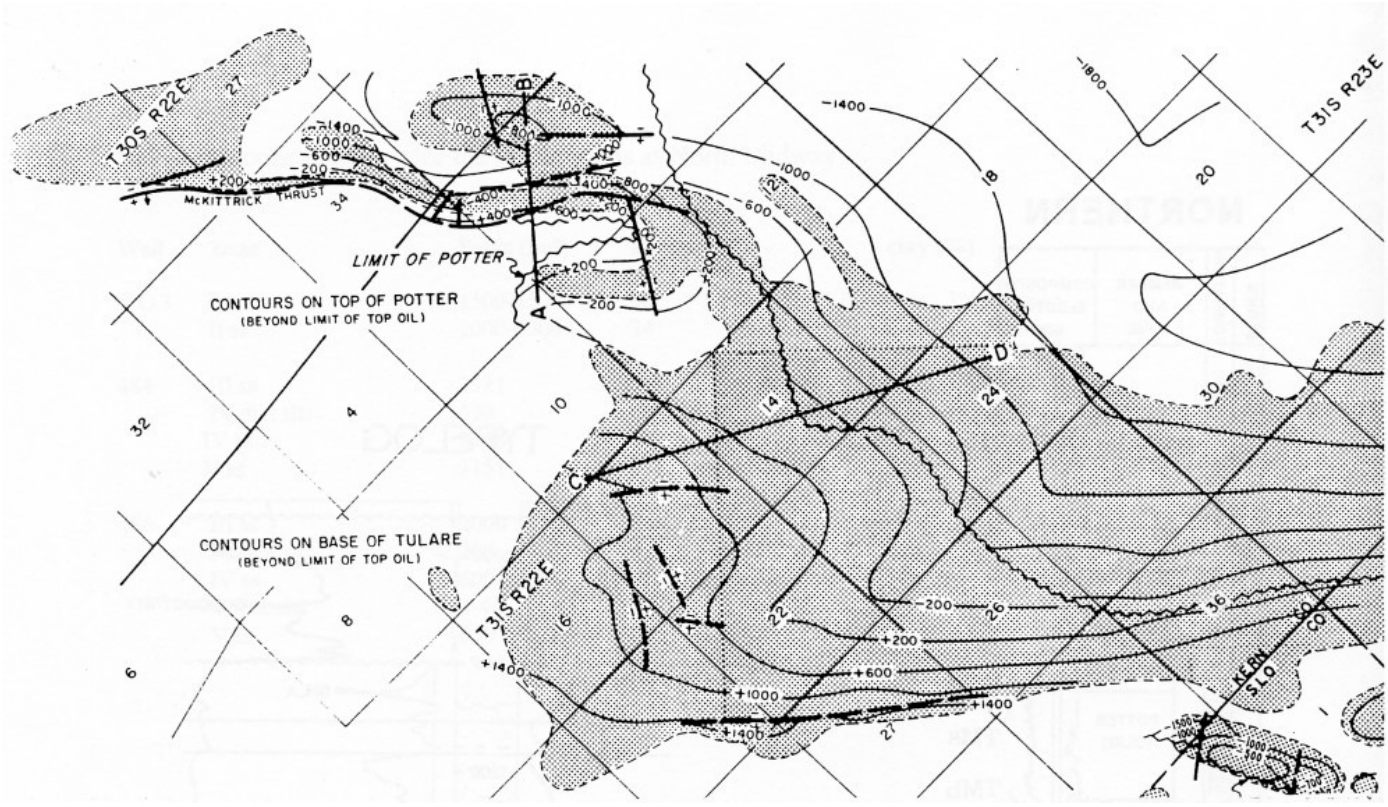

FIGURE 2: Midway-Sunset and North Midway structure map (from DOGGR, 1992).

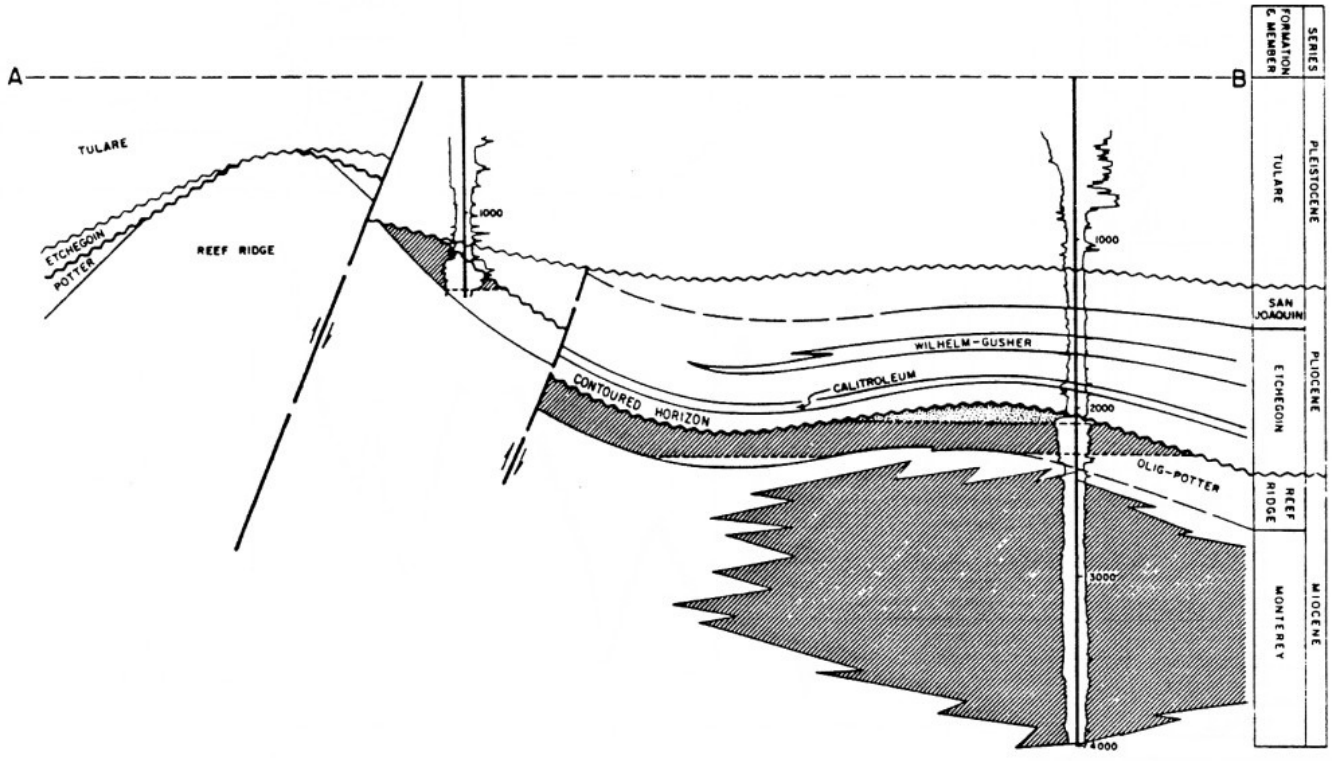

FIGURE 3: Midway-Sunset and North Midway cross-sections (from DOGGR, 1992).

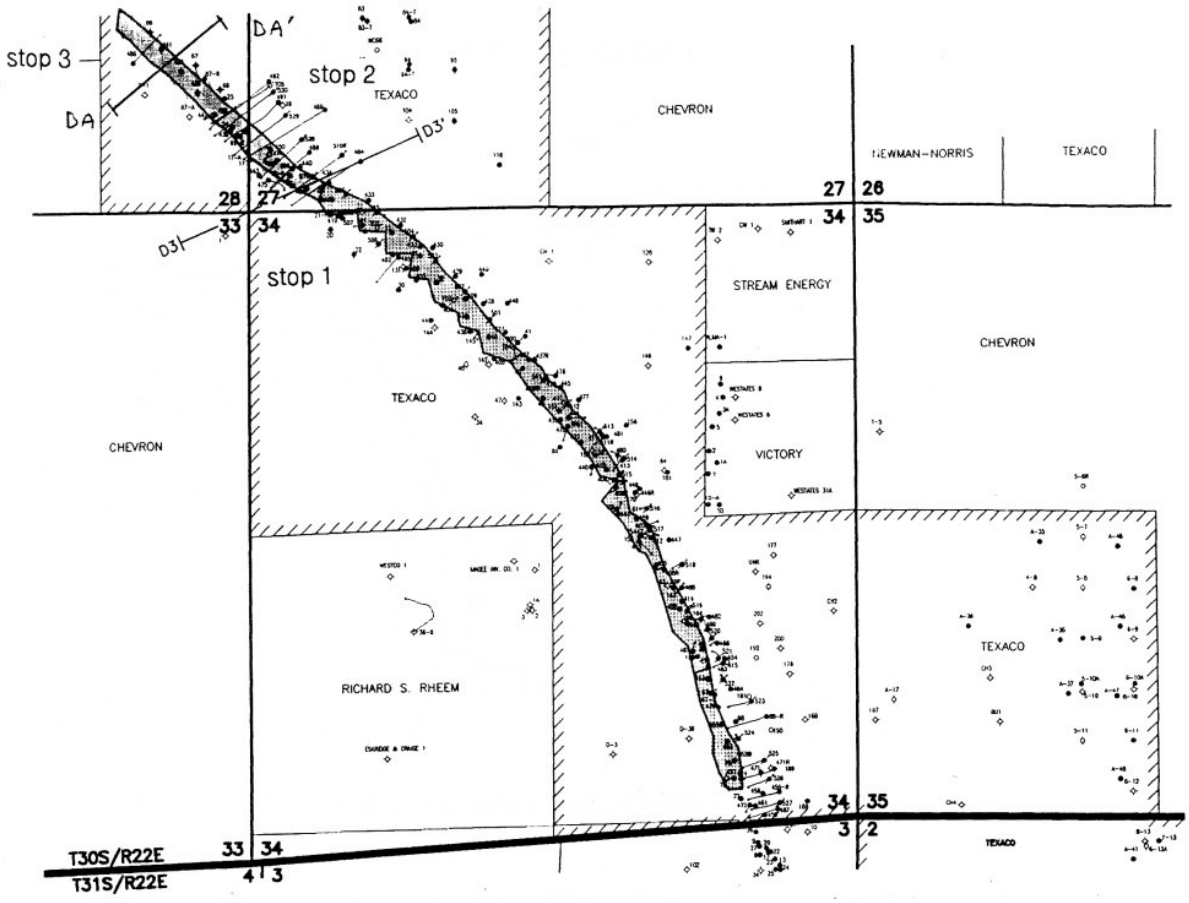

FIGURE 4: North Midway oil field map showing well locations.

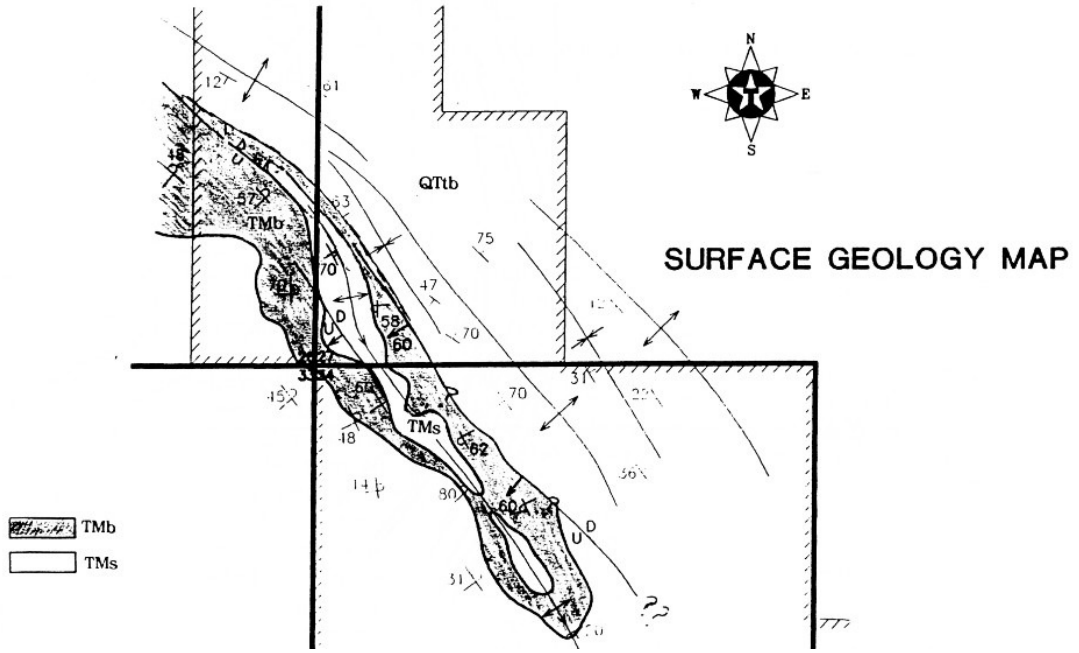

FIGURE 5: Surface geology of the northern portion of North Midway oil field.

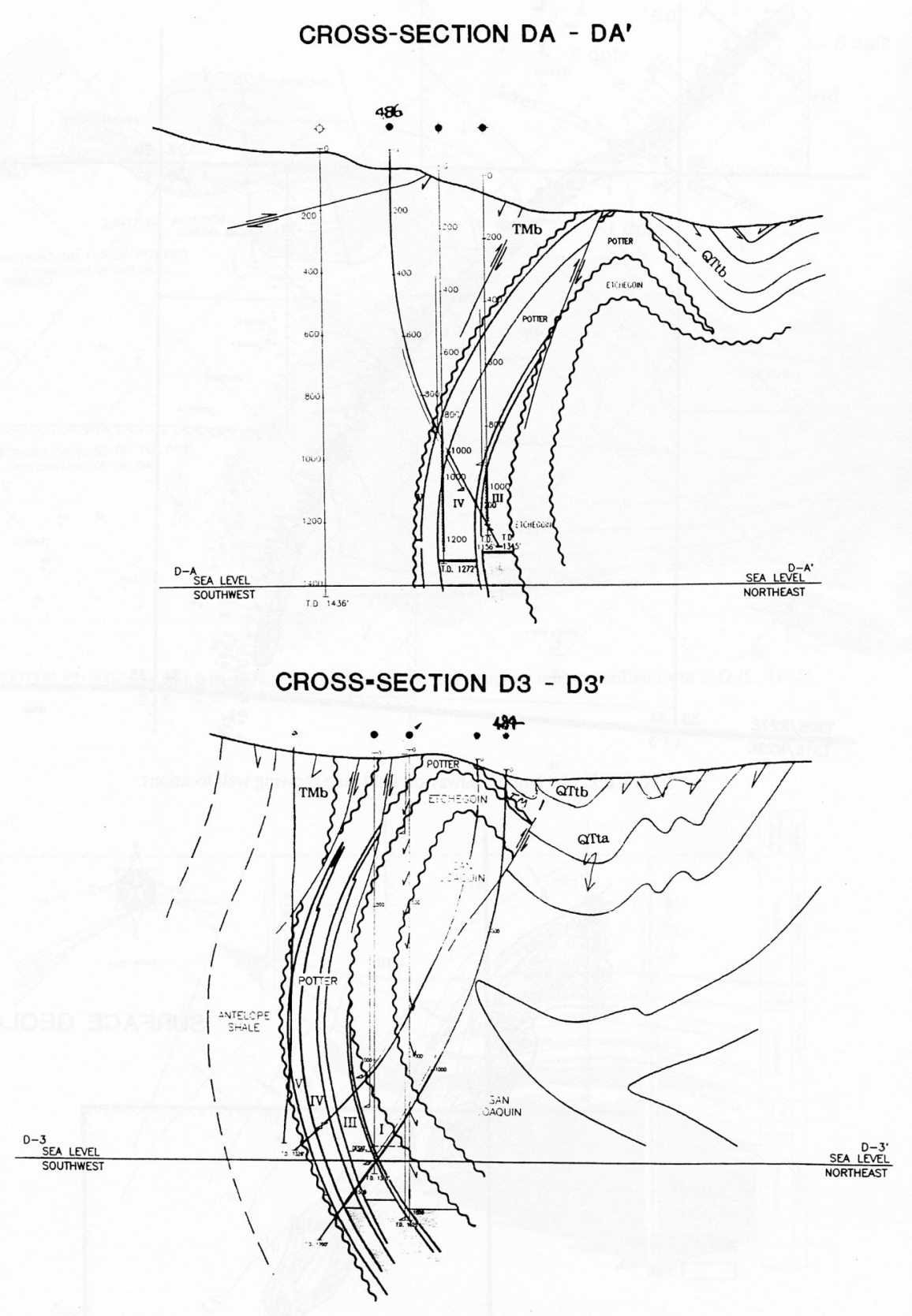

FIGURES 6 and 7: Cross-sections through northern portion of North Midway oil field.

FIELD TRIP STOP 4

The McKittrick Tar Pits

Located just off Highway 58, and not far from the town of McKittrick, there is an active, bubbling tar seep. This seep has literally been known for hundreds of years. Spanish explorers observed Indians in the area collecting tar from seeps such as this. Later, when this particular seep was located just off an old wagon road, pioneer settlers collected the tar to grease wagon wheels, and some even collected the tar to distill into kerosene for use as a lamp oil replacement. Most of the McKittrick seeps are gone now, having dried up as oil wells have tapped and drained the near-surface oil accumulations. But this one remains.

The McKittrick tar pits have also yielded a rich Pleistocene fauna of ice age mammals, many of which are on display today at the Page Museum, next to the La Brea tar pits in Los Angeles.

History of the Tar Pits and Tar Mines of McKittrick and Asphalto

Michael S. Clark

Spanish explorers traveling through California in the 1700s observed Indians using asphalt for many purposes. In particular, Yokuts Indians of the southern San Joaquin Valley collected asphaltum from natural seeps near the Yokuts village of Wogitu on the west side of the valley. This asphalt was molded into fist-sized tar balls used for trading, waterproofing, and as an adhesive. Decorating was accomplished by inlaying bits of abalone shell into tar stuck on pottery, knives, masks, and clothes.

When Pahmit, a member of the Dumna Yokuts tribe, was about 105 years old, he remembered watching San Joaquin Valley pioneers collect tar from the same seeps he and his family once mined. These pioneers used the tar primarily for waterproofing roofs and to grease wagon wheels.

Inevitably, the Wogitu tar seeps attracted the attention of entrepreneurs who sought to capitalize on this unusual resource. The most successful were John Hambleton and Judge Lovejoy who in 1864 dug shallow pits, 8 to 10 feet deep, near active seeps in what became known as the Asphalto area (Figure 1). They built a small still and refined the tar they collected into lamp kerosene which was shipped by wagon to their agents in Stockton.

Working the asphalt pits was difficult and dangerous. Valley temperatures often hovered around 120° F, reaching as high as 140° F in the pits. Consequently, work was limited to twenty-minute shifts, lest the workers become debilitated by the heat or overcome by noxious fumes rising from the seeps.

By 1891, several 5-foot by 6-foot foot shafts, many lined with railroad ties for stability, were sunk up to one-hundred feet deep into the McKittrick tar seeps. Because the miners working these shafts quickly became covered with asphalt, they usually worked naked. At days end, they cleaned themselves with case knives or wooden scrapers made for race horses, then washed with distillate. Because it was impractical to clean up at noon, they ate lunch ‘au naturale’ sitting on newspapers at the camp mess.

Rather than dig pits, some prospectors, many former Mother Lode miners, dug tunnels in search of the “black gold” of the San Joaquin (Figure 2). These mines were located just outside of McKittrick, a pioneer town that sprang up near the tar pits.

The mines, some up to 300 feet in length, yielded a high-quality asphalt, as much as 90-percent pure, that was better quality than asphalt produced on the island of Trinidad, then the world’s main supplier for this resource. Generally, McKittrick asphalt was used to pave streets and sidewalks in San Francisco or to grease log skids in the timber country. This commodity was valuable enough to command $30 a ton in the days when a nickel bought a decent meal.

Gradually, the tar mines were replaced by wells that drilled for the same oil which sourced the tar seeps (Figure 3). A new chapter in the story of the tar mines began in 1896 when the Shamrock gusher blew in at McKittrick field flowing 1,300 barrels of oil per day. Additional discoveries gave rise to nearby Midway-Sunset field, which today is one of the giant oil fields of the United States. Ultimately, the McKittrick and Midway-Sunset areas are expected to produce 3 billion barrels of oil over the lives of the fields.

Further Reading

Latta, F., 1949, Black gold of the Joaquin: Caxton Press.

Rintoul, W., 1976, Spudding In: Recollections of pioneer days in the California oil fields: California Historical Society.

Rintoul, W., 1990, Drilling through time: California Department of Conservation, Division of Oil and Gas, Sacramento, California.

More information on the McKittrick Tar Pits is available at the SJV Geology Web Site at http://www.sjgs.com/mckittrick.html

Figure 1: Prospectors mined asphalt near McKittrick by digging open pits like the one above.

Figure 2: Later tar prospectors in the 1880s and 1890s dug tunnels to mine asphalt in the area of North Midway. This was the so-called "black gold" of the San Joaquin. Much of this tar was used to pave roads in San Francisco prior to the Great 1906 Earthquake.

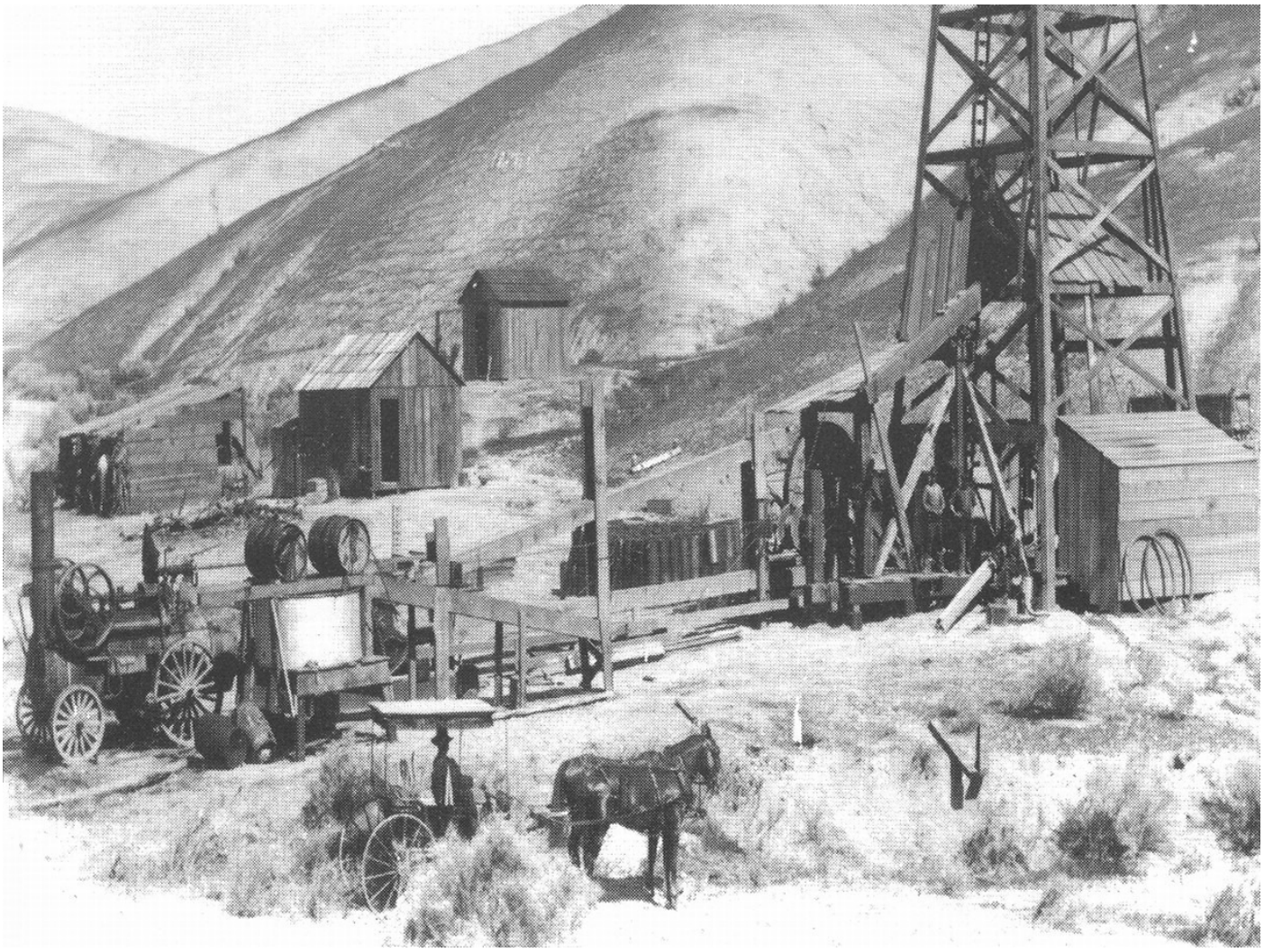

Figure 3: Turn of the century oil operations near the town of McKittrick on the westside of the San Joaquin Valley. Although some of the early wells in this area were drilled next to tar seeps, operators soon learned that the seep oils tended to be thick. smelly, and low-quality. Thus, they tried using geology to figure out where to drill down dip so that they could tap into where the seep oils originated from deep within the subsurface. Drilling deeper was more expensive, but paid off, as these oil pioneers were rewarded with lighter, sweeter-smelling crudes that brought better economic rewards.

FIELD TRIP STOP 5

Carneros Turbidites at Carneros Creek

The Lower Miocene (Saucesian stage) Carneros sandstone is a clastic facies of the Temblor Formation, a unit that contains deeper reservoir sandstones of the Phacoides, Agua and Oceanic sandstones of well. However, the Carneros is made up of turbidite sandstones that many interpret as deep-marine, basin floor submarine fans. By contrast, the Phacoides, Agua and Oceanic are shallow marine. Carneros deposition also coincides with the nearby onset of northward migration of the Mendocino triple junction during start up of offset along the San Andreas Fault. Thus, the Carneros was deposited during a tectonically active period associated with basin deepening.

The Carneros, which produces from a handful of fields on the west side of the basin, has gained notoriety from two important events in the recent history of the basin. The first is the spectacular 1998 blowout and well fire of the Belleview well no. 1 at Lost Hills field to the north of us from an over-pressured, tight gas reservoir inferred to be the Carneros (see Figure 7). The second is the discovery of the Gunslinger field to the south of us, a significant oil and gas accumulation in the Carneros that represents the largest new discovery in the basin in the last forty years.

The accompanying article by Jack Carter has been modified from the original through the inclusion of Figures 3-7 by the guidebook authors. The original did not include these figures. The unaltered article appears on pages 182-186 in the following publication by the Pacific Section—AAPG.

Graham, Steve. A., ed. (1985) Geology of the Temblor Formation, Western San Joaquin Basin, California, Pacific Section of the Society of Economic Paleontologists and Mineralogists, Los Angeles, Calif., Volume and Guidebook 44. 202 p.

Carneros Sandstone in Carneros Creek

Jack Carter and Michael S. Clark

The type section of the Carneros Sandstone is a well-exposed sequence of massive, amalgamated sandstones exposed at Carneros Creek on private property of the Twisselman Ranch (Figures 1, 2 & 3). Individual beds range in thickness from at least 1.5 m to 5 cm and define a crude upward thinning sequence between about 7 m above the base and the top of the section.

A few of the thicker beds near the base contain boulder-size clasts of dolomite (Figure 4). Presumably these clasts were incised from channel walls updip and rolled, slid or bounced downslope during large sediment gravity flows. They may be early-formed diagenetic dolomites exhumed from the subjacent Santos Shales. Visible amalgamation surfaces are generally sharp and marked by basal scour, flame structures, or textural contrasts. Bedding is often undulatory or convoluted, particularly near the base of the section in the thicker beds. This probably reflects tangential shear imposed by the passage of high-density flows and/or post-depositional slumping of water-charged sediment. Lamination and rare cross-stratification are locally developed.

Though difficult to identify in this outcrop, dish structures, pipes, and other fluid escape structures are present (Figure 5). Large slump structures are evident, and thin-shale interbeds are largely absent. The virtual absence of low-density turbidites (Bouma Td and Te divisions) between amalgamated beds indicates that this outcrop is made up largely of mud flows, high-density turbidites and some hybrid event beds (Figure 6). Alternatively the absence of low-density turbidites can be attributed to erosion and removal of those units by subsequent flows, and/or residual low-density turbidity currents bypassing this system to be deposited laterally in overbank settings, or transported basinward.

A thin interval of thin-bedded sandstones and shale is exposed about 3 m above the base. The thinner sandstone beds are wavy and discontinuous, have sharp bases and tops, and contain abundant clay rip-ups. A few of the thicker beds have poorly developed flute casts trending approximately S 30° E (dip corrected). This bedding style is rare in Carneros outcrops and may represent overbank deposits, and/or a temporary decrease in the grain size and volume of the sediment gravity flows.

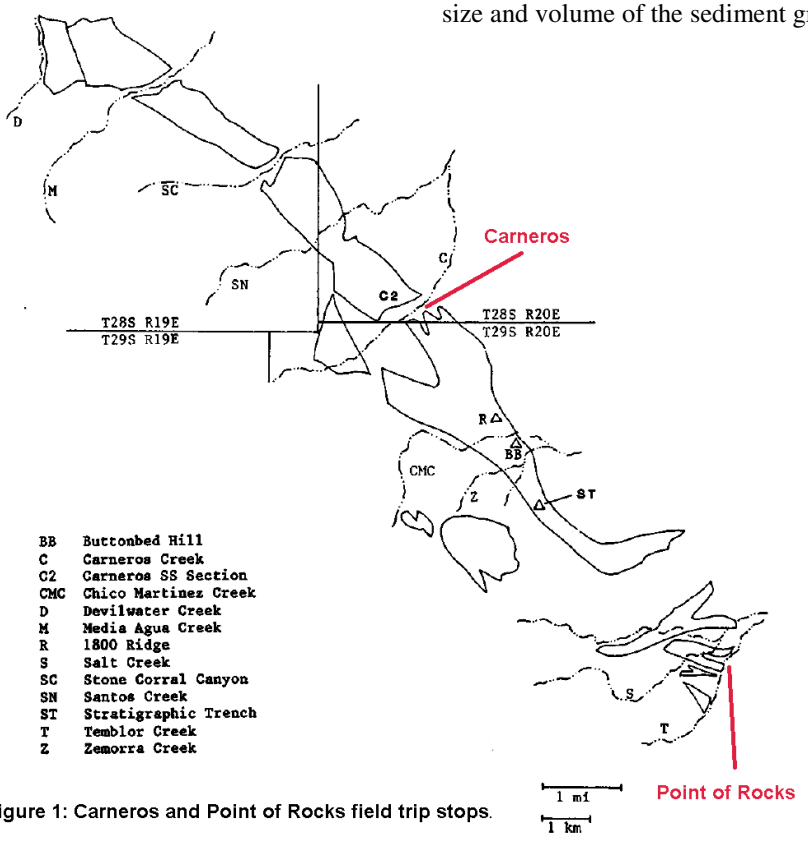

Figure 1: Carneros and Point of Rocks field trip stops.

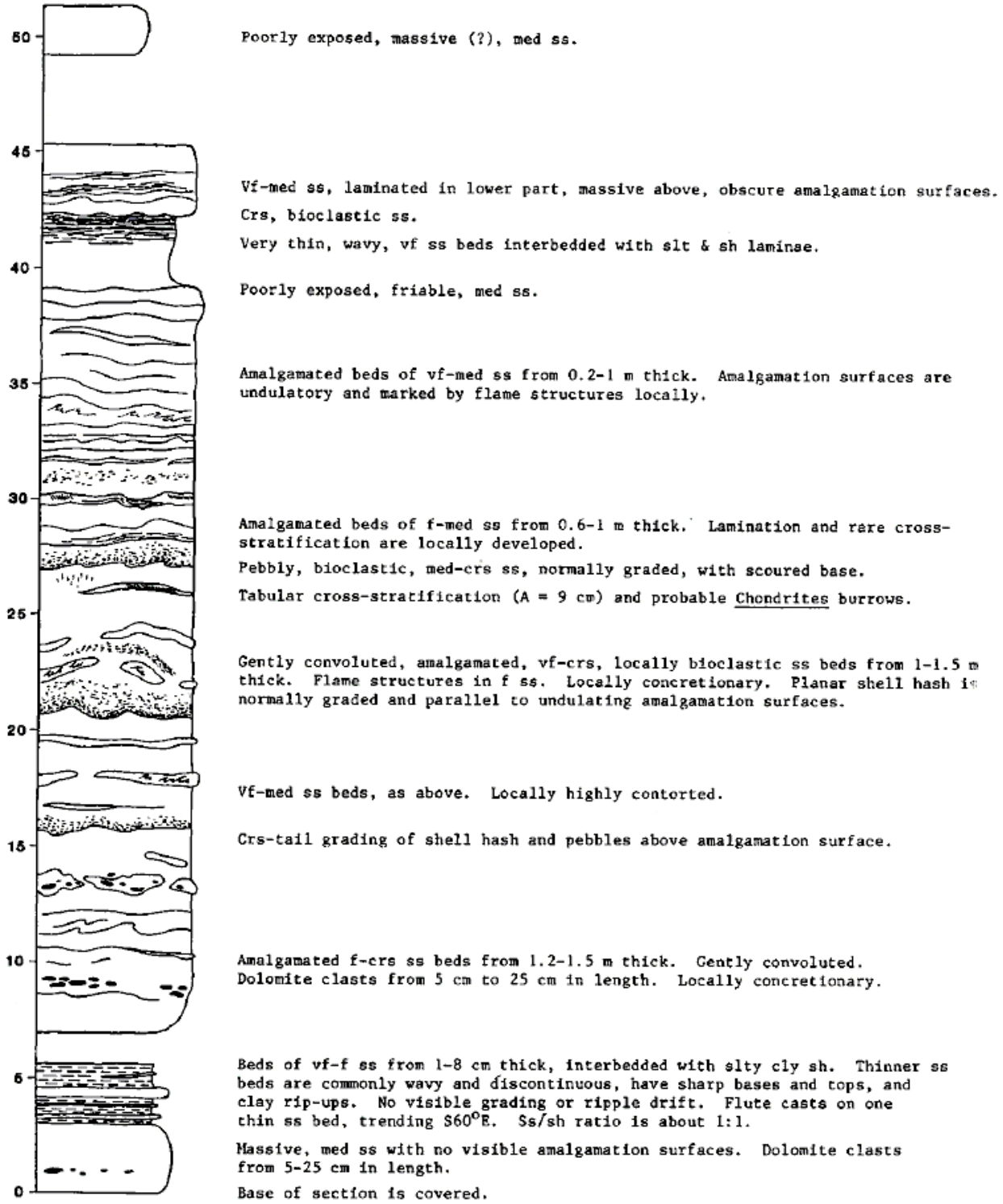

Figure 2: Measured section of the Carneros Sandstone in Carneros Creek. Locality is 800 ft east, 900 feet north of southeast corner, section 32-T28S-R20E. Scale is in meters.

Figure 3: The left photo shows cross-stratification (i.e., traction lamination) in the Carneros. The right photo shows a shale flame structure that indicates shear from an overlying bed.

Figure 4: Large dolomite clast in a sandstone block incorporated into a mass transport deposit.

Figure 5: Dish structures exposed at the top of a turbidite bed.

Figure 6: A linked debrite (hybrid event bed), with a light-colored turbidite (grain-supported) base and a darker debrite (mud-supported) top. Note the dewatering structure just above the turbidite-debrite transition at the red arrow.

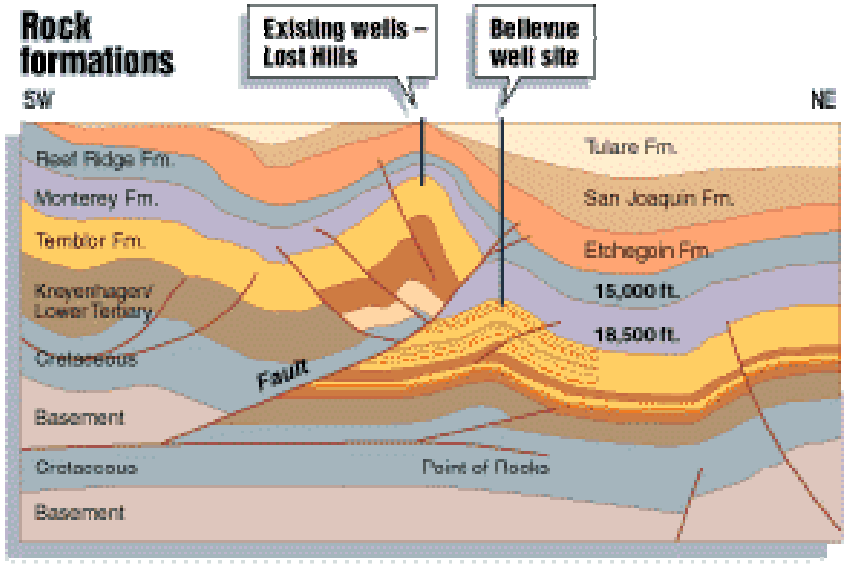

Figure 7: The Bellevue No. 1 well blew out and caught fire on November 23, 1998 at a 17,657 ft MD in what is believed to be the Carneros sandstone in the subthrust of Lost Hills field.

FIELD TRIP STOP 6

Point of Rocks Turbidites at Salt Creek

The Point of Rocks is an informal name for Eocene turbidite sandstones that represent a clastic facies of the diatomaceous Kreyenhagen Shale, which, like the Monterey, is an important source rock for the basin. Production from the Point of Rocks was first discovered in the 1930s, and has been the recent focus of several 14,000-ft to 15,000-ft deep wells drilled in the area of Cymric and McKittrick fields. The exposures we ill be examining at Salt Creek on private property of the Twisselman Ranch are some of the better Point of Rocks outcrops on the west side of the San Joaquin basin, and represent a very low-permeability reservoir that produces primarily from natural fractures. Although the outcrop here initially appears to be undeformed, it is actually cut by several faults that obscure the large-scale sedimentary features. Despite this complication, a wide variety of small-scale sedimentary structures are present that stand out especially well in the spring, after winter floods have washed the outcrop clean of mud and salt incrustations.

The Point of Rocks Sandstone, Temblor Range, California

Jack B. Carter

INTRODUCTION

The Point of Rocks Sandstone is an Eocene submarine fan complex that constitutes an important reservoir rock along the west side of the San Joaquin basin. It also has a larger significance for California geology in general, because at the time of its deposition, the fan straddled the proto-San Andreas fault before significant right lateral offsets occurred. Along with the Butano Sandstone of the La Honda basin in the Santa Cruz Mountains, its displaced equivalent, the Point of Rocks establishes a relatively well-defined cross-fault correlation and helps to constrain the timing and magnitude of offsets along the fault (Clarke & Nilsen, 1973).

The Point of Rocks attains a maximum thickness of 900 m (3000 ft) in outcrop and is mappable for 75 km (45 mi) along the southwest margin of the San Joaquin Valley. It is thickest adjacent to the San Andreas fault and thins to the north and east, where it wedges out into Kreyenhagen Shale. In the subsurface to the south it thickens to more than 1500 m (5000 ft). The formation is middle to upper Eocene in outcrop sections (Ulatisian to lower Narizian), but may range into the lower Eocene (Penutian or older) in the thicker subsurface sections to the south (Clarke, 1973).

Lithologically, the Point of Rocks is dominated by relatively blocky, arkosic sandstones interbedded with subordinate shales. The sandstones are medium- to coarse-grained and moderately well-sorted, generally intermediate between arenites and wackes (Clarke, 1973). In outcrop and in the subsurface the sands are commonly soft and friable, although calcite cement is locally pervasive. In outcrop the sands are buff to orange-brown, due to interstitial limonitic material, and often form prominent hogbacks. Well-exposed outcrops of shale are rare. The sandstone consists of 35-50 percent quartz, 14-18 percent potassium feldspar, 10-18 percent plagioclase feldspar, 1-5 percent other minerals (mostly biotite), and 8-10 percent lithic fragments, including chert, quartzite, shale, slate, argillite, phyllite, quartzofeldspathic metamorphic and plutonic rocks, and minor amounts of andesitic or basaltic volcanic rocks (Clarke, 1973).

FACIES ASSOCIATIONS AND DEPOSITIONAL SETTING

Based upon facies associations, foraminiferal biofacies and stratigraphic relationships observed in the Point of Rocks, Clarke (1973) inferred deposition on a large submarine fan system near the intersection of the suprafan with an upper fan valley. The dominant bedding style in the Point of Rocks is typical of facies B in the descriptive facies classification of deep-sea fan deposits of Mutti and Ricci Lucchi (1978). The thick sandstones exposed in outcrop consist of a series of stacked, 'amalgamated' sandstone beds averaging 1.3 m (4.3 ft) in thickness and ranging from 0.2 to 9.5 m (0.7-31 ft). Amalgamated sandstone beds commonly comprise sequences from 15 to 30 m (50-100 ft) thick that probably were deposited within or very near major suprafan channels (Clarke, 1973). Individual beds within these sequences frequently have scoured bases with erosional ridges or channels up to 2 m (6.5 ft) deep. Various sole marks are present, including very common flute and groove casts, load casts, and less common tool marks and organic trail and burrow fillings. The great majority of beds begin with thick, massive sandstones of Bouma's division Ta. Lamination occurs in about 25% of beds, but not always in the sequential position of Bouma's Tb division. Contorted or convoluted lamination and ripple cross-stratification are present in the upper interval of some beds, but rarely constitute a significant volume of the bed, particularly in amalgamated sequences. Various types of grading occur in over 90% of the beds examined by Clarke (1973), with continuous grading most common in thin beds, whereas delayed and coarse-tail grading are more common in thick beds. Dish structures are ubiquitous in many beds (Fig. 1), occurring most often in thick beds exhibiting coarse-tail and delayed grading. These water escape structures indicate a very high rate of direct suspension sedimentation. This stage of deposition from sandy high-density turbidity currents can form almost instantaneously sand beds that are many meters thick and devoid of traction sedimentation structures (Lowe, 1982).

Figure 1. Dish structures (discontinuous, concave-up lamina) in medium- to coarse-grained sandstone. These water-escape structures are locally abundant in most outcrops of the Point of Rocks.

Pebble to boulder-sized conglomerates have also been described in the Point of Rocks, particularly in the lower part of the formation (Clarke, 1973). These may correspond to facies A, although poor outcrop quality obscures most depositional features of these exposures. Volumetrically, they constitute a negligible part of the overall formation. The same is true of finer-grained rocks interbedded with the predominant sandstone. The average sand/shale ratio in the outcrops examined by Clarke (1973) is 11.5. As with the conglomeratic intervals, poor outcrop quality often hampers specific facies assignment. Clarke (1973) attributed the finer-grained sequences to shifts in the locus of sand deposition on the suprafan.

PALEOGEOGRAPHY

Neogene right-slip along the San Andreas fault bisected the Point of Rocks fan and has displaced its proximal half, the Butano Sandstone of the La Honda Basin, by 300-330 km (Clarke and Nilsen, 1973). This cross-fault correlation is one of the best documented examples of this relationship and is based on a number of striking parallels. Both formations are Eocene in age; the more proximal Butano is lower Narizian through Penutian, Point of Rocks is lower Narizian through Ulatisian and possibly Penutian in the more proximal southern penetrations. This possible discrepancy in the older part of the age assignment is not problematic if the fan developed progradationally from south to north, with oldest sediments generally restricted to the south. Both sandstones share similar vertical and lateral stratigraphic relationships with Eocene bathyal shales; the Kreyenhagen Shale on the east and the Twobar Shale Member of the San Lorenzo Formation on the west. Paleobathymetries indicated by foraminiferal biofacies are bathyal to abyssal in both formations (Clarke, 1973; Stanley, 1984). The sandstones are compositionally identical and indicate a provenance in rapidly eroding plutonic rocks having an average composition of quartz monzonite, with a subordinate sedimentary cover (Clarke, 1973).

Depositional facies observed in the Butano Sandstone are generally compatible with those described earlier in the Point of Rocks (Clarke and Nilsen, 1973). Nilsen (1983/1984) described inner-fan facies associations in the southern-most outcrop belt of the La Honda Basin, a facies not observed in the more distal Point of Rocks (Clarke, 1973). Paleocurrent indicators (flute casts, tool marks, pebble imbrication and other sole marks) are oriented to the north and northwest in both formations. The reconstructed Butano-Point of Rocks fan is on the order of 115 km (70 mi) long and 65 km (40 mi) wide (Fig. 2). This fan was shed from granitic uplifts of the Salinian block to the south, probably in the present day area of Monterey Bay and the northern Gabilan Range (Clarke and Nilsen, 1973).

SUBSURFACE PRODUCTION

The Point of Rocks Formation is productive in at least a dozen fields on the west side of the San Joaquin basin, including Belgian Anticline, Cymric, Pyramid Hills, Devils Den, Coles Levee (north), Antelope Hills, North Antelope Hills, McDonald Anticline, and McKittrick. The largest of these is the Belgian Anticline field located 7 miles southeast of the outcrop visited on this field trip. Cumulative production from the southeast part of this field through 1966 was 8.8 million barrels of oil and 67.2 billion cubic feet of gas, or about 1/3 of the total oil and 2/3 of the total gas production from that part of the field (Dunwoody, 1968). The trap is an intensely faulted anticlinal structure (Fig. 3). Interbedded shales from 15-120 m (50-400 ft) thick effectively seal hydrocarbons and create a stacked pay configuration in at least two separate sands. A faulted anticline in the Welport area of the Cymric field (8 km north of Belgian Anticline field) also produces oil and gas from the Point of Rocks. Peak annual production from this pool, covering about 300 acres near the crest of the structure, was 165,800 barrels of oil and 5.9 billion cubic feet of gas (California Oil & Gas Fields, Central California, 1985).

The Point of Rocks is also productive in several combination stratigraphic-structural traps, usually involving erosional truncation. The largest and most interesting example of this type is the Pyramid Hills field, located 55 km (34 mi) north of the outcrop visited on this field trip. The field is developed along the Pyramid Hills thrust fault and produces from three Point of Rocks sands in the hanging wall, truncated by basal Temblor and Monterey unconformities (Fig. 4). Oil is trapped against basinal Monterey shales within several broad, plunging anticlinal structures dipping away from the west-vergent fault. Interbedded shales as thin as 15 m (50 ft) appear to isolate individual sands within the formation and create multiple pay zones (California Oil & Gas Fields, Central California, 1985). A subthrust anticline is also productive in the field and may have a stratigraphic component on its east flank, again provided by basal Monterey truncation (Fig. 4). Cumulative production for the field through 1970 was 4.4 million barrels of oil, most of this from Point of Rocks (Webster and Ryall, 1972).

Reservoir parameters vary widely in the Point of Rocks. Porosities generally range between 20-25%, although in shallower penetrations at Devils Den and Pyramid Hills they are reported as high as 38% (California Oil & Gas Fields, Central California, 1985). Most reported permeabilities fall in the 100-500 md range, except at Pyramid Hills where values approach 5 darcies. Anomalously high porosity and permeability in that field is probably due to present burial depths as shallow as 180 m (600 ft) and possibly related to diagenetic enhancement under the basal Monterey and Temblor unconformities. Rapid changes in permeability and porosity locally accounts for lateral variations in productivity (Dunwoody, 1968). Highest flow rates are reported from the Belgian Anticline Field at 2,094 barrels of oil and 4,500 Mcf. of gas per day (Park et al., 1957).

OUTCROP DESCRIPTION

Excellent exposures of Point of Rocks sand and shale are found along Salt and Temblor Creeks at the southern end of the Temblor Range outcrop belt, located approximately 7 miles northwest of the Belgian Anticline field (Fig. 5). The measured section of Fig. 6 is located on the vertically dipping north flank of an east-plunging anticline, one of four such folds exposing Point of Rocks, lower Temblor, and basal Monterey strata. Several faults and a prominent joint pattern at this outcrop reflect the intensely structured local setting (Figs. 7 and 8). The section described is approximately 150 m (500 ft) below the top of the formation, here unconformably overlain by the Oligocene Cymric Shale Member of the Temblor Formation. Only the upper part of the Point of Rocks is exposed along this drainage.

The sand exposed here is approximately 25 m (82 ft) thick and is typical of the commonly occurring sand packages interpreted by Clarke (1973) to have been deposited within or very near major suprafan channels. The generally thinning-upward sequence exhibited here tends to support a

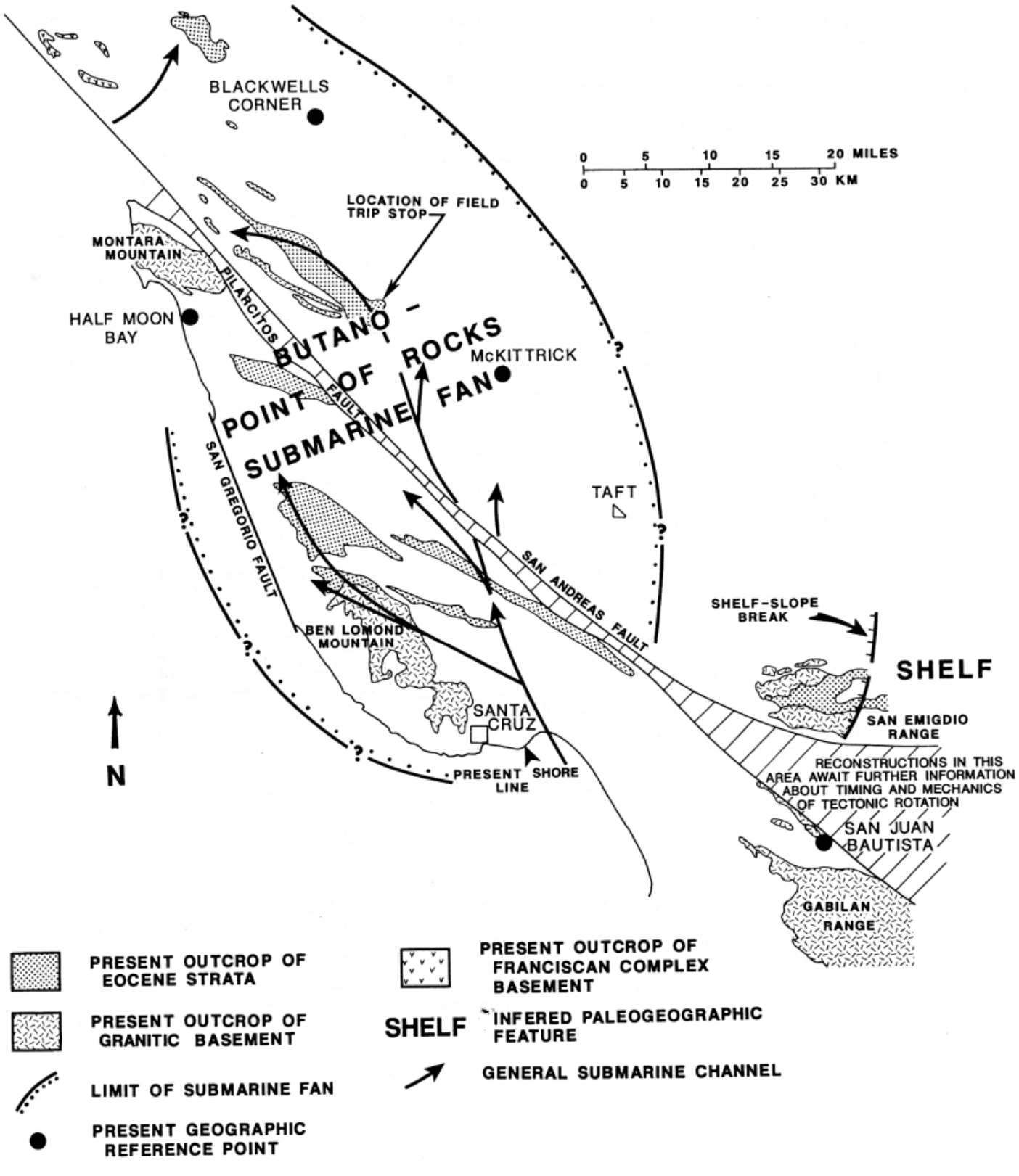

Figure 2. Middle Eocene paleogeography and sediment dispersal paths of central California. Map, redrawn from Clarke (1973), restores 300-330 km (186-205 mi) of right slip on the San Andreas fault. From Graham et al., 1989.

channelized setting. Unfortunately, the outcrop is not wide enough to determine lateral relationships of this sand body. The underlying shale has a few thin sand beds but overall is very fine-grained. Although poorly exposed below the measured section it appears to be at least 100 m (328 ft) thick and is probably not unlike the thick shale beneath the second Point of Rocks sand in the Belgian Anticline field (Fig. 3). It represents a significant local hiatus in sand deposition and is probably a distal overbank facies, possibly related to channel switching upslope.

The outcrop is dominated by a series of medium- to coarse-grained, amalgamated sand beds from 0.3 m (1 ft) to at least 2 m (6.5 ft) thick. Most of the beds appear to be rather uniform in thickness although several thin depositionally by as much as 25% over the width of the outcrop (about 60 m, or 200 ft). Basal scour is also common and erodes up to 1 m (3.3 ft) of the underlying bed (Fig. 8). Load and flame structures also characterize many basal contacts. Internally, the beds are massive or crudely graded and many display traction lamination (Fig. 8) or dish structures (Fig. 1). Carbonate concretions of oblate to spheroidal shape (popularly known as "cannonball" concretions) are common in this and most other outcrops, sometimes attaining diameters of 2 m (6.5 ft).

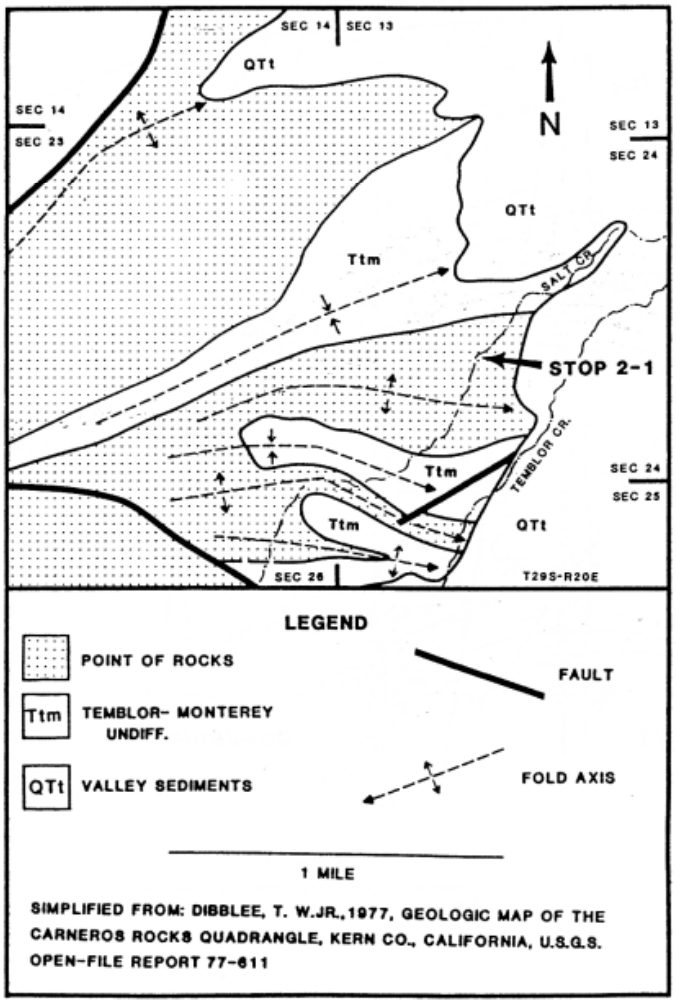

Figure 5. Location of Point of Rocks outcrop described in Figure 6 and visited on this field trip (Stop 2-1).

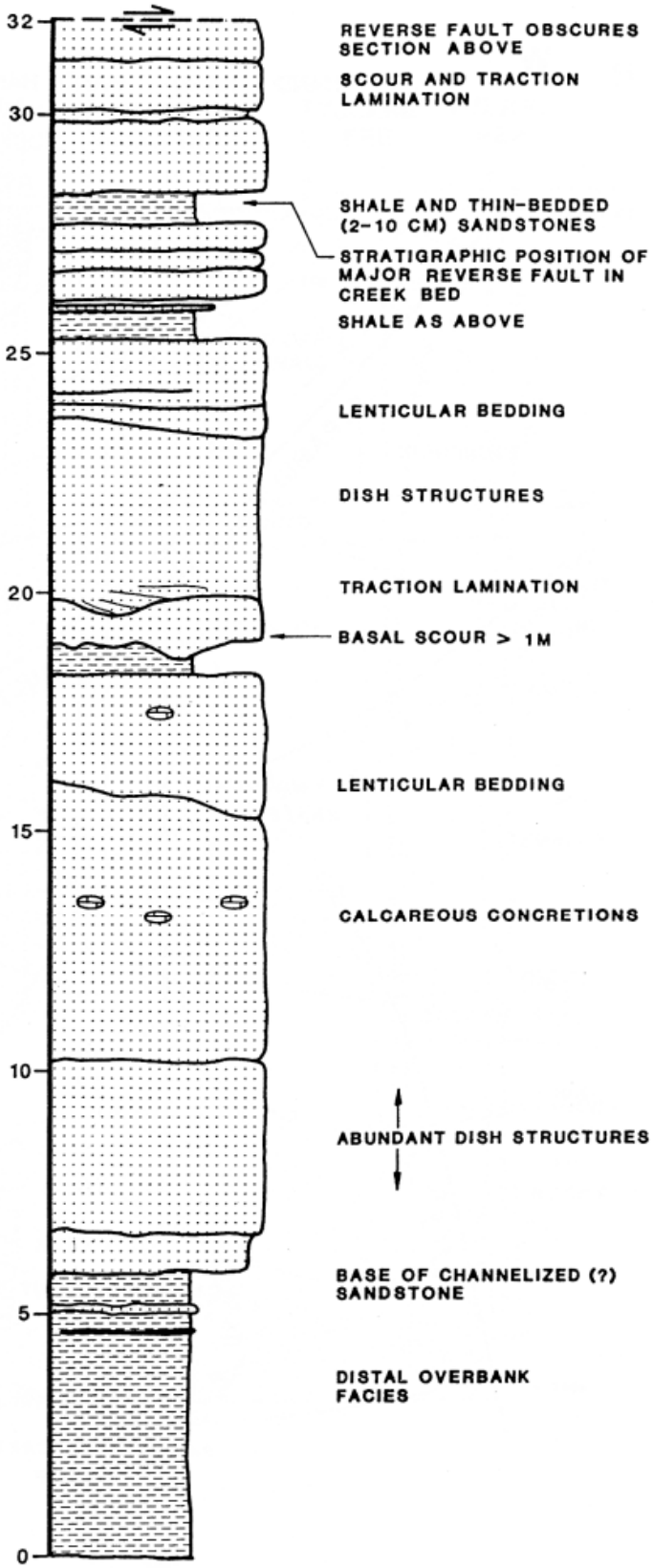

Figure 6. Measured section of the Point of Rocks sandstone, approximately 150 m (500 ft) below top of formation. Locality: in Salt Creek, 2000 ft east, 1350' north of southwest corner of Section 24, T29S, R20E, scale in meters. (Described by J. B. Carter, J. G. Kuespert, and S. A. Reid).

Figure 7. Structural deformation in the Point of Rocks outcrop on Salt Creek. A large reverse fault (center of photo) has offset strata by a minimum of about 30 m (100 ft) and created a prominent drag fold].

Figure 8. A deeply-scoured amalgamation surface (arrows) below a thick, high-density turbidite. Approximately 1 m (3.3 ft) of the underlying sand has been removed. Note traction lamination in the upper sand, prominent joint pattern, and concretions.

REFERENCES

California Division of Oil and Gas, 1985, California Oil and Gas Fields, Central California.

Clarke, S. H., Jr., 1973, The Eocene Point of Rocks Sandstone: Provenance, mode of deposition and implications for the history of offset along the San Andreas fault in central California (Ph.D. thesis): Berkeley, California, University of California, 302 p.

Clarke, S. H., Jr., and Nilsen, T. H., 1973, Displacement of Eocene strata and implications for the history of offset along the San Andreas fault, central and northern California, in Kovach, R. L., and Nur, A., eds., Proceedings of the Conference on Tectonic Problems of the San Andreas Fault System: Stanford University Publications in Geological Sciences, v. 13, p. 358-367.

Curtin, G., 1955, Pyramid Hills Oil Field: California Division of Oil and Gas, Summary of Operations -- California Oil Fields, v. 4, no. 2.

Dunwoody, J. A., 1968, Belgian Anticline oil field, southeast portion (main area), in Karp, S.E., ed., Geology and oil fields, west side southern San Joaquin Valley: 1968 Guidebook, Pacific Sections, American Association of Petroleum Geologists, Society of Exploration Geophysicists, Society of Economic Paleontologists and Mineralogists, p. 80-81.

Graham, S. A., Stanley, R. G., Bent, J. V., Carter, J. B., 1989, Oligocene and Miocene paleogeography of central California and displacement along the San Andreas fault: Geological Society of America Bulletin, v. 101, p. 711-730.

Lowe, D. R., 1982, Sediment gravity flows, II -- depositional models with special references to the deposits of high-density turbidity currents: Journal of Sedimentary Petrology, v. 52, no. 1, p. 279-297.

Mutti, E. and Ricci Lucchi, F., 1978, Turbidities of the northern Appenines -- introduction to facies analysis (translated by Nilsen, T. H.): International Geology Review, v. 20, no. 2, p. 125-166.

Park, W. H., Land, P. E., and Bruce, D. D., 1957, Belgian Anticline Oil Field: California Division of Oil and Gas, Summary of Operations, v. 43, no. 1.

Nilsen, T. H., 1983/1984, Submarine-Fan Facies Associations of the Eocene Butano Sandstone, Santa Cruz Mountains, California: Geo-Marine Letters, Vol. 3, p. 167-171.

Stanley, R. G., 1984, Middle Tertiary sedimentation and tectonics of the La Honda basin, central California: U.S. Geological Survey Open-File Report 85-596, 263 p.

Webster, C. B. and Ryall, P. L., 1972, West Side Oil Fields, in: Geology and oil fields, west side central San Joaquin valley: 1972 Guidebook, Pacific Sections, American Association of Petroleum Geologists, Society of Exploration Geophysicists, Society of Economic Paleontologists and Mineralogists, p. 26-27.

The previous article by Jack Carter, originally published in a 1990 guidebook, is modified from the original article by inclusion of new color photographs in Figures 1, 7 & 8. Also Figures 3 & 4 from the original are not included. The unaltered article appears on pages 391-395 in the following publication by the Pacific Section—AAPG.

Kuespert, J. G. and Reid, S. A. eds., 1990, Structure, Stratigraphy and Hydrocarbon Occurrences of the San Joaquin Basin, California: Pacific Section—SEPM and Pacific Section—AAPG, Fieldtrip Guidebook GB65, 366 p.

The next article by Glenn Sharman of Stanford University represents an updated interpretation of the Point of Rocks based on new evidence. It differs from the previous article by Carter (1990) in several aspects, and both are included to demonstrate the evolution in thinking on Point of Rocks provenance over the last twenty-five years.

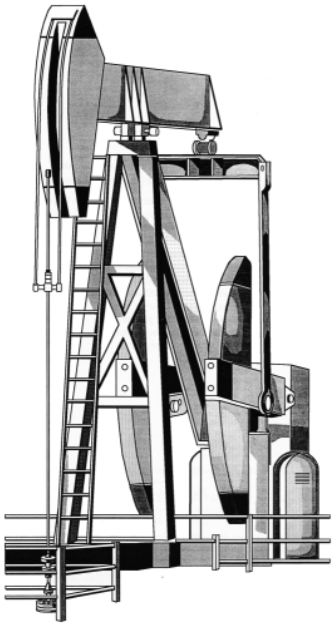

A New Paleogeographic Model for the Point of Rocks Sandstone, San Joaquin Basin, California

Glenn R. Sharman[1], Stephan A. Graham[1], and Christopher Sine[2]

[1] Department of Geological and Environmental Sciences, Stanford University 94305, USA
[2] Occidental Petroleum, Bakersfield, California 93311, USA

INTRODUCTION

The Point of Rocks Sandstone Member of the Kreyenhagen Formation is a middle Eocene sand-dominated unit that constitutes a historically important petroleum reservoir in the southwestern San Joaquin basin. The Point of Rocks Sandstone attains great thicknesses (likely over 2000 meters) and is present over a wide area, both in outcrop and in the subsurface (Fig. 1). Both sedimentary facies and recovered benthic foraminifera indicate that the Point of Rocks Sandstone was predominantly deposited in a deep-marine (lower bathyal to abyssal) environment as part of a submarine fan system (Clarke, 1973; see also Carter, this volume, for additional description of the Point of Rocks Sandstone).

In addition to its economic value, the Point of Rocks Sandstone has played an important role by influencing the historical development of paleotectonic and paleogeographic models in California. For example, the Point of Rocks Sandstone helped early workers to recognize and quantify strike-slip displacement along the San Andreas fault. In a seminal paper, Hill and Dibblee (1953) argued that the San Andreas fault had accumulated 100's of kilometers of dextral strike-slip motion since Cretaceous time, based in part upon correlation of Eocene deep-marine sequences of the Santa Cruz Mountains (Butano Sandstone) and Temblor Range (Point of Rocks Sandstone; Hill and Dibblee, 1953, p. 449). The recognition that large-scale, horizontal fault offsets could occur was a revolutionary and controversial idea that played an important role in reconciling continental and offshore geologic relationships in the emerging theory of plate tectonics (e.g., Atwater, 1970).

While the Butano-Point of Rocks correlation was proposed in the early 1950's, it was not until twenty years later that additional work done by Samuel Clarke and Tor Nilsen solidified the correlation within a coherent paleogeographic model (Clarke, 1973; Clarke and Nilsen, 1973; Nilsen and Clarke, 1975; see also Fig. 2 in Carter, this volume). In this model, the Butano Sandstone and Point of Rocks Sandstone formed two halves of a large, northeast-to-northwest flowing submarine fan that was derived from erosion of Salinian granitic rocks in the vicinity of the northern Gabilan Range and Monterey Bay area (Clarke, 1973; see also Fig. 2 in Carter, this volume). Portions of this submarine fan were deposited in the La Honda basin (modern-day Santa Cruz Mountains) and southwestern San Joaquin basin and constitute the Butano Sandstone and Point of Rocks Sandstone, respectively. Evidence for the Butano-Point of Rocks correlation includes many similarities between these units: 1) abrupt truncation of thick sand depocenters across the San Andreas fault, 2) great thickness (> 1,500 m) and widespread distribution, 3) age-equivalence, 4) similar depositional facies and paleobathymetry (outer neritic to bathyal/abyssal), 5) generally compatible paleocurrent distributions, 6) very similar sandstone composition and inferred provenance from a silicic-intermediate granitic terrane, and 7) shared stratigraphic positions overlying Paleocene mudstone and underlying middle-late Eocene mudstone (see discussion in Clarke, 1973, p. 225-230).

In addition to providing a paleogeographic model for the central California region, the Butano-Point of Rocks correlation provided a key constraint on the pre-Neogene offset history of the San Andreas fault (e.g., Nilsen and Clarke, 1975). For example, the middle Eocene Butano-Point of Rocks submarine fan (ca. 48-38 Ma) has approximately the same amount of offset (~315 km) as the ca. 23 Ma Pinnacles-Neenach volcanic field (Matthews, 1976; Graham et al., 1989), suggesting that the central San Andreas fault was inactive during late Paleogene time. Researchers have long recognized that restoration of ~315 km of Neogene San Andreas displacement does not fully account for the apparent offset of Salinian granitic rocks with respect to the main Cretaceous batholithic belt that runs through the Sierra Nevadan and Peninsular Ranges batholiths (e.g., Suppe, 1970). By one estimate, the amount of unaccounted slip is at least 100 km (Dickinson et al., 2005). This discrepancy has been accounted for by a dextral, proto-San Andreas fault that was hypothesized to have been active during latest Cretaceous-early Paleogene time (e.g., Nilsen and Clarke, 1975). However, the proto-San Andreas fault model has not been widely accepted and remains controversial (e.g., Atwater, 1989).

Since its proposal in the early 1950s, the Butano-Point of Rocks correlation has been widely accepted in the literature and has been used to constrain both paleogeographic and paleotectonic models (e.g., Graham et al., 1989; Dickinson et al., 2005). Perhaps a single exception was a regional study of

conglomerate clast and sandstone compositions by Seiders and Cox (1992) that noted a marked dissimilarity between conglomerate clast types within the Butano Sandstone and Point of Rocks Sandstone. In particular, the Butano Sandstone is enriched in felsic volcanic and granitic clasts compared to the Point of Rocks Sandstone that is enriched in chert (Seiders and Cox 1992, p. 28). Seiders and Cox (1992) also noted that Point of Rocks sandstone is enriched in quartz grains relative to the Butano Sandstone (Fig. 2). While the Butano Sandstone is compositionally similar to the German Rancho Formation, sandstone and conglomerate clast compositions of the Point of Rocks Sandstone closely resemble the lower Eocene Cantua Sandstone that is interpreted to have been derived from the Sierra Nevada (Graham and Berry, 1979; Seiders and Cox, 1992). In their conclusions, Seiders and Cox (1992) suggested that the Butano Sandstone and Point of Rocks Sandstone were derived from different source regions, in contrast to the prevailing paleogeographic model (Clarke, 1973).

The main purpose of this article is to further evaluate the Butano-Point of Rocks correlation using two complimentary methods: 1) detrital zircon U-Pb geochronology and 2) subsurface mapping of middle Eocene strata in the southern Joaquin basin using well log, biostratigraphic, and seismic datasets. Our results will be used to reassess current thinking regarding Eocene paleogeography of the central California margin (see also Sharman et al., 2013; Sharman et al., *in press*).

DETRITAL ZIRCON U-Pb GEOCHRONOLOGY

Detrital zircon U-Pb geochronology offers a method of determining sandstone provenance that can have distinct advantages over traditional methods (e.g., sandstone petrography, conglomerate clast assemblages, etc.). Individual crystallization ages of detrital zircon grains in sandstone can be directly linked with the ages of crystalline rocks in potential source regions. In California, igneous rocks are widespread due to the presence of a volcanic arc that extended north-south across the margin during Mesozoic time (Dickinson, 2008). Today, the remnants of this volcanic arc are primarily preserved as plutonic rocks in the Sierra Nevada Mountains, Salinian block, Transverse Ranges, and Peninsular Ranges. Although many of the plutonic rocks in California have similar compositions (e.g., quartz monzonite), detrital zircon geochronology is able to readily distinguish between compositionally-similar plutons on the basis of their crystallization age.

Sedimentary Provenance Analysis

Normalized and cumulative detrital zircon age distributions are presented in Figure 3 for twelve sandstone samples (early to middle Eocene) from the southern San Joaquin and La Honda basins (Sharman et al., 2013). All samples are dominated by late Permian-Cretaceous (ca. 280-80 Ma) zircon with lesser abundances of Paleogene and pre-Permian zircon (Fig. 3). In particular, all samples have variable proportions of mid-Cretaceous (ca. 125-80 Ma) and Jurassic-earliest Cretaceous (ca. 175-140 Ma) zircon (Fig. 3).

The dominance of ca. 280-80 Ma zircon in Eocene sandstone in the La Honda and southern San Joaquin basins suggests that these strata were derived in large part from igneous rocks of the Mesozoic arc (Fig. 3; Sharman et al., 2013). Although all samples share similar age populations, the details of the age distributions suggest that there are two distinct detrital zircon age assemblages that were derived from distinct source regions (Fig. 3).

The first age assemblage is represented by the Point of Rocks Sandstone and is characterized by a dominance of mid-Cretaceous zircon (ca. 125-80 Ma; 67%-80%) with lesser amounts of Jurassic zircon (10%-13%; Fig. 3). Eocene zircon (ca. 55-43 Ma) is also found in low abundances (1%-9%; Fig. 3). Strikingly similar detrital zircon age distributions are found in other Eocene fluvial and marine strata that extend ~400 km to the north along the San Joaquin and Sacramento basins (Fig. 4). We interpret this provenance signature to indicate that these sands were derived from the ancestral Sierra Nevada Mountains. The same age populations found in the forearc are present in the mid-Cretaceous Sierra Nevada batholith (125-85 Ma) and in local Jurassic rocks (Irwin and Wooden, 2001).

The second age assemblage is represented by Eocene strata from the La Honda basin (Butano Sandstone) and from the southernmost San Joaquin basin (Tejon Formation; Fig. 3). These samples are characterized by 1) approximately equal abundances of Cretaceous and Jurassic zircon, 2) a small population of Permian-Triassic zircon (5%-17%), and 3) a lack of Eocene zircon (Fig. 3). Very similar age assemblages are found in other Eocene sandstone units from the Salinian block, including samples from the Gualala block (German Rancho Formation; Doebbert et al., 2012) and Santa Lucia Range (Carmelo Formation and Rocks Sandstone; Sharman et al., *in press*) that also have abundant Permian-Jurassic zircon (Fig. 4). Because Permian-Jurassic rocks are very uncommon in the Salinian block (Kistler and Champion, 2001), the abundance of Jurassic (38%-62%) and Permian-Triassic (6%-17%) zircon in these units rules out a local Salinian source,

as traditionally interpreted (e.g., Nilsen and Clarke, 1975).

Kolgomorov-Smirnov Statistics

The Butano-Point of Rocks correlation can be quantitatively evaluated using the Kolgomorov-Smirnov (K-S) statistic that tests the null hypothesis that two distributions are derived from the same population (Press et al., 1986). This approach reveals that the two age assemblages are statistically distinct from each other at the 95% confidence level (i.e., P-value < 0.05; Table 1). In other words, differences in the detrital zircon age distributions between the Butano Sandstone and Point of Rocks Sandstone cannot be explained by random sampling of the same parent population, and these units were not likely derived from the same source region. In addition, the Point of Rocks samples, when compared to each other, are unable to be statistically distinguished by the K-S test (Table 1). Similarly, 31 of 36 sample pairs from the La Honda basin and San Emigdio Mountains are statistically indistinguishable at the 95% confidence level (Table 1).

Summary

Although the Butano-Point of Rocks correlation has been widely accepted and used to constrain paleogeographic and tectonic reconstructions (Clarke, 1973; Graham et al., 1989; Dickinson et al., 2005), our results demonstrate that the Butano and Point of Rocks Sandstones do not share a common provenance. These results are in agreement with the work by Seiders and Cox (1992) that found significant differences between sandstone and conglomerate clast compositions (Fig. 2). This interpretation casts doubt on the existence of the Butano-Point of Rocks submarine fan with a single source from the Salinian block.

SUBSURFACE INVESTIGATION

Isopach Mapping

Point of Rocks Sandstone

The Point of Rocks Sandstone is present over a wide area in the subsurface of the southwestern San Joaquin Basin and has been penetrated by numerous oil wells (Fig. 1). We mapped the thickness of the Point of Rocks Sandstone using a database of 43 wells of which 16 are interpreted to have penetrated the full thickness of the formation (see Appendix A). Our Point of Rocks isopach map closely resembles the excellent mapping of Clarke (1973), demonstrating that additional well penetrations in the last 40 years have not significantly altered our knowledge of the subsurface distribution of the Point of Rocks. However, we have extended the zero-thickness line farther east than Clarke's (1973) map, based on the presence of probable Eocene sand in the "Tupman USL 1-10" (API: 02947380) and 31X-10 "Great Basins" (API: 02947361) wells (Malmblorg, 2008).

The Point of Rocks Sandstone is thickest in the vicinity of Cymric oil field where it likely attains a thickness of over 2 kilometers in a deep well ("Cymric Unit" 1; API: 02929580) that reached total depth without exiting Eocene sandstone (CDOGGR, 1998). The Point of Rocks Sandstone systematically thins to the north and east (Fig. 1), where it pinches out within the encasing Kreyenhagen shale. The Point of Rocks is variably erosionally truncated along its western margin in outcrop and in the nearby subsurface (Clarke, 1973). The southern extent of the Point of Rocks Sandstone is poorly known due to deep burial and a lack of well penetrations, although the Point of Rocks is absent in Eocene exposures and well penetrations in the vicinity of the San Emidgio Mountains (Nilsen, 1987; Fig. 1).

Famoso Sandstone

The Famoso Sandstone is a poorly understood unit that occurs exclusively in the subsurface along the southeastern margin of the San Joaquin basin (Fig. 1). The Famoso Sandstone is inferred to have been deposited within a shallow-marine shelfal environment and grades into non-marine facies (Walker Formation) to the east (Reid, 1988; Fig. 1). The age of the Famoso Sandstone is poorly constrained but likely ranges from middle to late Eocene in age based on stratigraphic correlation with the underlying Domengine Sandstone (Reid, 1988) and by the presence of late Eocene (Refugian) benthic foraminifera within the formation (Bartow and McDougall, 1984; Fig. 5). Thus, the Point of Rocks Sandstone and Famoso Sandstone were likely deposited synchronously, in part (Fig. 5).

We mapped the thickness of the Famoso Sandstone using a database of 40 wells, all of which penetrated the full thickness of the formation (see Appendix A). Although the Famoso Sandstone reaches thicknesses up to 160 m, its average thickness is about 85 m over its mapped distribution (Fig. 1). The Famoso Sandstone forms a highly linear thickness trend that parallels the inferred position of the Eocene shoreline (Dickinson et al., 1979), an observation that is consistent with an inferred shallow-marine (shelfal) origin of the Famoso sands (Reid, 1988). The thickness distribution of the Famoso Sandstone is poorly constrained south of the Bakersfield Arch where the unit becomes deeply buried beneath younger valley fill (Fig. 1).

Metralla Sandstone

The middle Eocene Metralla Sandstone Member of the Tejon Formation is present both in outcrop in the San Emigido Mountains (Nilsen, 1987) and the nearby subsurface (Weber, 1973). The Metralla

Sandstone shares many similarities with the Famoso Sandstone including a middle Eocene age assignment (Fig. 5) and a shelfal depositional environment that grades into non-marine facies to the east (Tecuya Formation) and shale-dominated facies to the west (Nilsen, 1987). For these reasons, the Metralla Sandstone likely represents a southerly equivalent of the Famoso Sandstone.

The Point of Rocks-Famoso Depositional System

Although the deep-marine Point of Rocks Sandstone and shelfal Famoso Sandstone have previously been interpreted as depositionally unrelated (Clarke, 1973), several lines of evidence suggests that these units may have formed a genetically-linked, shelf-to-basin depositional system (Fig. 6). 1) Detrital zircon U-Pb age distributions indicate that the Point of Rocks Sandstone has a "Sierran" provenance signature that is distinct from coeval Eocene sands deposited atop or adjacent to the northern Salinian block (Figs. 3-4). Sierran-derived sand must have come from the east and would have passed through the shelf prior to entering the deep-marine basin. 2) The Famoso and Point of Rocks Sandstones overlap in age (Fig. 5), and thus could have been part of the same depositional system. 3) The thickness distributions of both units indicate that Famoso sands were located very closely to the Point of Rocks zero-thickness line (Fig. 1). 4) Paleocurrent measurements from the Point of Rocks Sandstone (n = 446; Clarke, 1973) indicate a mean west-northwesterly direction (296°) that is consistent with derivation from the east with lesser northward deflection.

Together, these observations are consistent with the interpretation that Famoso shelfal sands were routed into the deep-marine Point of Rocks basin (Fig. 6). We speculate that a submarine canyon linked the Famoso and Point of Rocks depocenters ("Point of Rocks canyon", Fig. 6), based in part on analogy to other well-documented Late Cretaceous-Paleogene submarine canyons in the Sacramento basin (e.g., Williams, Markley, Meganos, and Martinez canyons; Almgren et al., 1978; Williams et al., 1998) and central San Joaquin basin (Cantua canyon, Graham and Berry, 1979; Anderson, 1998). Any such canyon (if it existed) would be located on the Eocene shelf edge that was positioned "a short distance west of Belleview, Greely, and Wasco oil fields" (Clarke, 1973, p. 203) and also between the mapped distributions of the Point of Rocks and Famoso Sandstones (Figs. 1). Based on this reasoning, we depict the hypothetical "Point of Rocks canyon" to be located between the Tupman USL 1-10 and Mushrush 5 wells in our east-west cross section (Fig. 6).

CENTRAL CALIFORNIA EOCENE PALEOGEOGRAPHY

Both sandstone provenance (i.e., detrital zircon U-Pb geochronology) and subsurface mapping of the southern San Joaquin basin suggest that the prevailing paleogeographic model of central California during Eocene time requires significant modification (Fig. 7). Because the Butano-Point of Rocks correlation also constitutes an important piercing point used to constrain the offset history of the San Andreas fault (Nilsen and Clarke, 1975), our results have important implications for the tectonic development of the California margin (see discussion in Sharman et al., 2013).

Southern San Joaquin Basin

We argue that the Point of Rocks Sandstone was derived from the east and is the deep-marine equivalent of the shallow-marine Famoso Sandstone (Figs. 6, 7). This interpretation is primarily based upon detrital zircon U-Pb ages that are similar to other Eocene Great Valley sands that were derived from the Sierra Nevada batholith (Figs. 3-4) and proximity to age-equivalent shelfal sands (Fig. 5). We speculate that sand transported by alongshore currents along the paleo-Sierran shelf encountered a submarine canyon on the northwest flank of the Bakersfield arch and was routed into the deep-marine Point of Rocks basin (Fig. 7). This process was very effective in transporting a large volume of sand (~1,200-1,500 km^3; Fig. 1) into the southern San Joaquin deep-marine basin despite occurring during widespread middle Eocene marine transgression (Bartow, 1991). A potential analog for this system is the modern California coastline where similar processes transport sand offshore despite the present-day sea level highstand (e.g., Covault et al., 2009).

By analogy to the Cantua Sandstone to the north (Anderson, 1998), the Point of Rocks basin may have been structurally controlled by an actively rising accretionary complex that allowed great thicknesses of sand to accumulate in ponded depocenters (Fig. 7). We speculate that some amount of Point of Rocks sand may have bypassed the forearc to reach trench-slope basins through an outlet that may have existed in the trench-slope break (Fig. 7). Some evidence for this process is provided by early-middle Eocene sandstone present in trench-slope basins in the San Francisco Bay region that have a similar detrital zircon provenance character to the Point of Rocks Sandstone (Fig. 4; Sharman et al., *in press*).

Northern Salinian Block

An important, and surprising, observation is that the majority of zircon found in Paleogene sandstone of the Salinian block (e.g., Butano Sandstone) was not derived locally as previously thought (e.g., Nilsen and Clarke, 1975). This observation is at odds with

the "continental borderland" model which holds that local basement uplifts within the Salinian block supplied detritus to adjacent, bathyal basins (Nilsen and Clarke, 1975). Although the abundant Permian-Jurassic zircon found in the Butano Sandstone (and related units) could not have been derived from the Salinian block, plutonic and volcanic rocks of this age are abundant in the southeastern Sierra Nevada and western Mojave Desert region (Walker et al., 2002; Chapman et al., 2012). The presence of such source rocks is supported by locally preserved non-marine Paleogene basins in the southernmost Sierra Nevada region (Goler and Witnet basins) that contain significant amounts of Triassic-Jurassic zircon (Lechler and Niemi, 2011). We speculate that an extraregional fluvial system delivered sediment to marine basins atop the Salinian block from the southeastern Sierra and/or western Mojave regions (Fig. 7; Sharman et al., 2013).

The presence of western Mojave detritus in the Butano Sandstone (Sharman et al., 2013) and German Rancho Formation (Doebbert et al., 2012) is at odds with current paleogeographic models that depict the northern Salinian block juxtaposed northward against the southern San Joaquin basin during Eocene time (Fig. 7). Sharman et al. (2013) suggested that the Salinian block was positioned 50-100 km farther south in middle Eocene time than typically depicted in paleotectonic reconstructions (Fig. 7). This reconstruction has the advantage of 1) allowing sediment to be readily delivered from the western Mojave region to the northern Salinian block, and 2) negating the need for a late Cretaceous-early Paleogene proto-San Andreas fault by restoring the Salinian block to a position within the Cretaceous batholithic belt (Sharman et al., 2013)

CONCLUSIONS

- The Butano Sandstone and Point of Rocks Sandstone have quantitatively distinct detrital zircon U-Pb age distributions. As a result, these units were not likely part of a contiguous submarine fan system with a common source region from Salinian granitic rocks.
- The Point of Rocks Sandstone was derived from erosion of the ancestral Sierra Nevada Mountains. This interpretation is supported by 1) detrital zircon U-Pb ages in the Point of Rocks that closely resemble other Eocene Great Valley sands, and 2) the abundance of ca. 125-85 Ma detrital zircon that matches the age range of the mid-Cretaceous Sierra Nevada batholith.
- The Point of Rocks Sandstone is the deep-marine equivalent of the shelfal Famoso Sandstone and the non-marine Walker Formation. We speculate that a submarine canyon was positioned on the Eocene shelf-slope break and delivered shelfal sands to the adjacent deep-marine basin over much of middle Eocene time.
- The Butano Sandstone, and related Paleogene sandstone from the Salinian block, was derived from the southeastern Sierra Nevada and/or western Mojave region. This interpretation is supported by the abundance of late Permian-Jurassic zircon in these sands that lack a local source in the Salinian block.

ACKNOWLEDGEMENTS

This work benefited from discussion with I. Alark, M. Johns, B. Stupp, and the rest of the Oxy California Exploration group.

REFERENCES

Almgren, A.A., 1978, Timing of Tertiary submarine canyons and marine cycles of deposition in the southern Sacramento Valley, California, in Stanley, D.J., and Kelling, G., eds., Sedimentation in submarine canyons, fans, and trenches: Dowden, Hutchinson & Ross, Stroudsburg, p. 276-291.

Almgren, A.A., Filewicz, M.V., and Heitman, H.L., 1988, Lower Tertiary foraminiferal and calcareous nannofossil zonation of California: An overview and recommendation, in Filewicz, M.V., and Squires, R.L., eds., Paleogene Stratigraphy, West Coast of North America: Los Angeles, Pacific Section, SEPM (Society for Sedimentary Geology), v. 58, p. 83-106.

Anderson, K.S., Graham, S.A., and Hubbard, S.M., 2006, Facies, architecture, and origin of a reservoir-scale sand-rich succession within submarine canyon fill: Insights from Wagon Caves Rock (Paleocene), Santa Lucia Range, California, U.S.A.: Journal of Sedimentary Research, v. 76, p. 819-838.

Anderson, K.S., 1998, Facies architecture of two Paleogene structurally-controlled turbidite systems, central California [Ph.D. thesis]: Stanford University, 391 p.

Atwater, T., 1970, Implications of plate tectonics for the Cenozoic tectonic evolution of western North America: Geological Society of America Bulletin, v. 81, p. 3513–3536.

Atwater, T.M., 1989, Plate tectonic history of the northeast Pacific and western North America, in Winterer, E.L., Hussong, D.M., and Decker, R.W., eds., The Eastern Pacific Ocean and Hawaii: Boulder, Colorado, Geological Society of America, Geology of North America, v. N, p. 21–72.

Bartow, J.A., and McDougall, K., 1984, Tertiary stratigraphy of the southeastern San Joaquin

Valley, California: U.S. Geological Survey Bulletin 1529-J, 41 p.

Bartow, J.A., 1991, The Cenozoic evolution of the San Joaquin Valley, California: U.S. Geological Survey Professional Paper 1501, 40 p.

Carter, J.B., this volume, The Point of Rocks Sandstone, Temblor Range, California, in Clark, M., Sharman, G.R., and Carter, J.B., Westside Turbidite Field Trip, San Joaquin Valley – California, PS-AAPG Field Trip Guidebook.

Cassel, E.J., Grove, M., and Graham, S.A., 2012, Eocene drainage evolution and erosion of the Sierra Nevada batholith across northern California and Nevada: American Journal of Science, v. 312, p. 117-144.

CDOGGR, 1998, California Oil and Gas Fields, Volume 1 Central California: California Department of Conservation, Division of Oil, Gas, and Geothermal Resources, Publication No TR11.

Cecil, M.R., Ducea, M.N., Reiners, P., Gehrels, G., Mulch, A., Allen, C., and Campbell, I., 2010, Provenance of Eocene river sediments from the central northern Sierra Nevada and implications for paleotopography: Tectonics, v. 29, TC6010, 13 p.

Chapman, A.D., Saleeby, J.B., Wood, D.J., Piasecki, A., Kidder, S., Ducea, M.N., and Farley, K.A., 2012, Late Cretaceous gravitational collapse of the southern Sierra Nevada batholith, California: Geosphere, v. 8, p. 314-341.

Clarke, S.H., Jr., and Nilsen, T.H., 1973, Displacement of Eocene strata and implications for the history of offset along the San Andreas fault, central and northern California, in Kovach, R.L., and Nur, A., eds., Proceedings of the conference on tectonic problems of the San Andreas fault system: Stanford University Publications in the Geological Sciences, v. 13, p. 358-367.

Clarke, S.H., Jr., 1973, The Eocene Point of Rocks Sandstone: Provenance, mode of deposition and implications for the history of offset along the San Andreas fault in central California [Ph.D. thesis]: Berkeley, University of California, 302 p.

Covault, J.A., Normark, W.R., Romans, B.W., and Graham, S.A., 2009, Highstand fans in the California borderland: The overlooked deep-water depositional systems: Geology, v. 35, p. 783-786.

Critelli, S., and Nilsen, T.H., 1996, Petrology and diagenesis of the Eocene Butano Sandstone, La Honda basin, California: The Journal of Geology, v. 104, p. 295–315.

Dickinson, W.R., 2008, Accretionary Mesozoic-Cenozoic expansion of the Cordilleran continental margin in California and adjacent Oregon: Geosphere, v. 4, p. 329-353.

Dickinson, W.R., Ingersoll, R.V., and Graham, S.A., 1979, Paleogene sediment dispersal and paleotectonics in northern California: Geological Society of America Bulletin, v. 90, pt. I, p. 897–898; pt. II, p. 1458–1528.

Dickinson, W.R., Beard, L.S., Brakenridge, G.R., Erjavec, J.L., Ferguson, R.C., Inman, K.F., Knepp, R.A., Lindberg, F.A., and Ryberg, P.T., 1983, Provenance of North American Phanerozoic sandstones in relation to tectonic setting: Geological Society of America Bulletin, v. 94, p. 222–235.

Dickinson, W.R., Ducea, M., Rosenberg, L.I., Greene, H.G., Graham, S.A., Clark, J.C., Weber, G.E., Kidder, S., Ernst, W.G., and Brabb, E.E., 2005, Net dextral slip, Neogene San Gregorio–Hosgri Fault Zone, Coastal California: Geologic Evidence and Tectonic Implications: Geological Society of America Special Paper 391, 43 p.

Doebbert, A.C., Carroll, A.R., and Johnson, C., 2012, The sandstone-derived provenance record of the Gualala basin, northern California, U.S.A.: Journal of Sedimentary Research, v. 82, p. 841-858.

Dumitru, T.A., Ernst, W.G., Wright, J.E., Wooden, J.L., Wells, R.E., Farmer, L.P., Kent, A.J.R., and Graham, S.A., 2012, Eocene extension in Idaho generated massive sediment floods into the Franciscan trench and into the Tyee, Great Valley, and Green River basins: Geology, v. 41, p. 187-190.

Graham, S.A., and Berry, K.D., 1979, Early Eocene paleogeography of the central San Joaquin Valley: Origin of the Cantua Sandstone, in Armentrout, J.M., Cole, M.R., and Ter Best, H., Jr., eds., Cenozoic paleogeography of the western United States: Pacific Section, SEPM (Society for Sedimentary Geology), Pacific Coast Paleogeography Symposium 3, p. 119–127.

Graham, S.A., Stanley, R.G., Bent, J.V., and Carter, J.B., 1989, Oligocene and Miocene paleogeography of central California and displacement along the San Andreas fault: Geological Society of America Bulletin, v. 101, p. 711–730.

Harun, H., 1984, Distribution and deposition of lower to middle Eocene strata in central San Joaquin Valley, California: Stanford, Calif., Stanford University, M.S. thesis, 100 p.

Hill, M.L., and Dibblee, T.W., Jr., 1953, San Andreas, Garlock, and Big Pine faults, California: Geological Society of America Bulletin, v. 64, p. 443–458.

Irwin, W.P., and Wooden, J.L., 2001, Map showing plutons and accreted terranes of the Sierra Nevada, California with a tabulation of U/Pb isotopic ages: U.S. Geological Survey Open-File Report 2001-229.

Johnson, C.L., and Graham, S.A., 2005, Middle Tertiary stratigraphic sequences of the San Joaquin basin, California, in Scheirer, ed., A.H., Petroleum Systems and Geologic Assessment of Oil and Gas in the San Joaquin Basin Province, California: U.S. Geological Survey Professional Paper 1713, 18 p.

Kistler, R.W., and Champion, D.E., 2001, Rb-Sr whole-rock and mineral ages, K-Ar, 40Ar/39Ar, and U-Pb mineral ages, and strontium, lead, neodymium, and oxygen isotopic compositions for granitic rocks from the Salinian composite terrane, California: U.S. Geological Survey Open-File Report 01-453, 84 p.

Lechler, A.R., and Niemi, N.A., 2011, Sedimentologic and isotopic constraints on the Paleogene paleogeographic and paleotopography of the southern Sierra Nevada, California: Geology, v. 39, p. 379–382.

Ludington, S., Moring, B.C., Miller, R.J., Stone, P.A., Bookstrom, A.A., Bedford, D.R., Evans, J.G., Haxel, G.A., Nutt, C.J., Flyn, K.S., and Hopkins, M.J., 2007, Preliminary integrated geologic map databases for the United States Western States: California, Nevada, Arizona, Washington, Oregon, Idaho, and Utah: U.S. Geological Survey Open-File Report, v. 2005-1305, version 1.3.

Malmblorg, W.T., West, W.B., Brabb, E.B., and Parker, J.M., 2008, Digital coordinates and age of more than 13,000 foraminifers samples collected by Chevron petroleum geologists in California: U.S. Geological Survey Open-File Report 2008-1187.

Matthews, V., III, 1976, Correlation of Pinnacles and Neenach volcanic fields and their bearing on San Andreas fault problem: The American Association of Petroleum Geologists Bulletin, v. 60, p. 2128–2141.

McDougall, K., 2007, California Cenozoic biostratigraphy – Paleogene, in Hosford Scheirer, A., ed., Petroleum systems and geologic assessment of oil and gas in the San Joaquin Basin Province, California: U.S. Geological Survey Professional Paper 1268, p. 1-56.

Milam, R.W., 1985, Biostratigraphy and sedimentation of the Eocene and Oligocene Kreyenhagen Formation, central California [Ph.D. thesis]: Stanford University, 240 p.

Moxon, I.A.,1990, Stratigraphic and structural architecture of the San Joaquin and Sacramento valleys [Ph.D. thesis]: Stanford University, 371 p.

Nilsen, T.H., and Clarke, S.H., Jr., 1975, Sedimentation and tectonics in the early Tertiary continental borderland of central California: U.S. Geological Survey Professional Paper 925, 64 p.

Nilsen, T.H., 1987, Stratigraphy and sedimentology of the Eocene Tejon Formation, western Tehachapi and San Emigdio Mountains, California: U.S. Geological Survey Professional Paper 1268, 110 p.

Press, W.H., Flannery, B.P., Teukolsky, S.A., and Vetterling, W.T., 1986, Numerical recipes, The art of scientific computing: Cambridge, Cambridge University Press, 186 p.

PS-AAPG, 1957, Cenozoic correlation section across South San Joaquin Valley the San Andreas fault to Sierra Nevada foot hills, California: prepared by the San Joaquin Valley Sub-committee on the Cenozoic of the Geologic Names and Correlation Committee of the American Association of Petroleum Geologists, 1 sheet.

PS-AAPG, 1958, Correlation section across central San Joaquin Valley from Riverdale thru Tejon Ranch Area, California: prepared by the San Joaquin Valley Sub-committee of the Geologic Names and Correlation Committee of the American Association of Petroleum Geologists, Section 10S, 1 sheet.

PS-AAPG, 1959, Correlation section across westside San Joaquin Valley from Coalinga to Midway Sunset and across the San Andreas fault into southeast Cuyama Valley, California: prepared by the San Joaquin Valley Sub-committee of the Geologic Names and Correlation Committee of the American Association of Petroleum Geologists, Section 11, 1 sheet.

Reid, S.A., 1988, Late Cretaceous and Paleogene sedimentation along the east side of the San Joaquin Basin, in Graham, S.A., and Olson, H.C., eds., Studies of the geology of the San Joaquin Basin: Los Angeles, Pacific Section, Society of Economic Paleontologists and Mineralogists, book 60, p. 157-171.

Scheirer, A.H., and Magoon, L.B., 2007, Age, Distribution, and Stratigraphic Relationship of Rock Units in the San Joaquin Basin Province, California, in Scheirer, A.H., ed., Petroleum Systems and Geologic Assessment of Oil and Gas in the San Joaquin Basin Province, California: U.S. Geological Survey Professional Paper 1713, 38 p.

Seiders, V.M., and Cox, B.T., 1992, Place of origin of the Salinian block, California, as based on clast compositions of Upper Cretaceous and lower Tertiary conglomerates: U.S. Geological Survey Professional Paper 1526, 80 p.

Sharman, G.R., Graham, S.A., Grove, M., and Hourigan, J.K., 2013, A reappraisal of the early slip history of the San Andreas fault, central California, USA: Geology, v. 41, p. 727-730.

Sharman, G.R., Graham, S.A., Grove, M., Kimbrough, D.L., and Wright, J.E., *in press*, Detrital zircon provenance of the Late Cretaceous-Eocene California forearc: Influence

of Laramide low-angle subduction on sediment dispersal and paleogeography: Geological Society of America Bulletin.

Suppe, J., 1970, Offset of late Mesozoic basement terrains by the San Andreas fault system: Geological Society of America Bulletin, v. 81, p. 3253–3258.

Taylor, B.L., 2004, Petrography and diagenesis of the Eocene Point of Rocks Sandstone, McKittrick oil field, Kern County, California [M.S. thesis]: California State University, Bakersfield, 273 p.

Weber, G.E., 1973, Subsurface facies variations in the Metralla Sandstone Member of the Tejon Formation in the Wheeler Ridge and North Tejon oil fields, Kern County, California, in Vedder, J.G., chm., Sedimentary facies changes in Tertiary rocks – California Transverse and southern Coast Ranges: Society of Economic Paleontologists and Mineralogists Guidebook to Field Trip 2, Anaheim, California, p. 34-38.

Williams, T.A., Graham, S.A., and Constenius, K.N., 1998, Recognition of a Santonian submarine canyon, Great Valley Group, Sacramento Basin, California: Implications for petroleum exploration and sequence stratigraphy of deep-marine strata: American Association of Petroleum Geologists Bulletin, v. 82, p. 1575-1595.

Appendix A: Wells used to constrain isopach maps shown in Figure 1

Well Name	API	Top (MD)	Base (MD)	Thickness (ft)	Status
Point of Rocks Sandstone Well Penetrations					
Hand 35-28	03100157	1150	2020	870	Complete
2-32	03100193	2485	3430	945	Complete
Pyramid Hills 1-9	03120423	19109	19709	600	Complete
Levis 1	02911381	2465	3800	1335	Complete
Ocean Orchard 1	02935470	800	1940	1140	Complete
Maybury 3	02937117	1160	3800	2640	Complete
Texaco Beer 66-17	02919874	4115	6720	2605	Complete
OLC 10	02929571	1110	3460	2350	Complete
General Williamson 33	02917540	9000	9800	800 (?)	Complete
Hopkins B 35X-23	02913514	2200	5000	2800 (?)	Complete
31X-10 "Great Basins"	02947361	20600	20750	150	Complete
MST Theta 2	02936550	1000	3845	2845	Complete
AML 83-18	02952784	1807	6400	4593	Complete
AML 65X-18	02966363	1200	6025	4825	Complete
934H-29R	02974651	21650	23880	2230 (?)	Complete
9-363-31S	03026488	16680	17760	950	Complete
Texaco-2	02919869	6940	7240	<300	Partial
OLC 4	02929567	11330	12880	<1550	Partial
55-26	02935057	9450	10800	<1350	Partial
Cahn 58	02903956	10385	10400	<15	Partial
Layman 23	02935762	3150	6700	<3550	Partial
CWOD 75-20	02937643	6950	7190	<240 (?)	Partial
51X-33	02963779	12900	14565	<1665	Partial
Tupman USL 1-10	02947380	19875	20753	<878 (?)	Partial
Victory J-12	02936235	1700	2050	<350	Partial
Superior Cymric Unit 1	02929580	5000	12022	<7022	Partial
Bergen USL 1	02960381	8700	10106	<1406 (?)	Partial
PML 8-14	02913551	6660	7450	<790 (?)	Partial
CWOD 1	02938138	6150	8552	<2402	Partial
Seabord-Anderson 1	02919894	6760	7510	<750	Partial
555-15Z	02909446	10800	12700	<1900	Partial
534-16Z	02905802	9252	10522	<1270	Partial
733-17Z	03003315	8770	13682	<4912	Partial
572-18Z	02905307	9120	10800	<1680	Partial
Midway-McKittrick 'A' 33-30	02901077	5100	7000	<1900	Partial
Midway-McKittrick 'A' 22-30	02925785	5350	10867	<5517	Partial
52-33Z	02905341	6400	6935	<535	Partial
Rheem-Magee 36-X	02941289	8330	8572	<242	Partial
Dodds-Thomas 3	07900242	3239	3889	<650 (?)	Partial
Oceanic-Strickland 1	02935471	1140	1935	<795	Truncated
Corehole 17-13	02913620	50	562	<512	Truncated
Oil Explorers 31	02903649	0	1862	<1862	Truncated
Seabord-Bandini Government 41-10	02919887	900	2330	<1430	Truncated
38-19V	03100231	--	--	0	Absent
Bravo 1-31	03120135	--	--	0	Absent
Morris H C 1	10700112	--	--	0	Absent
S.F. & F.L. 4-2	02903645	--	--	0	Absent
Twisselman 1	02917530	--	--	0 (?)	Absent
Coles Levee A 26-29	02960650	--	--	0	Absent
Shell Posuncula 1	02918565	--	--	0	Absent
KCL 15X-24	02920544	--	--	0	Absent

Well Name	API	Top (MD)	Base (MD)	Thickness (ft)	Status
Famoso Sandstone Well Penetrations					
Churchhill 1	10700218	4999	5217	218	Complete
Hoffman 24	10700245	4879	5062	183	Complete
R.E.S. Hesse, et al 1	10720026	7073	7604	530	Complete
Transamerica 1	10720207	4853	5075	222	Complete
Moran 42-30	10700283	4263	4460	197	Complete
Pixley Comm. 1	10700374	6107	6569	463	Complete
Deer Creek 81	10700384	4543	4587	44	Complete
G.R.I. 65-20	10720029	10101	10246	146	Complete
Brunner B1	10700439	6997	7415	418	Complete
Beane 81-28	10700441	7051	7523	471	Complete
Curry 1	02930522	6276	6648	373	Complete
Mobile-Pan 86-35	02941957	14600	14960	360	Complete
Cities-Tenneco 35X	02948583	15221	15371	150	Complete
Mushrush 5	02909487	14926	15095	170	Complete
KCL 31-15	02940286	11324	11573	249	Complete
Famoso 12-1	02930718	6146	6489	343	Complete
Kuhn 81	02930721	7046	7420	374	Complete
KCL-A 58-8	02930725	8749	9112	363	Complete
D-L-K 1	02914763	4390	4520	131	Complete
Shell Fuhrman 1	02926316	4641	4682	41	Complete
Fee C 74	02924112	5653	5921	268	Complete
Kern County Land Lease 31 12-1	02916795	10413	10746	334	Complete
KCL 67 21-10	02940003	12491	12670	179	Complete
115	02908536	13336	13545	209	Complete
33	02930973	6810	6971	161	Complete
KCL A 57-13	02930978	7888	8143	255	Complete
KCL-B 45	02906949	10112	10502	389	Complete
Kramer 1	02908933	7157	7572	414	Complete
Section 5 34	02916269	6707	7107	400	Complete
Gow 1	02930728	7720	8029	309	Complete
Russell 73-17	02930755	13961	14155	194	Complete
McCulloch Camp et al 1-36	02956763	5607	5945	338	Complete
McKevitt-DiGiorgio Co. 1	10700444	5353	5478	125	Complete
Guinee 1	02942852	7318	7665	347	Complete
Occidental-KCL 18X-13	02930764	9011	9278	267 (?)	Complete
KCL 33-34	02900132	11171	11510	339 (?)	Complete
Lucy 1	10720142	8772	9033	261	Complete
KCL-A 85-35	02930606	9529	9791	262	Complete
Tenneco-Sun 11X-31	02970053	8434	8742	308	Complete
Parsons 1	03003222	7239	7606	367	Complete
Merritt Estate 1	10720008	--	--	0	Absent
Salyer 1-16	03120162	--	--	0	Absent
Boswell-Richardson 72-10	03100634	--	--	0	Absent
Hansen 1	03100004	--	--	0	Absent
Bravo 1-31	03120135	--	--	0	Absent
Elmer C. Von Glahn 1	03100739	--	--	0	Absent
S.F. & F.L. 4-2	02903645	--	--	0	Absent
Hahesy 36-1	03120005	--	--	0	Absent
Richgrove Community 1	02930540	--	--	0	Absent
Coles Levee A 26-29	02960650	--	--	0	Absent
Shell Posuncula 1	02918565	--	--	0	Absent
KCL 15X-24	02920544	--	--	0	Absent
Morris H C 1	10700112	--	--	0	Absent

Notes:
MD-measured depth in feet
Thicknesses queried when uncertain

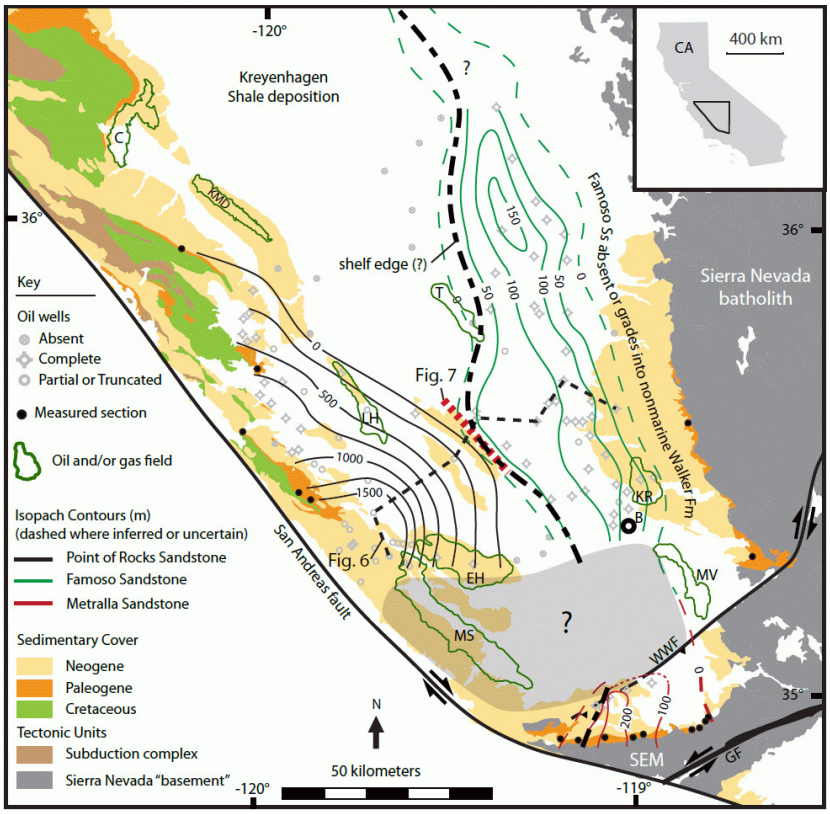

Figure 1. Isopach (thickness) maps of major sand-dominated units within the southern San Joaquin basin during middle Eocene time. Isopach maps of the Point of Rocks Sandstone, Famoso Sandstone, and Metralla Sandstone are modified from Clarke (1973), Weber (1973), Nilsen (1987), and Reid (1988). Region in gray shading is poorly constrained due to lack of well penetrations of Eocene strata. See Appendix A for oil wells used to constrain isopach mapping. Geologic map modified from Ludington et al. (2007). Fault locations follow Chapman et al. (2012). Oil Fields: C-Coalinga; KMD: Kettleman Middle Dome; LH-Lost Hills; EH-Elk Hills; MS-Midway-Sunset; MV-Mountain View; KR-Kern River; T-Trico. Other Abbreviations: B-Bakersfield; GF-Garlock fault; Fm-Formation; SEM-San Emigdio Mountains; Ss - Sandstone; WWF-White Wolf fault.

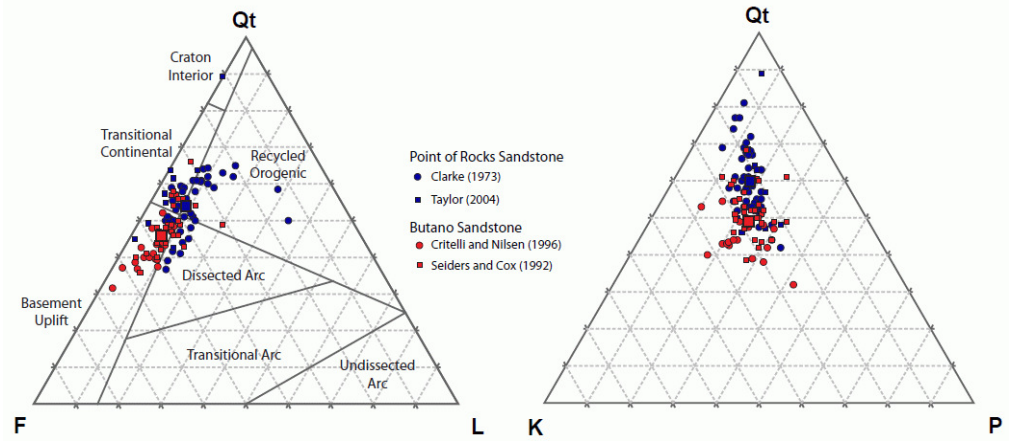

Figure 2. QFL diagram showing the sandstone composition of the Point of Rocks Sandstone (blue) and Butano Sandstone (red). Mean values are shown as larger squares. Data from Clarke (1973), Seiders and Cox (1992), Critelli and Nilsen (1996), and Taylor (2004). Tectonic setting overlay from Dickinson et al. (1983). Qt-total quartz; F-feldspar; L-lithic grains; K-potassium feldspar; P-plagioclase.

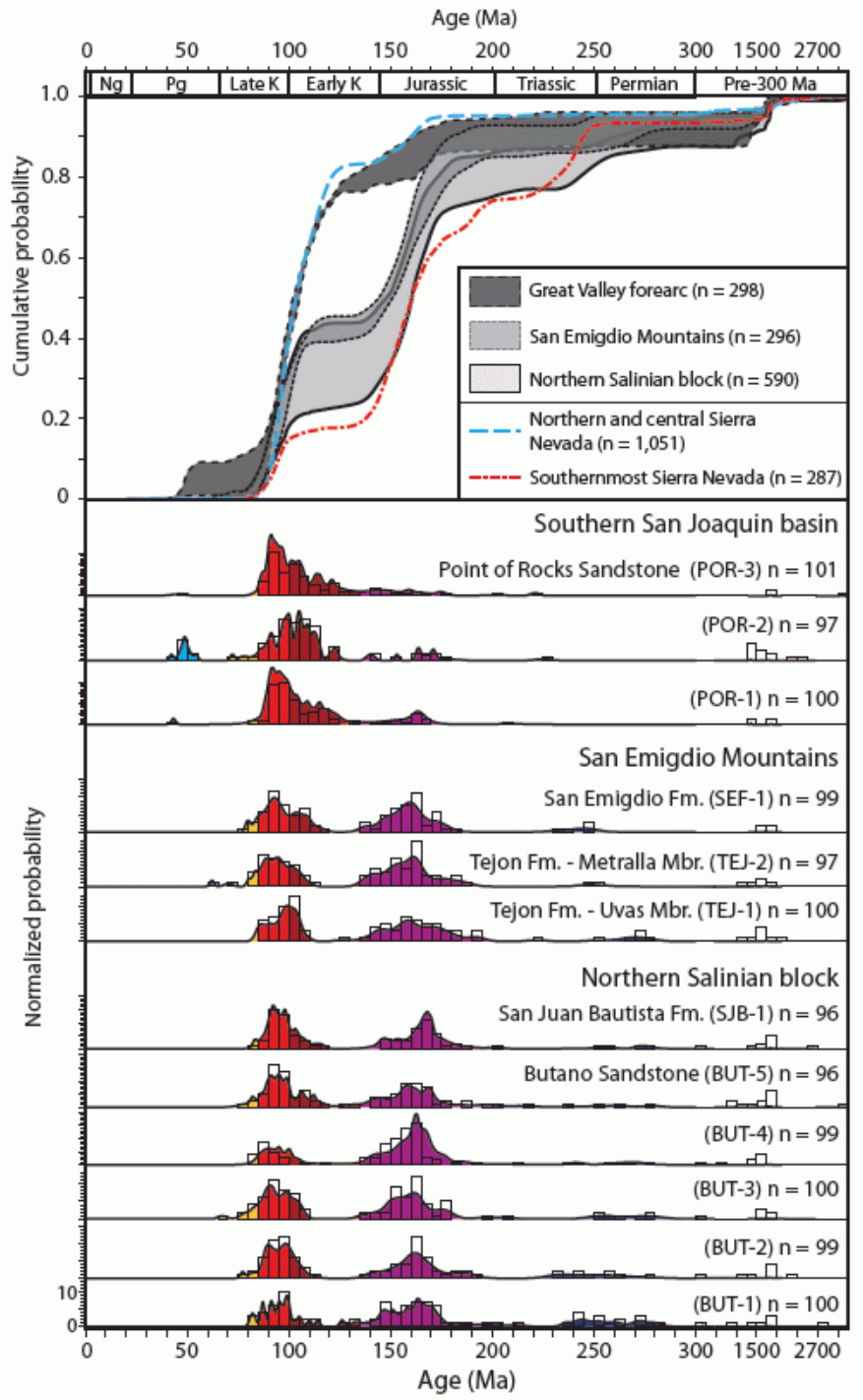

Figure 3. Cumulative (above) and normalized (below) detrital zircon U-Pb age distributions of Eocene sandstone from the southern San Joaquin basin, San Emigdio Mountains, and northern Salinian block. Data from Sharman et al. (2013). The gray shading in the cumulative distributions encompass all samples within each group. Northern and central Sierra Nevada samples from Cecil et al., 2010 and Cassel et al., 2012. Southernmost Sierra Nevada samples from Lechler and Niemi (2011). Ng-Neogene; Pg-Paleogene; K-Cretaceous; Fm-Formation; Mbr-Member.

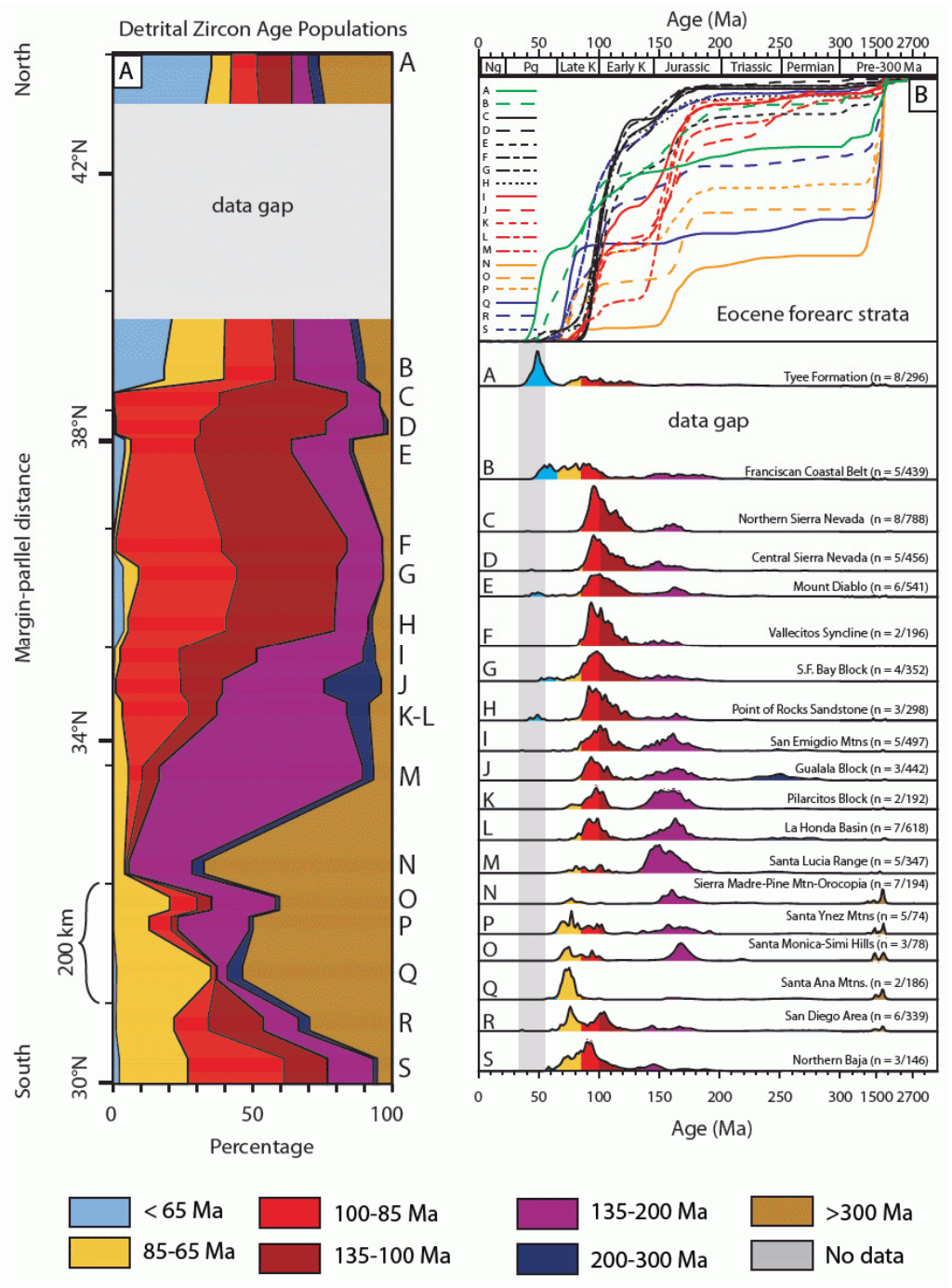

Figure 4. Regional compilation of detrital zircon U-Pb ages from Eocene sandstone along the southern Oregon-California-northern Baja forearc (modified from Sharman et al., *submitted*).

A) Bar graphs of major detrital zircon age populations.

B) Cumulative (above), and normalized (below) U-Pb age distributions for groups of forearc sandstone samples. Gray bar indicates depositional age range of the samples. Number of samples/grains in parentheses.

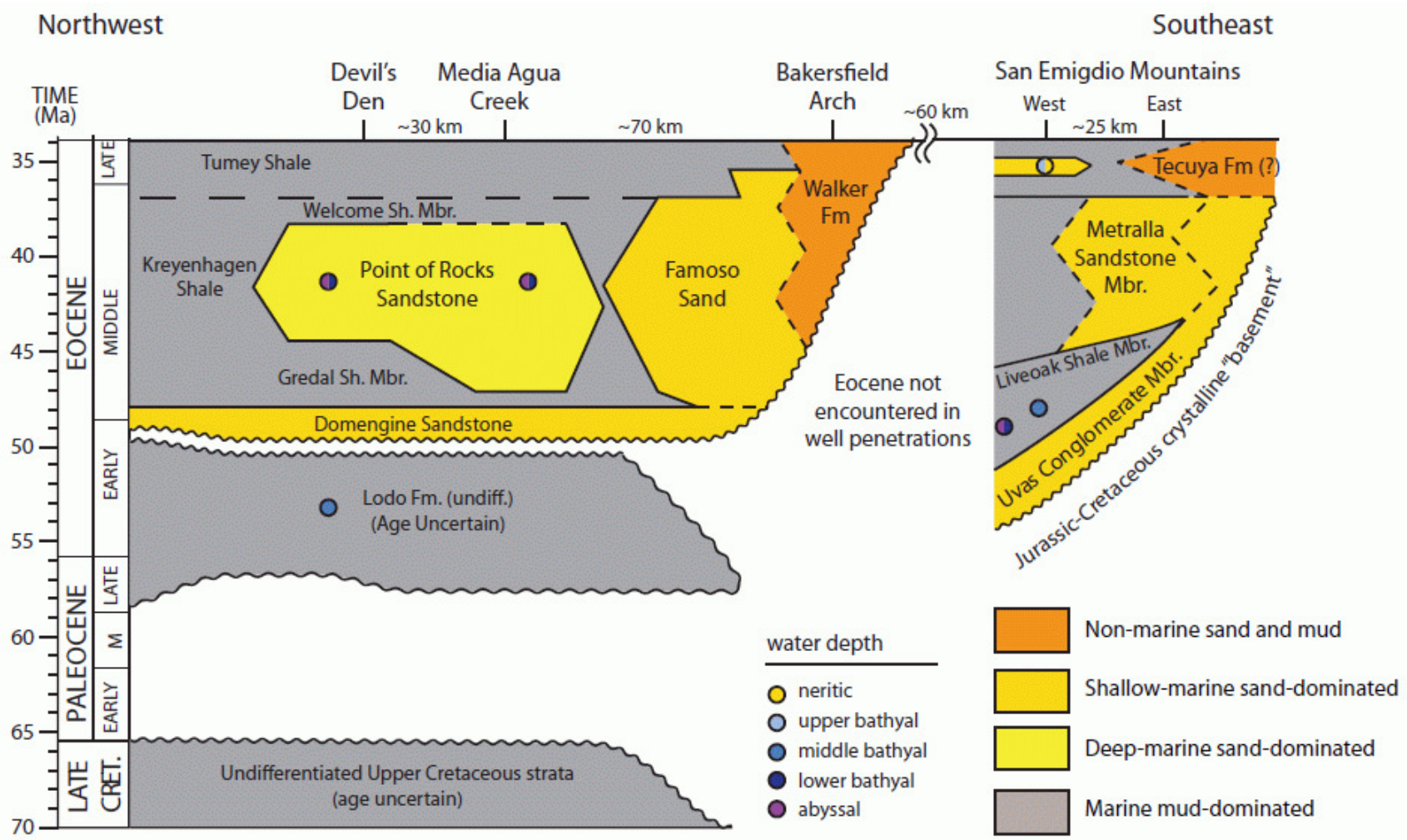

Figure 5. Chronostratigraphic diagram of the southern San Joaquin basin. Paleogene time scale from McDougall et al. (2007). Depositional age constraints from Bartow and McDougall (1984), Milam (1985), Nilsen (1987), Almgren et al. (1988), Reid (1988), Moxon (1990), Johnson and Graham (2005), Scheirer et al. (2007). Paleobathymetry (water depth) from Clarke (1973), Harun (1984), Nilsen (1987), and Moxon (1990).

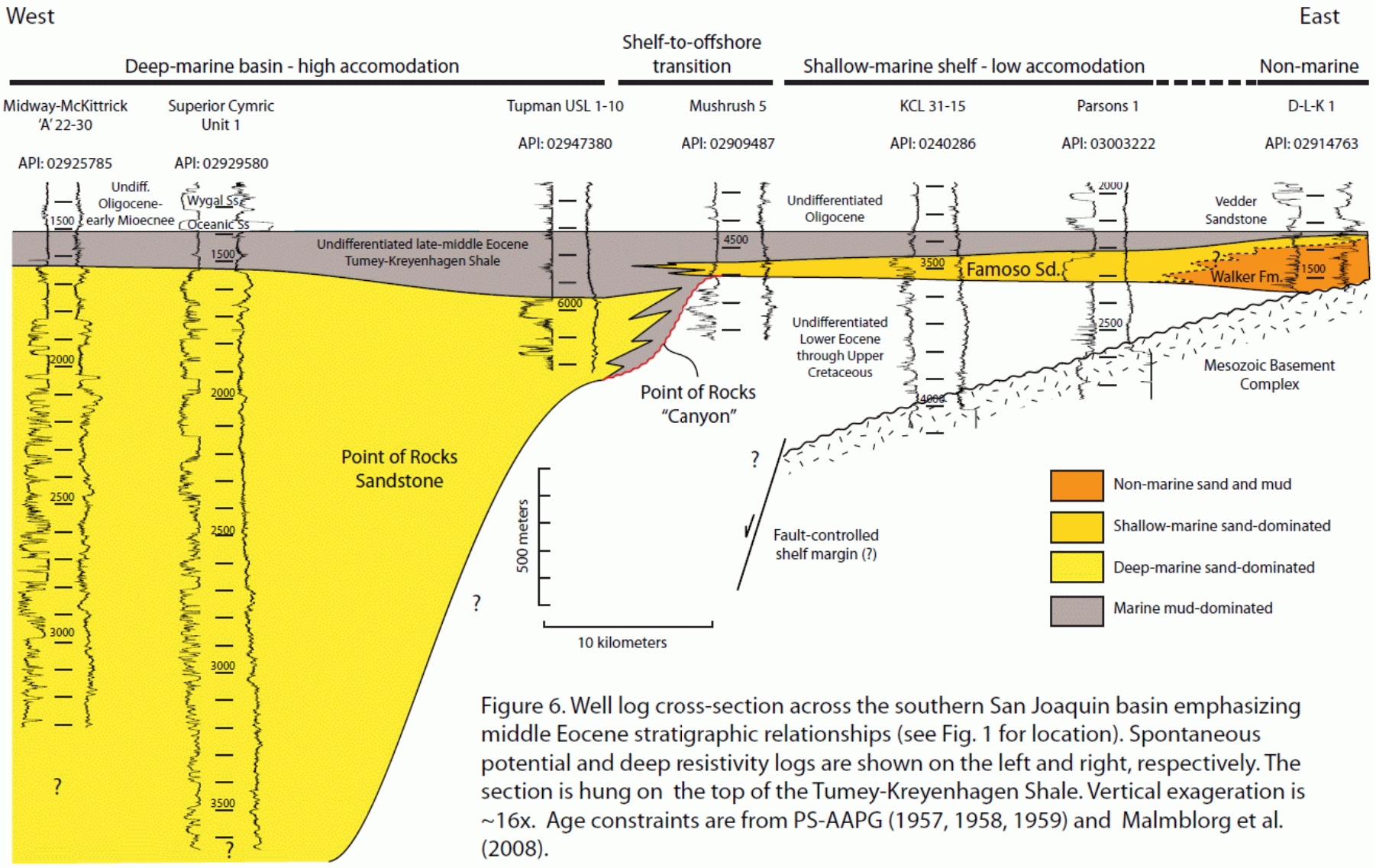

Figure 6. Well log cross-section across the southern San Joaquin basin emphasizing middle Eocene stratigraphic relationships (see Fig. 1 for location). Spontaneous potential and deep resistivity logs are shown on the left and right, respectively. The section is hung on the top of the Tumey-Kreyenhagen Shale. Vertical exageration is ~16x. Age constraints are from PS-AAPG (1957, 1958, 1959) and Malmblorg et al. (2008).

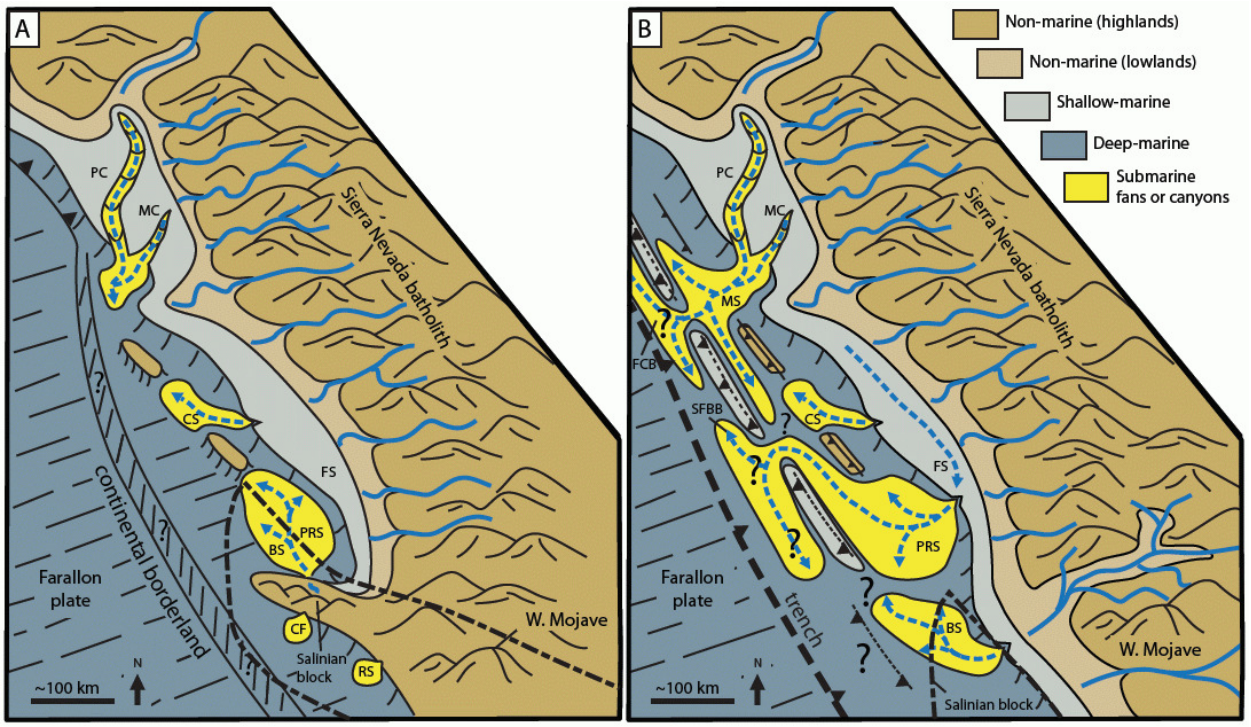

Figure 7. Cartoon of Paleogene paleogeography of the Great Valley forearc and northern Salinian block. A) Traditional paleogeographic model. Modified from Nilsen and Clarke (1975), Graham and Berry (1979), and Anderson et al. (2006). B) Revised paleogeographic model (this study). Modified from Dumitru et al. (2012) and Sharman et al. (2013). BS-Butano Sandstone; CF-Carmelo Formation; CS-Cantua Sandstone; FCB-Franciscan Coastal Belt; FS-Famoso Sandstone; MC-Markely Canyon; MS-Markley Sandstone; PC-Princeton Canyon; PRS-Point of Rocks Sandstone; RS-Rocks Sandstone; SFBB-San Francisco Bay Block.

Table 1: Kolgomorov-Smirnov (K-S) P-values of detrital zircon U-Pb age distributions

		P-values											
Sample	**N**	**POR-3**	**POR-2**	**POR-1**	**SEF-1**	**TEJ-2**	**TEJ-1**	**SJB-1**	**BUT-5**	**BUT-4**	**BUT-3**	**BUT-2**	**BUT-1**
Point of Rocks Sandstone (POR-3)	101		0.803	1.000	0.000	0.000	0.000	0.000	0.000	0.000	0.000	0.000	0.000
Point of Rocks Sandstone (POR-2)	97	0.803		0.936	0.000	0.001	0.000	0.001	0.000	0.000	0.000	0.002	0.000
Point of Rocks Sandstone (POR-1)	100	1.000	0.936		0.000	0.000	0.000	0.000	0.000	0.000	0.000	0.000	0.000
San Emigdio Formation (SEF-1)	99	0.000	0.000	0.000		0.999	0.518	0.795	0.511	0.040	0.991	0.612	0.050
Tejon Formation - Metralla (TEJ-2)	97	0.000	0.001	0.000	0.999		0.214	0.862	0.561	0.023	0.989	0.680	0.066
Tejon Formation - Uvas (TEJ-1)	100	0.000	0.000	0.000	0.518	0.214		0.829	0.914	0.233	0.212	0.393	0.695
San Juan Bautista Formation (SJB-1)	96	0.000	0.001	0.000	0.795	0.862	0.829		1.000	0.034	0.994	1.000	0.265
Butano Sandstone (BUT-5)	96	0.000	0.000	0.000	0.511	0.561	0.914	1.000		0.053	0.942	0.997	0.360
Butano Sandstone (BUT-4)	99	0.000	0.000	0.000	0.040	0.023	0.233	0.034	0.053		0.038	0.011	0.697
Butano Sandstone (BUT-3)	100	0.000	0.000	0.000	0.991	0.989	0.212	0.994	0.942	0.038		1.000	0.164
Butano Sandstone (BUT-2)	99	0.000	0.002	0.000	0.612	0.680	0.393	1.000	0.997	0.011	1.000		0.117
Butano Sandstone (BUT-1)	100	0.000	0.000	0.000	0.050	0.066	0.695	0.265	0.360	0.697	0.164	0.117	

P-values use error in the cumulative distribution function

Samples that are statistically distinct at a 95% confidence level (P-value < 0.05) are shaded

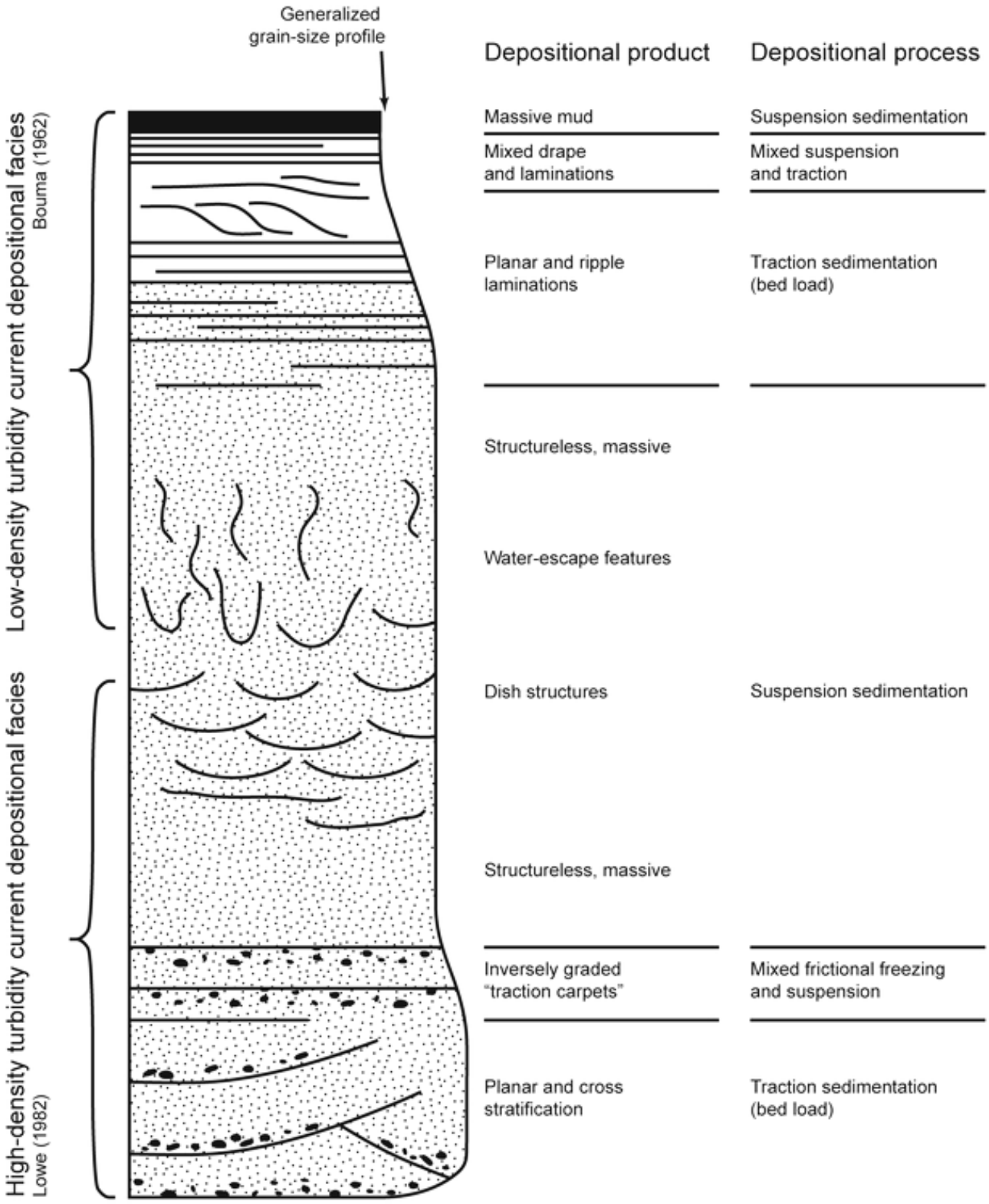

Diagram by Lowe (1982) and Bouma (1962) showing the ideal vertical succession of sedimentary structures in deposits resulting from high-density turbidity currents. These types of deposits characterize many of the outcrops described in this field guide.

Terminology and Theory of Sediment Gravity Flows

Michael S. Clark

Sediment gravity flows are currents in which sediment carried by the current moves in response to the force of gravity, and not in response to the actual movement of the current itself. Although various classification schemes can be proposed, most geologists differentiate these flows by the dominant sediment support mechanisms, which can be difficult to distinguish as flows move and evolve downslope, transitioning from one type of support mechanism to the next.

Sediment support mechanisms

Most geologists recognize four end-member processes that keep grains in a sediment gravity flow in suspension (Middleton & Hampton, 1873; Postma, 1986); Visher, 1999). These are summarized as follows (Figure 1).

Grain flows – Grains in the flow are kept in suspension by grain-to-grain interactions, with the fluid acting only as a lubricant. As such, the grain-to-grain collisions generate a dispersive pressure that helps prevent grains from settling out of suspension. Although common in terrestrial environments on the slip faces of sand dunes, pure grain flows are rare in subaqueous settings. However, grain-to-grain interactions in high-density turbidity currents are very important as a contributing mechanism of sediment support (Lowe, 1982).

Liquefied and fluidized sediment flows – Form in cohesionless granular substances. As grains at the base of a suspension settle out, fluid that is displaced upward by the settling generates pore fluid pressures that may help suspend grains in the upper part of the flow. Application of an external pressure to the suspension will initiate flow. This external pressure can be applied by a seismic shock, which may turn transform loose sand into a highly viscous suspension, as in quicksand. Generally as soon as the flow begins to move, fluid turbulence results, and the flow rapidly evolves into turbidity current. Flows and suspensions are said to be liquefied when the grains settle downward through the fluid and displace the fluid upwards. By contrast, flows and suspensions are said to become fluidized when the fluid that moves upward through the grains is able to temporarily suspend them. Most flows are liquefied, and many references to fluidized sediment gravity flows are in fact incorrect and may actually be referring to liquefied flows (Lowe, 2006).

Debris flows or mudflows – Grains are supported by the strength and buoyancy of the matrix. Mudflows and debris flows have cohesive strength, which makes their behavior difficult to predict using the laws of physics. Thus, these flows exhibit non-Newtonian behavior (Gani, 2004). Because mudflows and debris flows have cohesive strength, unusually large clasts may be able to literally float on top of the mud matrix within the flow.

Turbidity currents – Grains are suspended by fluid turbulence within the flow. Because the behavior of turbidity currents is largely predictable, they exhibit Newtonian behavior, in contrast to flows with cohesive strength, such as mudflows and debris flows (Gani, 2004). The behavior of turbidity currents in subaqueous settings is strongly influenced by the concentration of the flow, as closely packed grains in high-concentration flows are more likely to undergo grain-to-grain collisions and generate dispersive pressures as a contributing sediment support mechanism, thereby keep additional grains in suspension. Thus, it is useful to distinguish between low-density and high-density turbidity currents (Lowe, 1982). A powder snow avalanche is a type of turbidity current where air is the supporting fluid. Glowing avalanches (gas-charged flows of super-heated volcanic ash) are another non-marine example of turbidity currents.

Types of flows

Although the deposits of all four types of sediment support mechanisms are found in nature, pure grain flows are largely restricted to aeolian settings, whereas subaqueous environments are characterized by a spectrum of flow types with debris flows and mud flows on one end of the spectrum, and high-density and low-density turbidity currents on the other end. It is also useful in subaqueous environments to recognize transitional flows that are in between turbidity currents and mud flows. The deposits of these transitional flows are referred to by a variety of names, some of the more popular being "hybrid-event beds (HEB)", “linked debrites" and "slurry beds" (Haughton et al., 2009).

Grain flow deposits are characterized by a coarsening-upward distribution of grain sizes (inverse grading) within the bed. This results from smaller grains within the flow falling down in between larger grains during grain-to-grain collisions, and thereby depositing preferentially at the base of flow (Middleton & Hampton, 1973). Although present as grain avalanches in terrestrial sand dunes, grain flows are rare in other settings. However, inverse graded beds resulting from grain flow processes do make up so-called "traction carpets" in the lower intervals of some high-density turbidites (Lowe, 1982).

Liquefied flow deposits are characterized by de-watering features, such as dish structures, that result from upward escaping fluid within the flow (Middleton & Hampton, 1973). As with pure grain flows, pure liquefied flows seldom occur in nature. Nonetheless, liquefied flow processes are very important as grains within turbidity currents begin to settle out and displace fluid upwards. Thus dish structures and related features, such de-watering pipes, are often found in turbidites.

Debris flow deposits are characterized by a bimodal distribution of grain sizes, in which larger grains and/or clasts float within a matrix of fine-grained clay. Because the muddy matrix has cohesive strength, unusually large clasts may be able to float on top of the muddy material making up the flow matrix, and thereby end up preserved on the upper bed boundary of the resulting deposit (Middleton & Hampton, 1973).

Low-density turbidity current sandstones (i.e., "classic turbidites") are characterized by a succession of sedimentary structures referred to as the Bouma sequence, which result from decreasing energy within the flow (i.e., waning flow), as the turbidity current moves downslope (Lowe, 1982).

High-density turbidity current sandstones are characterized by much coarser grain size than in low-density turbidites, with the basal portions of the deposits often characterized by features that result from the close proximity of the grains to each other. Thus indications of grain-to-grain interactions (i.e., grain flow processes), and interaction of grains with the substratum (i.e., traction) are generally present in the lower portions of these deposits. Complete Bouma sequences are rare, and generally only the Bouma A and B layers are evident (Lowe, 1982).

Hybrid event beds (HEB) are characterized by textures indicative of both cohesionless (turbulence-supported) and cohesive (mud-supported) flow, with no separating bed boundary between the two. In most cases, these deposits are represented by grain-supported (turbidite) textures that grade upward into mud-supported (debrite) textures. These deposits are also referred to as linked debrites. They are generally attributed to debris flows and mud flows that evolved downslope, and partitioned into a turbidity current component at the front that is "linked" to a trailing mud-supported component (Haughton et al., 2009) (Figure 2).

Basal mud-supported textures capped by sand-supported textures have also been described, generally where the bed in question is much thicker relative to other beds in the section. These are generally attributed to seismically-triggered turbidity currents that eroded into and incorporated muddy strata that the flow moved across, thereby creating a mud-supported layer at the base of the flow. Alternatively, an earthquake-triggered mud-supported flow might be followed by sandy turbulent flow triggered by the same event (Hampton, 1972; Haughton et al., 2009).

There are also so-called "slurry beds" with alternating dark, mud-rich and lighter, sand-rich bands. The banding is attributed to sandy flows with a significant mud component that internally transitioned upward, back and forth from cohesive to non-cohesive processes (Lowe & Guy, 2000; Haughton et al., 2009).

Geologic Significance

Sediment gravity flows, primarily turbidity currents, but to a lesser extent debris flows and mud flows, are thought to be the primary processes responsible for depositing sand on the deep ocean floor. Because anoxic conditions at depth in the deep ocean basins are conducive to the preservation of organic matter, which with deep burial and subsequent maturation can generate oil and gas, the deposition of sand in deep ocean settings can ultimately juxtapose potential petroleum reservoirs with organic-rich source rocks. In fact, a significant portion of the oil and gas produced in the world today is found in reservoirs originating from sediment gravity flows (Weimer and Link, 1991).

Terminology for low-density turbidites

Bouma (1962) originally proposed a classification to describe the ideal vertical succession of sedimentary structures that develop in turbidite sandstone beds deposited by low-density

(i.e., low-concentration, fine-grained) turbidity currents. Although Bouma's terminology is widely used, beds with a complete "Bouma sequence" are rarely observed in outcrop. There are several reasons for this. First, the lower units of the Bouma sequence may not be deposited if the flow has insufficient energy to transport a coarse-grained component and/or the flow is made up primarily of mud. Second, the upper units may not be deposited if the flow "freezes" in place during a sudden drop in flow energy. Third, the upper units may be eroded off by successive flows. Fourth, most turbidites, but certainly not all, preserved in outcrop resulted from sand-rich, high-concentration (i.e., high-density) flows in which grain-to-grain collisions are an important contributing process of keeping grains in suspension, and which result in a slightly different succession of sedimentary structures (Lowe, 1982).

The Bouma (1962) sequence is divided into five distinct layers labeled A through E, with A being at the bottom and E being at the top (Figure 3). Each layer described by Bouma has a specific set of sedimentary structures and a specific lithology, with the layers overall getting finer-grained from bottom to top. Most turbidites found in nature have incomplete sequences - Bouma describes the ideal sequence where all layers are present (Middleton and Hampton, 1973). The layers are described as follows, from the top of the sequence to the base.

Bouma E: Massive, ungraded mudstone. Trace fossils may be present. The Bouma E layer is often missing, or difficult to differentiate from the Bouma D layer below.

Bouma D: Parallel-laminated siltstone.

Bouma C: Ripple-laminated, fine-grained sandstone. The ripple laminations may be deformed into convolute laminations and/or flame structures.

Bouma B: Planar-laminated fine- to medium-grained sandstone. The base of Bouma B often has features known as sole markings, such as flute casts, groove casts and parting lineation.

Bouma A: Massive to normally graded, fine- to coarse-grained sandstone, often with pebbles and/or shale rip-up clasts near the base. Dish structures may be present. The base of the A layer is sometimes eroded into underlying strata. Rare trace fossils may indicate shallow-water deposition, and/or organisms "rafted in" from settings where the flow originated.

Processes in low-density turbidity currents

The Bouma sequence is deposited during waning flow as turbidity currents move downslope. In other words, flows steadily lose energy as they react to changes in the slope of the surface over which they travel, and/or as flows move from being confined within a channel to unconfined when they exit the channel and spread out. Surges and/or hydraulic jumps caused by changes in slope can reinvigorate flows briefly to increase flow energy, but ultimately energy decreases as flows move away from their points of origin (Middleton and Hampton, 1973).

When energy within a flow is highest, it can carry the maximum amount of sediment and the largest grain sizes, but as energy decreases, the carrying capacity reduces, and the coarsest grains quickly settle out, sometimes almost instantaneously. High-energy flows may also erode into underlying beds, thereby incorporating new material into the flow, which will tend to decrease flow energy. Flows in channels can also undergo flow stripping, in which the upper part of the flow, where the finer grains tend to concentrate, separates and travels out over the top of the channel. Thus, the lower part of the flow, where the coarser-grained fraction tends to accumulate, remains within the channel. Ultimately, only clay particles remain, suspended in a stagnant water column with essentially no current movement (Middleton and Hampton, 1973).

As flows move downslope the following processes take place to create the layers of the idealized Bouma sequence (Middleton and Hampton, 1973). As already noted, not all layers of the Bouma sequence may be deposited by a given flow.

Bouma A is the first layer deposited by a turbid flow, provided the flow has sufficient energy and sand content. Otherwise Bouma B, C or D will be the first layer deposited. Bouma A is deposited when the flow energy is high enough that fluid turbulence is able to keep the coarsest grains in suspension. When energy drops below a critical level, the grains tend to settle out all at once to create a massive bed. If flow energy drops more slowly, then the coarse grains may settle out first, leaving the fine grains still in suspension. This results in coarse-tail graded bedding, which means that there is a bimodal distribution of grain sizes with the coarse grains becoming progressively smaller towards the top of the bed, and the finer grains being randomly distributed between the coarse grains (i.e., the finer grain sizes are ungraded). As grains settle out, water displaced by

grain compaction can move upward to create dish structures. Also, erosion can take place at the base of the flow and tear up shale from an underlying bed so that shale-rip clasts are incorporated into the base of the Bouma A layer. If there is some buoyancy to the rip-up clasts, then they may form a layer some distance above the base of Bouma A.

Bouma B is deposited during upper flow regime conditions where the flow energy is high enough to carry sand grains by traction, wherein grains slide and roll across the surface beneath the flow. The current energy is such that sole marks such as groove casts, flute casts and parting lineation can form on top the bed beneath the flow, and be preserved as molds and casts on the base of the Bouma B layer.

Bouma C is deposited under lower flow regime conditions where there is enough energy for the flow to carry fine sand by saltation, wherein grains hop and bounce across the surface beneath the flow. As grains settle out, current ripples develop, with climbing ripples developing if sedimentation rates are high enough. If shear is imposed on the ripple beds by an earthquake and/or by an overlying turbidite/turbidity current, the ripple laminations can be deformed into convolute laminations and flame structures.

Bouma D is deposited by suspension settling where a slight current exists. Subtle changes in current energy causes alternating laminations of coarser and finer grains of silt to settle out.

Bouma E is the last layer deposited. It results from suspension settling where essentially no current exists. Clays generally remain suspended until the water chemistry changes and allows the clays to flocculate and settle out. Because the Bouma E layer, if deposited at all, is easily eroded by subsequent turbidity currents, it is often not present.

Terminology for high-density turbidites

Lowe (1962) has proposed a classification to describe the succession of sedimentary structures that develop in turbidite sandstones deposited by high-density (i.e. sand-rich, high-concentration) turbidity currents) Lowe's terminology is intended to complement, not replace, the better known Bouma sequence, which applies primarily to turbidites deposited by low-density (i.e., low-sand concentration) turbidity currents.

Description of Lowe's terminology

Lowe's (1982) terminology adds three layers labeled S1 through S3 to Bouma's (1962) terminology, with Lowe's S1 layer at the bottom of a sandy turbidite bed, and the S3 layer at the top. As in the Bouma sequence, each layer has a specific set of sedimentary structures and lithology (Figure 4). Similarly,, the layers become finer grained from bottom to top. The layers are described as follows.

S3 - Massive to graded, fine- to coarse-grained sandstones that overlie the S2 layer represent deposition from a turbulent suspension. Sometimes dish structures and dewatering pipes are present. This layer is essentially the same as the Bouma A layer.

S2 - Inverse (reverse) graded, fine- to coarse-grained sandstone layers that overlie the S1 layer represent deposition as traction carpets, where grain-to-grain collisions are an important process.

S1 - Sandstone to conglomerate that are at the base of the turbidite and display parallel-laminated to cross-laminated beds that indicate traction deposition, wherein the current moves grains, pebbles and large clasts by rolling and sliding them across the surface beneath the flow.

As previously mentioned, the Lowe sequence is intended to complement, not replace the Bouma sequence. Fine-grained turbidites resulting from low-density turbidity currents, in which the Bouma A through Bouma E terminology applies, are referred to in the Lowe classification as Ta through Te, in which the T acronym derives from "Traction". By contrast, because the S1-S3 terminology describes sand-rich turbidites deposited by high-density turbidity currents, the S acronym derives from "Sandstone". Lastly, R1-R3, which uses the same descriptive criteria as S1-S3, applies to conglomerates, wherein the R acronym derives from "Rubble". In practice, the S1-S3 terminology is widely used, Ta-Te is used sometimes, and R1-R3 is seldom used.

Processes in high-density turbidity currents

Initially grains, pebbles and large clasts in a high-density turbidity current (i.e., a high-sand concentration flow), are moved by traction (rolling and sliding) to generate a coarse-grained to conglomeratic, parallel-laminated to cross-laminated S1 layer. However, as grains settle out and move closer together, grain-to-grain collisions begin to generate dispersive pressures that help

prevent further settling. This results in smaller grains moving between larger grains and preferentially settling out beneath them. Thus, an inverse graded layer develops that is called a traction carpet, since it is thought to move as a single unit. At some point, the grains move close enough together that collisions no longer generate enough energy to keep the grains in suspension, and the entire layer freezes to create an S2 layer. This process can then repeat to create additional traction carpets (Lowe, 1982).

When grains move closer together and settle out, the water between them is displaced and moves upward into the flow, helping to keep grains above the traction carpets in suspension. Because the flow is in motion, this upward movement of fluid quickly becomes turbulent. When the energy of the flow drops low enough so that the flow can no longer sustain turbulence, then the entire flow freezes to create the massive to normally graded S3 layer. Subsequent reworking of the top of this new deposit by overlying remnant currents or by new currents unrelated to the original flow can create laminations that resemble the Bouma B layer. When reworking stops, suspension settling may deposit massive mudstone (Bouma E) directly on top of the laminated layer. Alternatively, if new sediment is introduced during this reworking phase, or if sediment is sufficiently remobilized and transported, then a more complete Bouma sequence may develop on top of the S3 layer (Lowe, 1982).

References

Bouma, Arnold H. (1962), Sedimentology of some Flysch deposits: A graphic approach to facies interpretation, Elsevier, p. 168.

Gani, M.R. (2004), From turbid to lucid: a straightforward approach to sediment gravity flows and their deposits, The Sedimentary Record (A publication of the SEPM Society for Sedimentary Geology), v. 2, n. 3 (Sept.), p. 4-8.

Hampton, M.A. (1972). The role of subaqueous debris flows in generating turbidity currents, Journal of Sed. Petrology, v. 42, p. 775-793.

Haughton, P., Davis, C., McCaffrey, W. & Barker, S. (2009), Hybrid sediment gravity flow deposits - classification, origin and significance, Marine ad Petroleum Geology, v. 26, p. 1900-1918.

Lowe, D.R. (1982), Sediment gravity flows: II. Depositional models with special reference to the deposits of high-density turbidity currents, Journal of Sedimentology, v. 52, p. 279–297.

Lowe, D.R. (2006), Subaqueous liquefied and fluidized sediment flows and their deposits, Sedimentology, v. 23, p. 285-308.

Lowe, D.R. & Guy, M. (2000), Slurry-flow deposits in the Britannia Formation (Lower Cretaceous), North Sea: a new perspective on the turbidity current and debris flow problem, Sedimentology, v. 47, p. 31-70.

Middleton, G.V. and Hampton, M.A. (1973), "Sediment gravity flows: mechanics of flow and deposition" in Turbidites and deep-water sedimentation (Pacific Section of the Society of Economic Paleontologists and Mineralogists, Short Course Lecture Notes), p. 1–38.

Postma, G. (1986), Classification for sediment gravity-flow deposits based on flow conditions during sedimentation, Geology Magazine, v. 14, p. 291–294.

Visher, G.S. (1999), Stratigraphic systems: origin and application, Academic Press, v. 1, p. 521.

Weimer, P. & Link, M.H., eds. (1991), Seismic facies and sedimentary processes of submarine fans and turbidite systems, Springer-Verlag, 447p

This article is modified from various short articles written previously by the author and posted on www.wikipedia.com

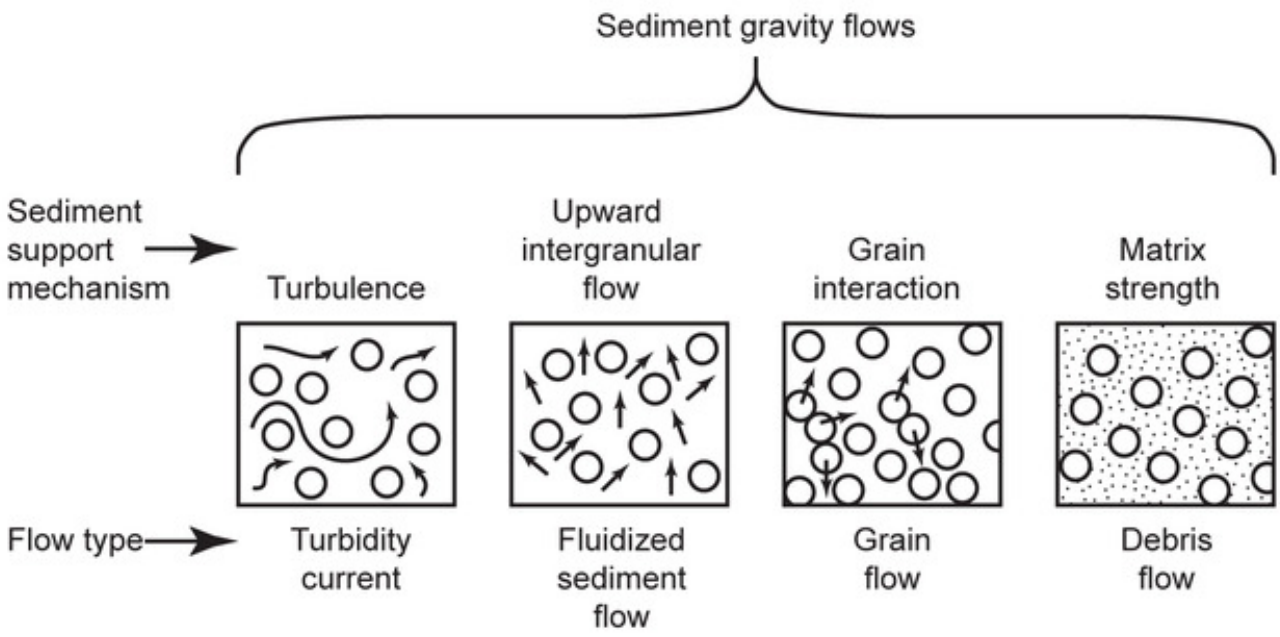

Figure 1: Diagram showing the sediment support mechanisms commonly used to differentiate sediment gravity flows (modified from Middleton & Hampton, 1973).

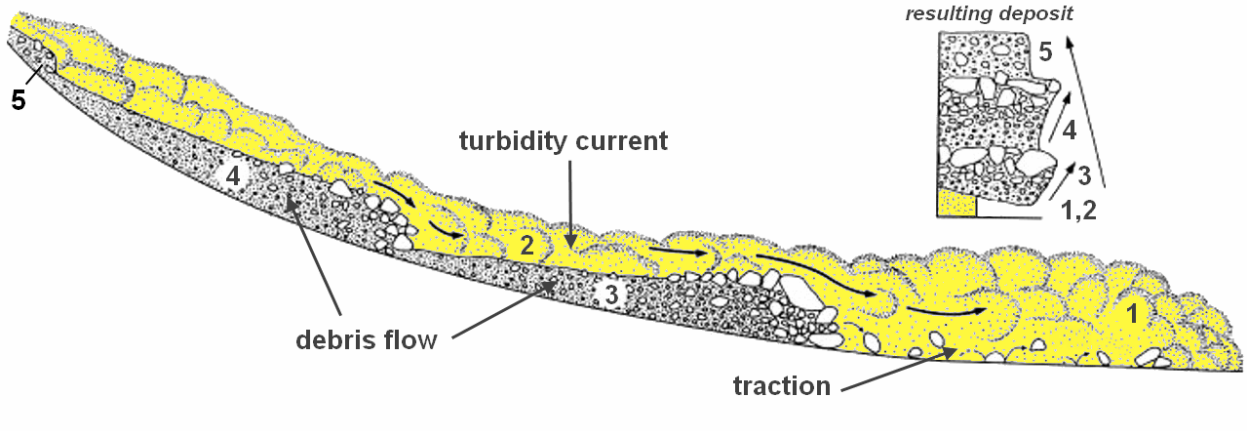

Figure 2: Diagram showing debris flow, turbidity current and traction processes in a single sediment gravity flow. The resulting deposit, which some geologists call a linked debrite, exhibits features of all three processes (from Wikipedia).

Figure 3a (above): Photograph of a turbidite from the Pigeon Point Formation (Lower Cretaceous), Pescadero Beach, California showing Bouma A-D divisions. **Figure 3b (below):** Diagram showing divisions of the Bouma sequence (from Bouma, 1962).

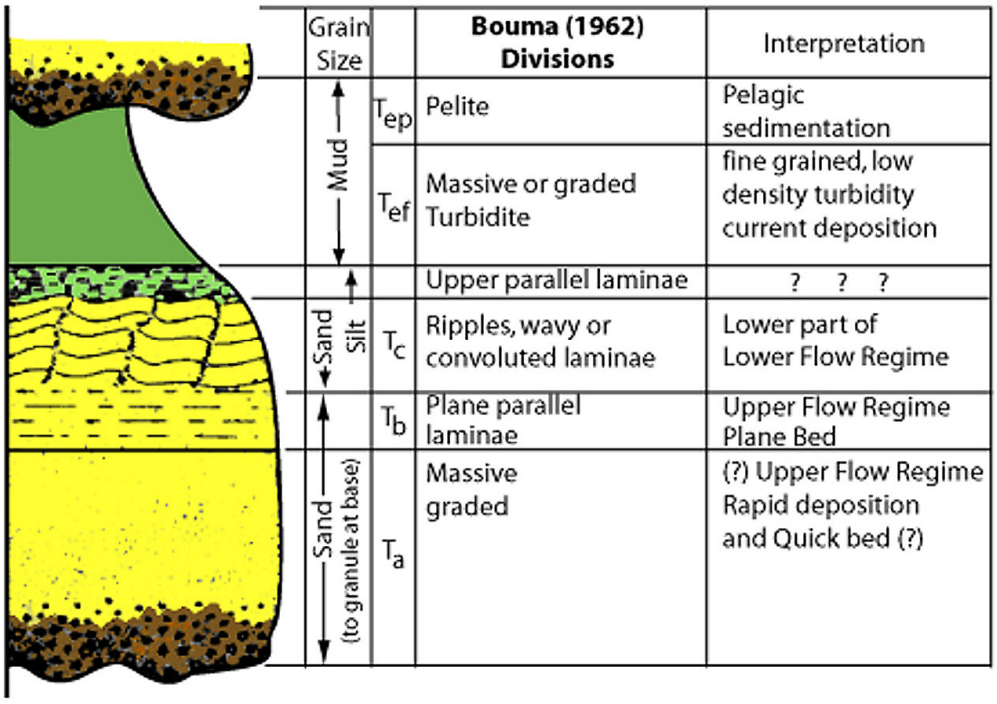

Grain Size		Bouma (1962) Divisions	Interpretation
Mud	T_{ep}	Pelite	Pelagic sedimentation
Mud	T_{ef}	Massive or graded Turbidite	fine grained, low density turbidity current deposition
Mud / Silt		Upper parallel laminae	? ? ?
Sand / Silt	T_c	Ripples, wavy or convoluted laminae	Lower part of Lower Flow Regime
	T_b	Plane parallel laminae	Upper Flow Regime Plane Bed
Sand (to granule at base)	T_a	Massive graded	(?) Upper Flow Regime Rapid deposition and Quick bed (?)

Figure 4a (above): Incredible photograph by Zoltan Sylvester showing a high-density turbidite exposed near Talara, Peru with a basal S1 division (traction lamination), a middle S2 division (inverse-graded traction carpets), and an S3 division (turbidite with dish structures) at the top. This unit represents a single depositional event.
Figure 4b (below): Diagram of Lowe's divisions (modified from Lowe, 1982).

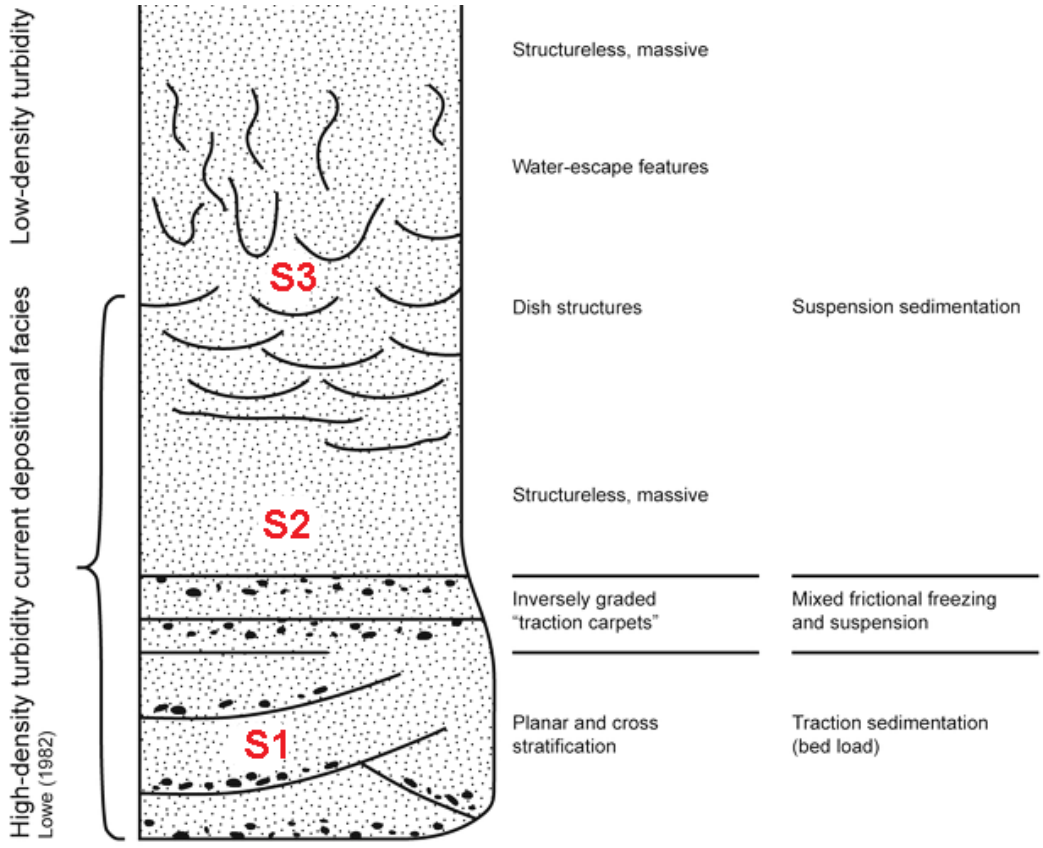

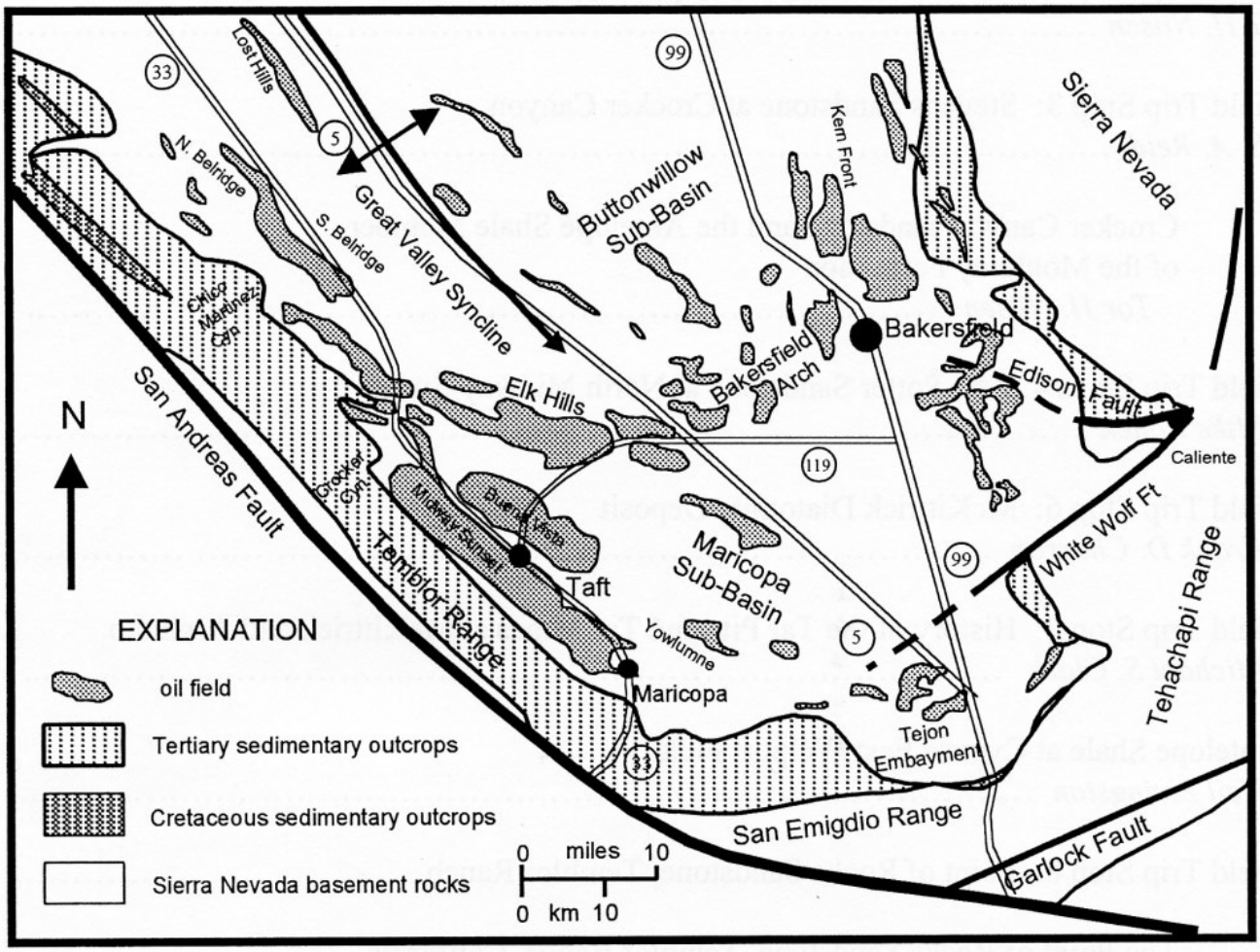

Geologic map of the southern San Joaquin basin to accompany the following Road Log for the Westside Turbidite Outcrops field trip (modified from Jennings, 1977, Geologic Map of California, Calif. Div Mines and Geology, scale 1:750,000)

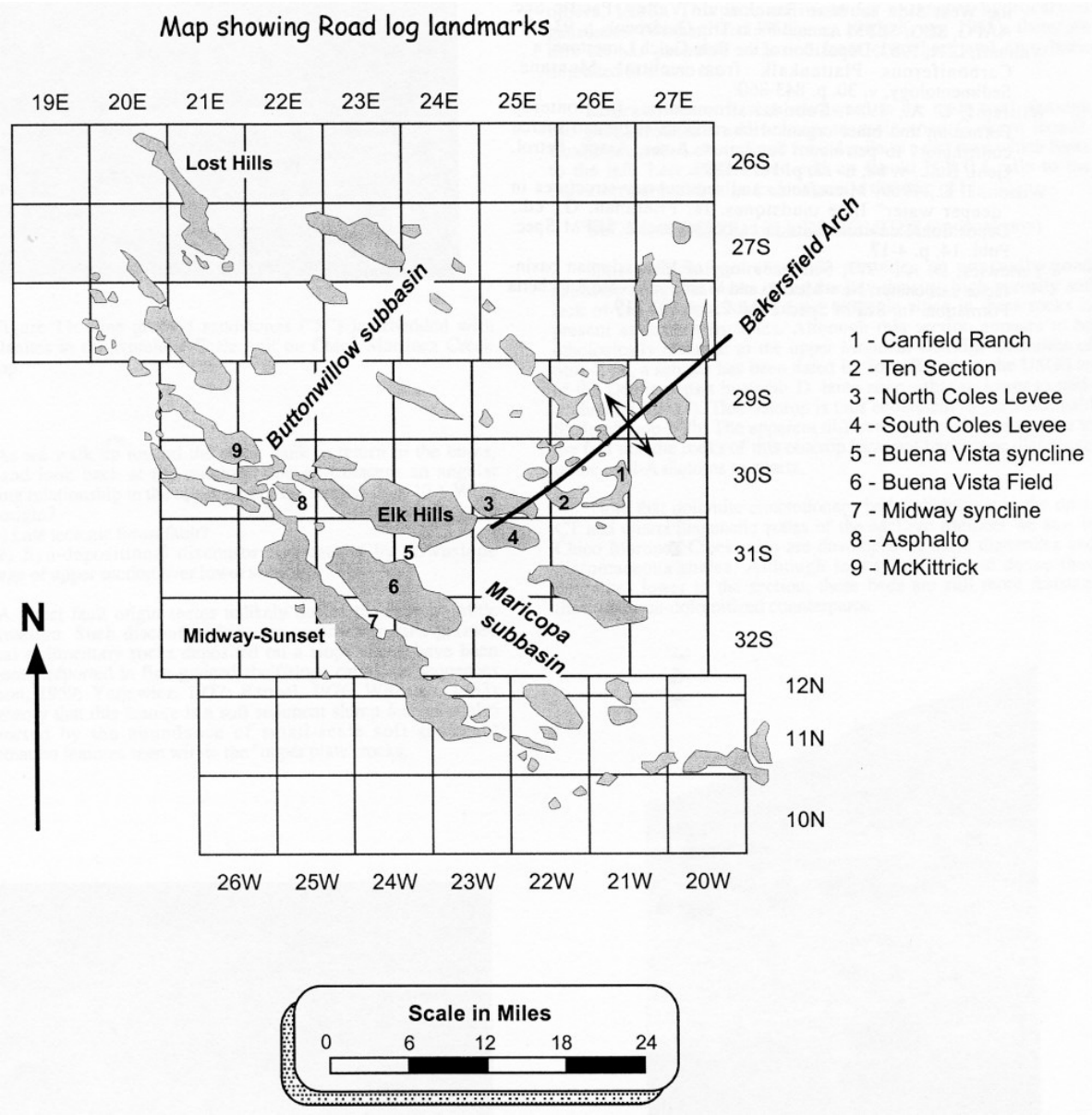

Figure 1: The map above shows some of the oil fields mentioned in the following Road Log. The map also shows the trend of the Bakersfield Arch, which is a subsurface regional high, with no surface expression, that separates the Maricopa (White Wolf) depocenter in the south part of the San Joaquin basin from the Buttonwillow depocenter to the north. The field guide begins in the city of Bakersfield and follows a line of oil fields (numbers 1-4) that trend along the crest of this subsurface feature. The guide then leads through three en echelon giant anticlines (numbers 5-7) that correspond to billion-barrel oil fields. These anticlines result from compression associated with the San Andreas fault, which is located near the west margin of the above map. The guide then turns north, leads through Asphalto Field (#7), and pauses at McKittrick Field (#8), the planned lunch stop, before continuing north.

Road Log for Turbidite Outcrops on the West Side of the San Joaquin Valley

Michael S. Clark, S. A. Reid and Michael L. Simmons

Cumulative Mileage	*Field trip stops are highlighted yellow* *Oil fields and other sites of interest are highlighted green*	miles to next landmark
0.0	Start at parking lot across the street from the California Well Sample Repository on the California State University campus. Turn left (south) out of the lot, heading towards the Edwards Cinema. We will proceed generally along the crest of the Bakersfield Arch (see Figure 1 on opposite page), a subsurface regional high that controls much of the production in the central part of the San Joaquin basin. Despite the economic importance of the Arch, it has no surface expression.	1.8
	Turn right on Camino Media and proceed west.	
	Turn left on Old River Road and proceed south.	
1.8	Turn right on Ming Avenue and proceed west.	1.4
	Turn left on Buena Vista Road and proceed south.	
3.2	CANFIELD RANCH OIL FIELD – The pumping jacks on the right (west) side of the road represent the East Gosford area of Canfield Ranch field, which produces from Miocene Stevens sandstones at depths of 7,000 to 8,000 feet. The field is primarily a stratigraphic trap controlled by the updip (eastward) lensing out of the oil-bearing sands. Also, several faults clearly influence the shape of the oil pool. Canfield Ranch is the first of several Stevens fields we will pass through that sit on the Bakersfield Arch, a regional northeast-to-southwest trending high that separates the southern San Joaquin Valley into the Tejon subbasin, on the south side of the Arch, from the Buttonwillow subbasin, on the north. The Arch continues through Ten Section and the Coles Levee fields before merging with the Elk Hills anticline (Figures 1 and 2).	1.6
4.8	Turn right on Panama Lane and proceed west.	4.7
9.5	TEN SECTION OIL FIELD – The tank farm and pumping jacks on the left (south) side of the road indicate Ten Section field, an anticline with no surface expression that was discovered in 1936 in the first application of seismic exploration in California. Production was established from a previously unknown, Miocene package of sandstones which was named the “Stevens” after the nearby Stevens Siding railroad stop. Today, the Stevens is one of the most important reservoirs in the basin, responsible for roughly 15% of the 12 billion barrels of oil that has been produced from the San Joaquin Valley since the turn of the century.	2.3
11.8	Turn left on Enos Lane and proceed south. The low hills visible in the foreground straight ahead are the Elk Hills anticline, better known as the former U. S. Naval Petroleum Reserve No. 1.	1.9
13.7	Turn right on the Taft Highway (Route 119) and proceed west.	2.0
15.7	COLES LEVEE OIL FIELDS – The tank farms and structures on either side of the road are facilities for North and South Coles Levee fields which sit in the middle of the Coles Levee Ecosystem Preserve. Both fields were discovered in 1938-1939, and North Coles Levee has the distinction of having supplied most of the crude oil used to make aviation fuel during World War II. North Coles Levee, with a cumulative production of over 160 MMBO, is also one of the giant oil fields of the San Joaquin Valley. Both fields are seismically defined anticlinal structures, with no surface expression, which produce from Stevens sandstones at depths of 7,500 to 10,000 feet. The Ecosystem Preserve is a in which the Coles Levee surface acreage will to be turned over the state as a wildlife sanctuary when the field is abandoned.	1.2

16.9	ELK HILLS ANTICLINE AND OIL FIELD – As we cross over the California Aqueduct, the Taft Highway (Route 119) climbs up into Elk Hills, one of the largest oil fields in the United States. Outcrops of the Tulare Formation mark the flanks of an enormous anticlinal dome, over 12 miles long and more than 4 miles wide. Beneath this anticline, at depths down to 10,000 feet, there are three major anticlinal structures that contain Miocene (Stevens sandstones and Monterey shales) and Pliocene (Etchegoin and San Joaquin Formation) reservoirs. The field has produced over 1 billion barrels of oil and currently produces 55,000 barrels of oil and 350 million cubic feet of gas per day.	3.2
20.1	U.S. NAVAL PETROLEUM RESERVE No. 1 – A sign on the right (west) side of the road indicates the entrance to the Elk Hills field office, previous headquarters for U.S. Naval Petroleum Reserve No. 1. The Naval Petroleum Reserves were established early in the century to provide oil for the U.S. Navy in the event of a national emergency. With a strong upswing in oil prices in the mid-1970s, the Federal government decided to cash-in on the elevated oil revenues and open-up Elk Hills to full production. Pressure from corporations subsequently convinced the Government to sell their interest in the field. Occidental Petroleum successfully bid $3.65 billion in 1997 and recently assumed operation of the field.	3.6
23.7	BUENA VISTA SYNCLINE – At about this mileage, the highway passes through Buena Vista Valley, the axis of a giant syncline that separates Elk Hills (behind us) from the Buena Vista Hills anticline (in front of us). BUENA VISTA HILLS ANTICLINE – The wooden derrick and pumping jack on the right (west) side of the road date to the early days of Buena Vista field. Since its 1909 discovery, the field has produced 660 million barrels of oil. The pumping jacks spreading from here south to Taft, on either side of the road, produce from Miocene and Pliocene reservoirs in the Buena Vista anticline, which corresponds to the hilltop west of the highway. Of particular interest is deeper production from both Stevens sandstones and fractured Antelope shale.	3.3
27.0	Turn right on Midway Road and proceed west.	2.7
29.7	MIDWAY SYNCLINE – The valley we are passing through represents the Midway Valley syncline, a trough separating the Buena Vista Hills anticline (in back of us) from the Temblor anticlinorium (in front of us). More important, the valley represents the separation between Buena Vista field and billion-barrel Midway-Sunset field. We immediately enter Midway-Sunset in an area of primarily Pliocene production, which has largely been abandoned. Here stratigraphic traps have formed on the east flank of the Temblor anticlinorium by the onlap of thin Pliocene sands onto a basal Pliocene unconformity.	1.4
31.1	Stop sign. Stay on Midway Road, continue across Highway 33, and proceed west.	0.2
31.3	Stay left at a Y-intersection, continue on Midway Road into the town of Fellows.	0.5
31.8	Turn left in Fellows at the T-intersection onto Midoil Road, which winds into the oil field, and proceed south. MIDWAY-SUNSET FIELD – The town of Fellows, which we are now passing through, is a company-owned community originally established as living quarters for employees working Midway-Sunset field. With a daily production of 160 to 170 thousand barrels, Midway is the largest oil field in the continental United States. The cumulative production currently stands at 2.3 billion barrels. As we continue driving northwest, we enter an area dominated by Miocene production resulting from the updip truncation of Potter sandstones (Reef Ridge equivalents) beneath the basal Pliocene unconformity.	2.2
34.0	Look for a white sign indicating the way to the 17X Lease and turn right off the main road into confusing maze of oil field roads and pumping jacks. Try to stay on the north (right) side of an obvious draw, and proceed west into the field.	0.9
34.9	When you reach H2S plant at the back of the draw, take the lower (left-hand) road at a Y junction just past the H2S plant. Then drive uphill on the main road.	0.7
35.6	**Park** on the crest of the main road, at the far edge of the field, and walk to granite boulders on the top of the hill to the south. This is the first of three short stops. STOP 1a: STEVENS CANYON FILL AT 17X LEASE: OVERVIEW – please see page 8 of field guide	

	Return to the cars, and make a U-turn. Drive down the short steep hill and leave the main road at first opportunity to take a dirt track on the right. Continue to near a fence on the edge of the oil field, turn east on the main dirt road proceed downhill, aiming for an interesting looking road cut.	0.3
35.9	**Park** in the large, flat pad for the 235X well head, with a large road cut to the north.	
	STOP 1b: STEVENS CANYON FILL AT 17X LEASE - CANYON CROSS-SECTION	
	Return to the cars and continue straight ahead (east). The dirt track ahead soon rejoins the the main road you drove up earlier. Turn left (west) back onto the main road, then quickly vere off to the right on a dirt track that takes off from the head of a sharp curve.	0.4
36.3	**Park** between the 202 and 243 well heads, with a road cut to the west.	
	STOP 1c: STEVENS CANYON AT 17X LEASE - FAULTED DIATOMITE	
	Return to the cars and retrace the route back through the oil field to the main highway.	1.7
38.0	Turn left on Mocal Road. Then proceed north to the town of Fellows,and drive through the town past the post office.	2.4
40.4	Turn left onto Midway Road and proceed west.	0.4
40.8	MIDWAY GUSHER – The historical marker on the right side of the road commemorates the Chanslor-Canfield Midway No. 2-6, simply called the Midway Gusher, which blew out on November 27, 1909. Flowing at a rate of about 2,000 barrels of per day, this well foreshadowed development of Midway-Sunset field.	3.3
44.1	MIDWAY-SUNSET STEAM FLOOD – Most oil produced on the west side of the San Joaquin Valley is heavy crude, with an API gravity of 15 degrees or less, that flows with difficulty. Consequently, Midway-Sunset crude was sub-economic for many operators to produce until the advent of steam recovery in the 1960s. Today, steam injection into the subsurface, to increase mobility of the oil and facilitate its recovery, has made Midway-Sunset the most prolific oil field in the continental United States.	1.8
45.9	Turn left onto Crocker Springs Road and proceed west.	2.1
48.0	COGENERATION PLANT – Unknown to many, most steam produced in the valley is first used to turn turbines and generate electricity before being injected into the ground. The steam plant on the right (north) side of the road, with three 78-megawatt turbines, is one of the larger cogeneration facilities in the valley. Although the electricity generated here exceeds the energy needs for all of Kern County, little is used locally and most is sent south to Los Angeles.	2.1
50.1	**Park** just past the farmhouse and complex of cattle pens.	

CROCKER CANYON IS PRIVATE PROPERTY. PLEASE DO NOT CONTINUE WITHOUT PERMISSION.

	STOP 2: STEVENS TURBIDITES AT CROCKER CANYON – please see page 16 of field guide.	
	Return to the cars, and retrace the route to the intersection of Crocker Springs and Mocal Road.	4.0
54.1	Turn left onto Mocal Road, and proceed north. When the enters the oil field a short distance ahead, go right at a Y-junction. A short distance ahead the road curves to the right.	0.6
54.7	Turn right off the main road just in front of an obvious east-west line of oil tanks, and proceed east. Continue east after passing the tanks, proceed into the abandoned part of the field, and aim for Highway 33 up ahead.	0.6
55.3	Turn left onto Highway 33 and proceed north toward the town of McKittrick, passing through the town of Derby Acres. About the time you pass the junction with Highway 58, look for the black remnants of ancient tar seeps exposed on either side of the Highway 33 road cut.	6.5
61.8	Turn right onto Reserve Road at intersection on the far side of McKittrick and proceed east towards the La Paloma congeneration plant.	1.0

62.8	Turn right onto dirt road before you reach the La Palomas plant, and proceed south into the hills ahead, passing under a line of electircal wires. The road is rough at first, then becomes paved when it enters the oil field.	1.2
64.0	Turn left when a good view of the La Paloma plant appears on the left. This will be just past a vapor recovery plant on the right. The road goes down left, then switchbacks right to the large well pad below. Then cross over to the next large well pad to the south.	0.1
64.1	**Park** next to the 494 pumping jack. There will be obvious diatomite outcrops to the west and sandstone outcrops to the east.	
64.1	STOP 3: POTTER SUBMARINE CANYON – please see page 22 of field guide. OPTIONAL STOP – OIL-STAINED TULARE SANDS AND HISTORIC TAR MINES – Gullies to the south of this stop contain shafts and tunnels, dating to the 1880s, that were used to mine asphalt seams. Dark, oil-stained rocks around the mine entrances are trough cross-stratified sandstones of the Pleistocene Tulare Formation that unconformably overlie Potter sandstones and Belridge diatomaceous shales. Oil-stained, flat-lying beds above the mines represent ancient tar seeps that were originally sourced by the asphalt seams.	
64.1	Return to the cars, and retrace the route back to Reserve Road.	1.3
65.4	Turn left (west) onto Reserve Road, continue to McKittrick, cross highway 33 and continue west.	1.6
67.0	**Park** at the Chevron production office, which will be on the right. RESTROOM STOP AT CHEVRON McKITTRICK FIELD OFFICE	
67.0	Retrace the route back to the town of McKittrick	0.6
67.6	Turn right onto Highway 33 and proceed south.	0.6
68.2	McKITTRICK FIELD – Pumping jacks in this area are part of McKittrick field, which is one of the oldest fields in the valley and dates back to the 1860s when commercial production was first established by collecting tar from nearby oil seeps. Hand-dug pits and asphalt mines soon followed. Modern production began in 1896 when the first genuine oil well in the area, the Shamrock gusher, blew out an estimated rate of 1,300 barrels of oil per day. Since then, the field has produced over 280 million barrels of oil to qualify it as one of the valley's giant oil fields.	
68.2	Turn right on Highway 58 and proceed west McKITTRICK TAR PITS – The McKittrick tar pits which have yielded a Pleistocene fossil fauna that rivals that found in the La Brea Tar Pits of Los Angeles.	1.6
69.8	**Park** on the right side of the road at a long conspicuous road cut. STOP 4: LUNCH AT McKITTRICK OIL SEEPS - see page 28 of field guide.	
69.8	Return to the cars, turn around, and retrace the route back down the hill to Highway 33, staying to the left of a paved junction part way down the hill.	1.6
71.4	Turn left onto Highway 33 and proceed north. WELPORT AREA OF CYMRIC FIELD – The wells on the left (west) side of the highway since we left McKittrick, and which we will continue to see until we reach Twissleman Ranch, produce from Cymric field. This complex accumulation, which has produced 280 million barrels of oil since its 1909 discovery, is characterized by several different types of traps and produces from reservoirs that range in age from Eocene to Pleistocene. Of particular interest is recent development of fractured Monterey Shale production.	10.9
82.3	Turn left onto Seventh Standard Road, which is just past the Missouri Triangle Café, and proceed west. The route passes the Aera Energy field office at 1.9 miles, the South Belridge school at 4.0 miles, and Chico Martinez oil field at 5.5 miles. SOUTH BELRIDGE OIL FIELD - This is a giant anticline with more than a billion barrels of production, most of which comes from Opal A facies diatomites of the Reef Ridge Formation (Delmontian Stage) that must be fracture stimulated to produce.	5.7
88.0	CHICO-MARTINEZ OIL FIELD - This is a small oil field that produces from fractured Monterey shales. Although most of the wells produce only a few barrels a day, the field has witnessed a revitalization that has resulted in the drilling of many new wells.	

88.0	Make a sharp curve to the right to stay on Seventh Standard, just after passing through Chico-Martinez oil field, and proceed in a northwesterly direction to reach Twisselman Ranch.	3.2

TWISSELMAN RANCH IS PRIVATE PROPERTY.
PLEASE DO NOT CONTINUE WITHOUT PERMISSION.

91.2	McDONALD ANTICLINE OIL FIELD - The field evident several hundred years away on the road ahead is similar to the Chico-Martinez Creek field that we just passed through. However, McDonald Anticline field is not as prolific as Chico-Martinez, and the revitalization of the field has not attracted as much investment.	
91.2	Take the left fork at a Y-junction and proceed only if you have permission to Carneros Creek. The right goes fork to McDonald Anticline oil field. There are gates here that must be unlocked in order to continue past the ranch house and horse corrals.	1.1
92.3	**Park** at a curve near the top of the hill beyond the ranch house. Down at the bottom of the creek on the right is the Carneros Creek type section.	
92.3	STOP 5: CARNEROS TURBIDITES AT CARNEROS CREEK - please see page 32 of field guide.	
92.3	Return to the cars and retrace the route back Highway 33 and proceed south to the intersection of Highway 33 with Lokern Road.	20.3
112.6	Turn right onto Lokern Road and proceed west on a deteriorating paved road.	5.6
	SALT CREEK AREA OF CYMRIC FIELD – The pumping jacks to the left (south) side of the road produce from the Salt Creek area of Cymric field, which represents the easternmost production from the field complex. Southeast of us is the crest of Cymric (Welport Lease) that we drove by earlier.	
118.2	TWISSLEMAN RANCH – This ranch, also known as the Temblor Ranch, has belonged to the Twisselman family for more than a hundred years. The road log ends here at a point just before reaching the ranch house.	

THIS IS PRIVATE PROPERTY.
PLEASE DO NOT CONTINUE WITHOUT PERMISSION.
(The Point of Rocks outcrop is another 1.3 miles beyond)

STOP 6: POINT OF ROCKS TURBIDITES AT SALT CREEK (page 38 of field guide).